MONITORING BONE MICRO-ARCHITECTURE WITH A SPECIAL FOCUS ON BONE STRENGTH

A Thesis Proposal Submitted to the

College of Kinesiology

in Partial Fulfillment of the Requirements

for the Degree of Doctorate of Philosophy

in the College of Kinesiology

University of Saskatchewan

Saskatoon

By

Chantal E. Kawalilak

PERMISSION TO USE

In presenting this thesis/dissertation in partial fulfillment of the requirements for a postgraduate degree from the University of Saskatchewan, I agree that the libraries of this university may make it freely available for inspection. I further agree that permission for copying of this thesis/dissertation in any manner, in whole or in part, for scholarly purposes may be granted by the professor or professors who supervised my thesis/dissertation work or, in their absence, by the head of the department or the dean of the college in which my thesis work was done. It is understood that any copying or publication or use of this thesis/dissertation or parts thereof for financial gain shall not be allowed without my written permission. It is also understood that due recognition shall be given to me and to the University of Saskatchewan in any scholarly use which may be made of any material in my thesis/dissertation.

Requests for permission to copy or to make other uses of materials in this thesis/dissertation in whole or part should be addressed to:

Dean of the College of Kinesiology

University of Saskatchewan

Saskatoon, Saskatchewan

S7N 5B2

ABSTRACT

Introduction. Osteoporosis is a chronic disease characterized by the loss of bone mass and the deterioration of bone micro-architecture leading to a subsequent increase in fracture risk. High-resolution peripheral quantitative computed tomography (HR-pQCT) provides non-invasive measures of bone micro-architecture and strength in live humans but its ability to monitor small skeletal changes is yet poorly understood. The objectives of this thesis were to 1) determine HR-pQCT precision for volumetric density, geometry, cortical and trabecular micro-architecture, as well as estimates of bone strength; 2) determine the monitoring time interval (MTI) and least significant change (LSC) metrics; and 3) to characterize annual changes in bone area, density, and micro-architecture at the distal radius and tibia using HR-pQCT in postmenopausal women.

Methods. To determine precision error as well as monitoring and change metrics of the distal radius and tibia, 34 postmenopausal women (mean age 74, SD±7 years) from the Saskatoon cohort of the Canadian Multicentre Osteoporosis Study (CaM*os*) were measured using HR-pQCT. To characterize the annual change in bone outcomes of this same cohort, 51 women (mean age±SD: 77±7 years) were measuring at baseline and again 1 year later. Precision errors were calculated as coefficient of variation (CV% and $CV\%_{RMS}$). The LSC was determined from precision errors and then divided by the median annual percent changes to define MTIs for bone area, density, and micro-architecture. Repeated measures analysis of variance (ANOVA) with Bonferroni adjustment for multiple comparisons were used to characterize the mean annual change in total density, cortical perimeter, trabecular and cortical bone area, density, content, and micro-architecture. Significant changes were accepted at $P<0.05$.

Results and Discussion. HR-pQCT precision errors were <10% for bone densitometric, geometric, and mechanical properties; while precision errors were <16% for cortical and trabecular micro-architectural outcomes. Further, the use of either automatic or modified contour methods for the dual-threshold technique for cortical micro-architectural analysis provided similar precision. Densitometric and geometric outcomes had longer monitoring times (>3 years), while micro-architecture had monitoring times of ~2 years. The observed annual changes were statistically significant for several outcomes; however, only cortical and trabecular area, as well as cortical density at the distal tibia changed beyond the LSC. Overall, thesis findings will assist design and interpretation of prospective HR-pQCT studies in postmenopausal women.

PREFACE AND CANDIDATE'S ROLE

Sections of this thesis have been published or submitted for publication as multi-authored papers in refereed journals. This section aims to define the role of the candidate and that of the co-authors for each publication and the conference presentations.

Study 1: HR-pQCT Precision

Publication 1: Kawalilak CE, Johnston JD, Olszynski WP, Leswick D, Kontulainen SA (2014). Comparison of short term in vivo precision of bone density and micro-architecture at the distal radius and tibia between postmenopausal women and young adults. *Journal of Clinical Densitometry, 17*(4): 541-517.[1]

Chantal Kawalilak (CK) co-developed study design and research protocol together with supervisor Saija Kontulainen (SK). CK performed all HR-pQCT measurements, image analyses, and statistical analyses. CK drafted the manuscript and revised versions based on the feedback from SK and JD Johnston (JDJ), Wojciech Olszynski (WO), and David Leswick (DL).

The results in this study were presented at local and international conferences:

i. *Local Meeting*: University of Saskatchewan Life and Health Sciences Research Day; Saskatoon, Saskatchewan, Canada; March 9, 2012.
ii. *International Meeting:* American Society for Bone and Mineral Research; Minneapolis, Minnesota, USA; October 15, 2012 (MO0308).

Publication 2: Kawalilak CE, Johnston JD, Cooper DML, Olszynski WP, Kontulainen SA (2015). Role of endocortical contouring methods on precision of HR-pQCT-derived cortical micro-architecture in postmenopausal women and young adults. *Osteoporosis International. E-pub ahead of print.*[2]

CK co-developed study design and research protocol together with SK. CK performed all HR-pQCT measurements, image analyses, and statistical analyses. CK drafted the manuscript and revised versions based on the feedback from SK and JDJ, WO, and Dave Cooper (DC).

The results in this study were presented at national and international conferences:

i. *International Meeting:* American Society for Bone and Mineral Research; Houston, Texas, USA; September 15, 2014 (MO0021).

Publication 3: Kawalilak CE, Kontulainen SA, Lanovaz JL, Amini MA, Johnston JD (2015). *In vivo* precision of three HR-pQCT-derived finite element models of the distal radius and tibia in postmenopausal women. *Submitted.*

CK co-developed study design and research protocol together with SK and JDJ. CK performed all HR-pQCT measurements, image analyses, and statistical analyses. CK programmed the single and dual tissue finite element (FE) models, and together with the help of Morteza Amini (MA), CK helped in the programming of the E-BMD model into the XtremeCT FE solver. CK drafted the manuscript and revised versions based on the feedback from SK, JDJ, MA, and Joel Lanovaz (JL).

The results in this study will be presented at an international conference:

i. *International Meeting*: American Society for Bone and Mineral Research; Seattle, Washington, USA; October 9-12, 2015 (SA0032).

Study 2: Monitoring Skeletal Changes

Publication 4: Kawalilak CE, Johnston JD, Olszynski WP, Kontulainen SA (2015). Least significant changes and monitoring time intervals for high-resolution pQCT-derived bone outcomes in postmenopausal women. *Journal of Musculoskeletal and Neuronal Interactions, 15*(2):190-196.[3]

CK co-developed study design and research protocol together with SK. CK obtained all HR-pQCT measurements and executed all image analyses. CK performed statistical analyses together with SK and JDJ. CK drafted the manuscript and revised versions based on the feedback from SK, JDJ, and WO.

The results in this study were presented at national and international conferences:

i. *International Meeting:* Black Forest Forum for Musculoskeletal Interactions; Bad Liebenzell, Baden-Wurttemburg, Germany; May 24-26, 2013.
ii. *National Meeting:* Canadian Multicenter Osteoporosis Meeting; Montreal, Quebec, Canada; April 24-26, 2014.

Study 3: Characterizing Skeletal Changes

Publication 5: Kawalilak CE, Johnston JD, Olszynski WP, Kontulainen SA (2014). Characterizing micro-architectural changes at the distal radius and tibia in postmenopausal women using HR-pQCT. *Osteoporosis International, 25*(8): 2057-2066.[4]

CK co-developed study design and research protocol, together with SK. CK performed all HR-pQCT measurements and image analyses. CK performed statistical analyses together with SK. CK drafted the manuscript and revised versions based on the feedback from SK, JDJ, and WO.

The results in this study were presented at local, national, and international conferences:

i. *Local Meeting*: University of Saskatchewan Life and Health Sciences Research Day; Saskatoon, Saskatchewan, Canada; March 15, 2013.
ii. *International Meeting:* Black Forest Forum for Musculoskeletal Interactions; Bad Liebenzell, Baden Wurttemburg, Germany; May 24-26, 2013.
iii. *International Meeting:* American Society for Bone and Mineral Research; Baltimore, Maryland, USA; October 7, 2013 (MO0072). *[ASBMR President's Choice Poster Presentation Award 2013]*.
iv. *National Meeting:* Canadian Student Health Research Forum (CSHRF) hosted by the Canadian Institutes for Health Research (CIHR); Winnipeg, Manitoba, Canada; June 10-13, 2014.

ACKNOWLEDGEMENTS

I would like to extend my gratitude and sincerest thanks to all those individuals who have made the completion of my PhD possible. Foremost I would like to thank Dr. Saija Kontulainen for being an insightful, supportive, and encouraging supervisor. I greatly appreciate her patience and collaboration regarding my many inquiries and ideas, thesis study modifications, and additional research projects. I am also grateful for her encouragement and promotion of my research and teaching independence, for her support in my taking on research projects outside of my PhD work, for her trust regarding the management of the XtremeCT (HR-pQCT), and in helping with the mentoring of more novice researchers.

I would also like to thank my committee and cognate members: Dr. JD Johnston, Dr. Joel Lanovaz, and Dr. David Cooper for their time, guidance, expertise, and valuable contributions regarding this thesis. I would particularly like to extend many thanks and appreciation to Dr. JD Johnston for his patience, teachings, and guidance regarding the mechanics and engineering principles underpinning finite element modeling and the use of this tool.

I would also like to recognize Scanco Medical, specifically Nicolas Vilayphiou, for the invaluable help and support during my PhD and the learning process surrounding the use, maintenance, and management of the XtremeCT.

I would like to extend the warmest gratitude to my family for their ongoing support throughout my studies. I would also like to acknowledge CaM*os*, particularly Dr. Olszynski, Jola Thingvold, and Andrew Frank-Wilson for coordinating the study measurements

Finally, I would like to thank the University of Saskatchewan and the Canadian Institute of Health Research (CIHR) for funding my PhD work.

TABLE OF CONTENTS

LIST OF TABLES

LIST OF FIGURES

LIST OF ABBREVIATIONS

Mathematical Methods and Properties

$CV\%_{RMS}$	Root-Mean-Squared Percent Coefficient of Variation (precision error) [%]
E-BMD	Young's modulus scaled per image voxels' bone mineral density (BMD) [Pa]
FEA	Finite Element Analysis (also abbreviated: FE Analysis)
FEM	Finite Element Modeling (also abbreviated: FE Modeling)
LOA	95% Limits of Agreement
LSC	Least Significant Change [%]
MTI	Monitoring Time Interval [Years]
ρ	Density (as used in the E-BMD FE model) [mg HA/cm^3]
ν	Poisson's Ratio [-]
σ	Stress [Pa; N/mm^2]
ε	Strain [%]
E	Young's Modulus, Elastic Modulus, or Stiffness [Pa; N/mm^2]

Imaging Modalities

DXA	Dual-energy X-ray Absorptiometry
HR-pQCT	High Resolution peripheral Quantitative Computed Tomography

Bone Related Properties

General Bone Properties:

aBMD	Areal Bone Mineral Density (DXA-derived) [mg/cm^2]
BMC	Bone Mineral Content (measured using DXA and calculated for HR-pQCT) [g of HA]
HA	Hydroxyapatite (calcium phosphate; $Ca_5(PO_4)_3OH$)
vBMD	Volumetric Bone Mineral Density (e.g., HR-pQCT derived) [mg HA/cm^3]

Total Bone Properties:

D100	Total Bone Density [mg HA/cm^3]

Cortical Bone Properties:

CortArea	Cortical Area [mm^2]
CtBMD	Cortical bone mineral density [mg HA/cm^3]
CtBV	Cortical bone volume [mm^3]
CtPm	Cortical bone perimeter (i.e., periosteal perimeter) [mm]
CtPo	Cortical Porosity [%]
CtPoDm	Cortical Pore Diameter [mm]
CtPoV	Cortical Pore Volume [mm^3]
CtTh	Cortical Bone Thickness [mm]
CtTV	Cortical bone total volume [mm^3]
Dcomp	Cortical Bone Density [mg HA/cm^3]
EndoCtPm	Endocortical perimeter [mm]

Trabecular Bone Properties:

BV/TV Trabecular bone volume fraction defined as the ratio of trabecular Bone Volume: Total Volume [%]

Dtrab Trabecular Bone Density [mg HA/cm^3]

Inn Trabecular bone density calculated as the inner 60% of the trabecular area [mg HA/cm^3]

Meta Trabecular bone density calculated as the inner 40% of the trabecular area [mg HA/cm^3]

TrabArea Trabecular Area [mm^2]

TbN Trabecular Number [1/mm]

TbTh Trabecular Thickness [mm]

TbSp Trabecular Separation [mm]

TbSpSD Trabecular heterogeneity (i.e., inhomogeneity). Same as Tb1/NSD (*below*).

Tb1/NSD Standard deviation of 1/Tb.N representing the inhomogeneity of the trabecular network (i.e., trabecular heterogeneity and trabecular inhomogeneity. Same as TbSpSD (*above*)).

DEFINING EQUATIONS

Bone Mineral Content (BMC):

$$BMC = vBMD \; x \; Volume$$

Cortical Porosity (CtPo)[5]:

$$CtPo = \frac{Cortical\ Pore\ Volume}{\sum(Pore\ Volume + Bone\ Volume)}$$

E-BMD[6]:

$E = b\ (\rho/\rho_o)^p$

Where:

b - Constant (15004)s[7]

ρ_o - Reference density assuming fully mineralized bone (1200 mg HA/cm^3)

ρ - Imaged based density per voxel

p - Constant (1.7)[7]

LOA[8]:

$$95\%\ LOA = \bar{d} \pm (1.96 \; x \; SD_{meas})$$

Where:

$\bar{d}$ - Average measurement bias

SD_{meas} - Standard deviation of the differences between the two measurements

Least Significant Change (LSC)[9,10]:

$$LSC = 2.77 \; x \; CV\%_{RMS}$$

Monitoring Time Interval (MTI)[9]:

$$MTI = \frac{LSC}{Median\ Annual\ Percent\ Change}$$

Poisson's Ratio (ν)[11]:

$$Poisson's Ratio = \frac{Transverse\ Strain}{Longitudinal\ (Axial)\ Strain}$$

Precision Error (defined as: root-mean-squared percent coefficient of variation, $CV\%_{RMS}$)[12]:

$$CV\%_{RMS} = \sqrt{\sum_{j=1}^{m} \frac{CV\%_j^2}{m}}$$

Where:

$$CV\% = \left(\frac{\sum_{j=1}^{m} \frac{SD}{\bar{x}_j}}{m} \right) x\ 100\%$$

SD - Standard deviation between the two measurements
x_j - Mean of the two measurements
m - Number of participants in the analysis

Stress (σ)[11]:

$$Stress = \frac{Force}{Area}$$

Strain (ε)[11]:

$$Strain = \frac{Change in\ Length}{Original\ Length}$$

Tissue Stiffness (E)[11]:

$$E = \frac{Stress}{Strain} = \frac{\sigma}{\varepsilon}$$

Trabecular Number (TbN)[13,14]:

$$TbN = \left(\frac{1}{p}\sum_{j=1}^{i=p} DT(MAT(Image))_j\right)^{-1}$$

Where:

MAT - Mid-axis transformation between trabecular bone ridges (*sphere*)
DT - Distance transform between trabecular bone ridges (*sphere diameter*)
p - Distances between the ridges, expressed as an average over all inter-ridge voxels

Trabecular Thickness (TbTh)[13,14]:

$$TbTh = \frac{\left(\frac{BV}{TV}\right)}{TbN}$$

Where:

BV/TV - Bone volume fraction
TbN - Trabecular number

Trabecular Separation (TbSp)[13,14]:

$$TbSp = \frac{\left(1 - \frac{BV}{TV}\right)}{TbN}$$

Where:

BV/TV - Bone volume fraction
TbN - Trabecular number

Trabecular Heterogeneity (TbSpSD)[13,14]:

$$TbSpSD = \frac{SD\left(\frac{Meta}{Inn}\right)}{TbN}$$

Where:

Meta - Trabecular density in the meta region (inner 60% of the trabecular region)
Inn - Trabecular density in the inner region (inner 40% of the trabecular region)
TbN - Trabecular number

Trabecular Heterogeneity (Tb1/NSD)[13,14]:

$$TbSpSD = \frac{SD\left(\frac{Meta}{Inn}\right)}{TbN}$$

Where:

Meta - Trabecular density in the meta region (inner 60% of the trabecular region)

Inn - Trabecular density in the inner region (inner 40% of the trabecular region)

TbN - Trabecular number

LIST OF APPENDICES

1 INTRODUCTION

1.1 Overview

Osteoporosis is a chronic disease characterized by the loss of bone mass and the deterioration of bone micro-architecture which results in an increase in fracture risk[15]. Osteoporosis is colloquially referred to as the "silent disease" or the "silent thief" because bone loss occurs gradually over many years and presents no obvious signs or symptoms until fracture occurs[16,17]. Osteoporosis and related fractures occur at multiple skeletal sites; the most common fracture site, however, is at the distal forearm and wrist[18].

Bone strength is the ability to resist fracture when the bone is subjected to an applied load. Bone mineral content (BMC, or bone mass) and areal bone mineral density (aBMD) are important factors for bone stiffness[19,20], and are clinically monitored to estimate bone strength as well as diagnose osteoporosis[21]. However, the exclusive use of these measures does not predict osteoporotic fracture risk[19,20,22], as evidenced by more than half of the women who suffer an osteoporotic fracture being diagnosed with osteopenia, not osteoporosis[21,23,24]. This indicates that other factors influence bone strength independent of bone mass and density, such as: bone size/geometry and micro-architecture[25,26], bone material properties[20,26,27], as well as other risk factors such as: age, sex, medication, and falls[28]. To date, much of our understanding of bone micro-architecture and strength in the elderly has come from cadaveric specimens and cross-sectional evidence[29-35], making it impossible to determine how bone micro-architecture and strength change over time. Further, dual-energy x-ray absorptiometry (DXA)—the currently used clinical tool for monitoring bone strength and diagnosing osteoporosis—is neither capable of measuring bone micro-architecture[36] nor can it predict fractures on an individual basis[37].

There is a need for a clinical tool to non-invasively assess and monitor age-related changes in bone micro-architecture and strength in living people (i.e., *in vivo*). Various studies have indicated that the micro-architecture of the outer cortical and inner trabecular bone tissues are important for bone strength (determined by finite element (FE) modeling), and that these tissues are compromised in fracture cases compared to non-fracture controls[29,38-44]. However, there is a lack of prospective information pertaining to how the micro-architecture of these tissues change with age and how this affects bone strength. In order to separately measure cortical and trabecular bone micro-architecture, 3-dimensional (3D) imaging tools with high resolution are required. High resolution peripheral quantitative computed tomography (HR-pQCT) is an x-ray based 3-dimensional (3D) imaging modality that provides high resolution (82 µm, isotropic) for *in vivo* measures of bone density, geometry, and micro-architecture at the periphery of the human skeleton (distal radius and distal tibia)[13,45].

Beyond density, geometry and micro-architectural outcomes, HR-pQCT can provide estimates of bone strength through the use of FE modeling. FE modeling is an engineering-based computational technique that simulates mechanical testing to failure and evaluates how the structure behaves when subjected to the loads[11]. Direct mechanical testing of bone to failure is the gold standard to determine bone strength; however, the destructive nature of this technique renders it unacceptable for use *in vivo*. Therefore, FE modeling is the best known tool to non-invasively estimate bone strength *in vivo*. The use of the integrated FE modeling with HR-pQCT images could help explain the role of bone micro-architecture in determining bone strength and define how these outcomes change with age.

There is presently a lack of information for monitoring micro-architecture and strength in elderly individuals. High precision (low precision error) is essential to reliably monitor small

bone changes over time, changes due to drug therapy or intervention, and to compare minute differences between groups of people[9,12]. Precision information can be used to plan prospective and longitudinal studies and facilitate the interpretation of the longitudinal results[9,12]. Once precision is estimated it can be used in conjunction with a selected level of statistical confidence to determine the least significant change (LSC) and the monitoring time interval (MTI)[9]. The MTI is important in order to determine the length of time required between measures to have skeletal change. Further, the LSC will help establish whether skeletal change was captured beyond the precision error of the scanner[12]. To date, there is no evidence-based MTIs available for HR-pQCT and the reported LSC relies on long term measures of precision estimates[46], which incorporates both precision error and skeletal change and should be interpreted with caution[12].

The overall goal of this thesis was to investigate HR-pQCT precision for all outcomes, establish the least significant change (LSC) and monitoring time interval (MTI) as tools to determine if true change in bone outcomes has occurred, and use prospective data to characterize changes in bone density, geometry, and micro-architecture in postmenopausal women using HR-pQCT.

1.2 Anatomy and Physiology of Long Bones

Generally, the adult human has 206 bones of various shapes and sizes in the axial and appendicular skeleton[47]. There are 5 categories for bone shapes: long bones (e.g., radius, tibia), short bones (e.g., carpals), flat bones (e.g., mandible), irregular bones (e.g., vertebrae), and sesamoid bones (e.g., pisiform)[47]. Of particular interest to this dissertation are the long bones of the appendicular skeleton—particularly the radius and tibia.

1.2.1 Long Bone Anatomy

1.2.1.1 Gross Anatomy

Long bones are divided into 3 regions: epiphysis, metaphysis, and diaphysis[47]. The epiphyses are situated at the distal and proximal regions of all long bones and form the subchondral bony regions of joints[47] (Figure 1.1). Each epiphysis transitions into a flute-shaped metaphyseal region (or metaphysis; Figure 1.1)[47]—the location of osteoporosis-related fractures of the distal forearm and wrist[18,48]. The epiphysis and metaphysis originate from two independent ossification centers and are consequently separated by a developmental zone called the growth plate—which fuses during late adolescence and early adulthood[47]. The middle division of long bones is a pipe-like region called the diaphysis[47] (Figure 1.1). The metaphyseal and epiphyseal regions are primarily comprised of trabecular (or cancellous, spongy) bone, surrounded by a thin layer of cortical (or dense, compact) bone—called the thin cortical shell. The diaphysis, however, is typically made of thick cortical bone.

Macroscopically, cortical bone appears to be a solid tissue (hence it is synonymously termed dense or compact bone), comprising approximately 80% of the skeleton[47,49,50] (Figures 1.1-1.3). Younger individuals and males have been shown to have thicker cortices at all sites and cortical thickness has been reported to decline with age and disease status (e.g., osteoporosis)[29]. For instance, the cortex at the distal radius metaphysis of young adult women (mean age: 34 years) has been reported to be approximately 1.0 mm thick, while in postmenopausal women (mean age: 69 years) cortical thickness was reported to be as thin as 0.5 mm[29] (Figure 1.2). This age-related decrease in cortical thickness has been attributed to increased voids within the cortex (cortical pores), particularly along the cortical-trabecular junction—called the endocortex[51,52] (Figures 1.1 and Figure 1.2). The diaphyseal regions of long bones do not escape this age-related decline in cortical thickness. At the 30% site of the radial shaft, cortical thickness has been

shown to be 3.5 mm in young adults (mean age: 28 years)[53], and 1.9 mm in aged radii (mean age: 78 years)[54] (Figure 1.7). Just as cortical thickness varies along the longitudinal axis of the bone, research has also illustrated that the thickness of the cortex is not uniform around the bone cross-section. For instance, the cortices of the distal radius and tibia tend to be thicker on the anterior and posterior surfaces, although thinner on the medial and lateral surfaces at distal bone sites[55].

Trabecular bone is noticeably different from cortical bone—macroscopically spongy in appearance. In trabecular bone, there are large spaces between the bony lattice-like network of horizontally and vertically oriented plates and rods that comprise approximately 20% of the skeleton[47,50] (Figure 1.1 and Figure 1.2). Trabecular bone is found primarily at long bone epiphyses and metaphyses, as well as within vertebral bodies[47,50] (Figure 1.1 and Figure 1.2). Spaces within the trabeculae (trabecular pores) are filled with bone marrow, which is continuous with the medullary cavity of long bone diaphyses[56]. The thickness of the trabeculae (i.e., plates and rods) have been reported to be, on average, 50-150 μm thick in young adults (age range: 20-35 years)[57,58] (Figure 1.2). In postmenopausal women with osteoporosis, however, trabeculae can be as thin as 20 μm[32] (Figure 1.2). With increased age, cross-sectional cadaveric research suggests that trabecular erosion occurs, which explains the thinning trabeculae[59] (Figure 1.2 and Figure 1.6). Further, trabecular erosion can progress into the perforation of plates and rods resulting in a loss in trabecular number[59] (Figure 1.2 and Figure 1.6).

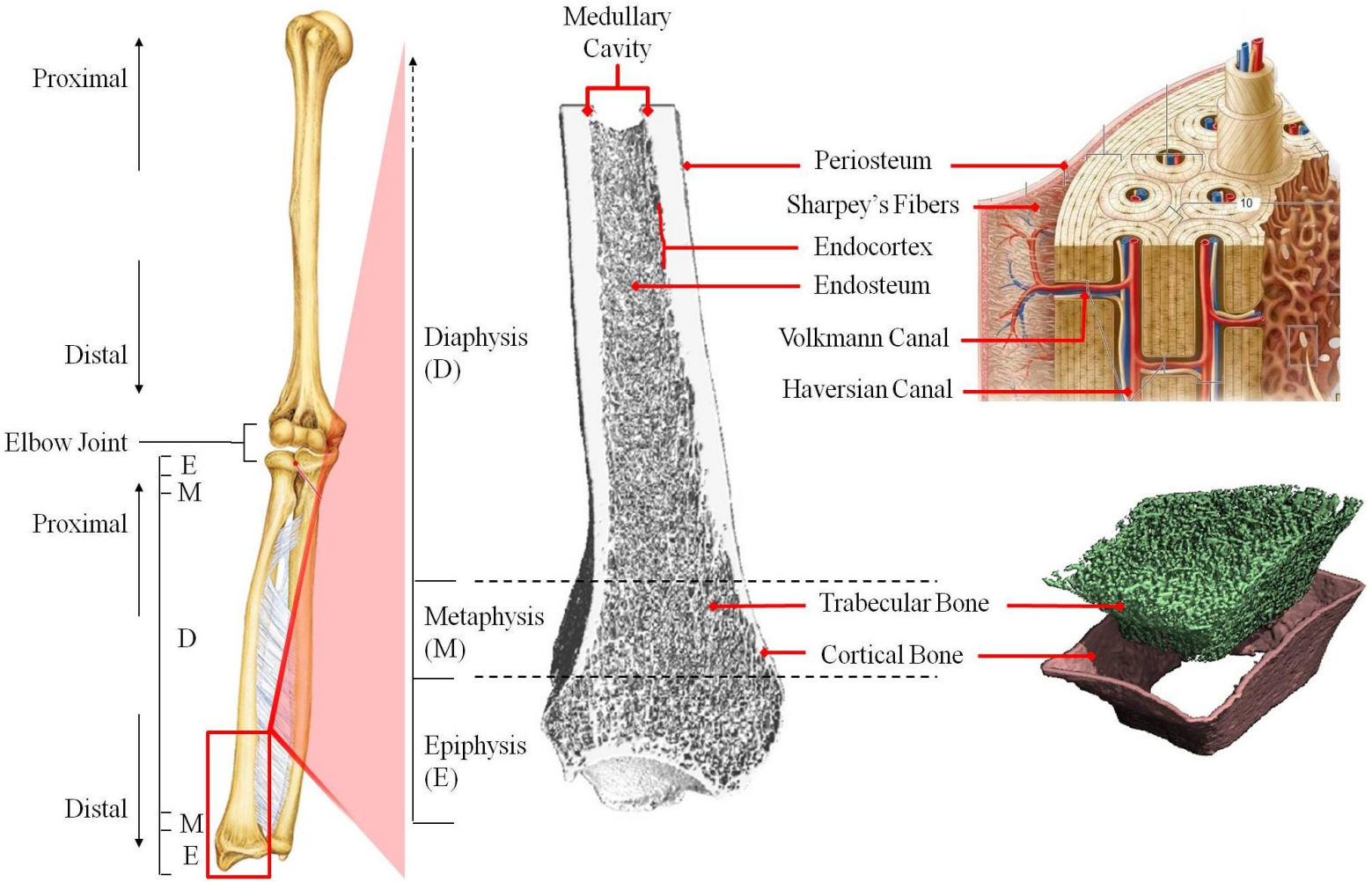

Figure 1.1. Anatomy of long bones. *Left*: Distal and proximal bone locations illustrating the 3 regional divisions: epiphysis (E), metaphysis (M), and diaphysis (D). *Middle:* Enlarged distal radius highlighting the 2 bone tissues and 3 bone surfaces: outer periosteum, inner endosteum, and cortical-trabecular divisional endocortex. *Far Right, Top:* Enlarged cortical region illustrating the outer periosteum (with anchoring Sharpey's fibers), cortical bone osteons (with neurovascular supply), longitudinal Haversian canals and transverse Volkmann canals. *Far Right, Bottom:* Exploded section of the distal radius metaphysis showing the outer, cortical (pink) and inner, trabecular (green) bone tissues. [*Modified from: Martini et al (2012)*[47], *Mueller et al (2009). Bone*[33]].

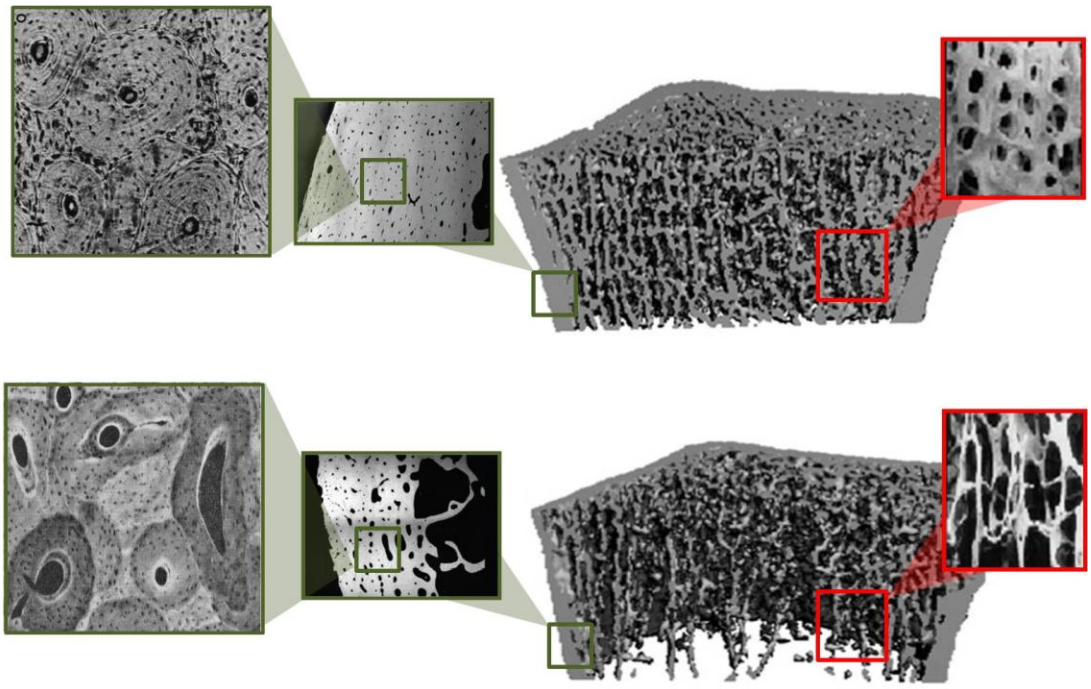

Figure 1.2. Cortical and trabecular micro-architecture. *Top:* Section through a young distal radius. Illustrating dense cortical (green) and trabecular (red) bone mass. Trabeculae are numerous and thick (right insert), while cortical pores are small and evenly distributed through the cortex (left inserts). *Bottom:* Section through an osteoporotic distal radius, illustrating low cortical (green) and trabecular (red) bone mass. Trabecular micro-architecture have thin plates and rods with large separations (right insert), while cortical pores are large and irregularly shaped (left inserts). [*Modified from: Zebaze et al (2010). Lancet*[51] *and Guesens et al (2014). Nature Reviews: Rheumatology*[60]].

1.2.1.2 Bone Histology

At the tissue level, bone exists in two distinct forms: woven bone and lamellar bone[56]. Woven bone is disorganized bone found in fetus' and in the callus produced during the reparation of injury or fracture[56,61]. Lamellar bone replaces woven bone and is organized in concentric rings of tissue called lamellae[56,62]. Lamellar bone can be further divided into primary and secondary bone. Secondary lamellar bone is developed through a process called remodeling—formed by the replacement of existing primary bone[63]. Of interest to this thesis is the mature secondary lamellar bone which can be subdivided into cortical and trabecular (cancellous) tissues.

Cortical bone consists of numerous densely arranged osteons (~280 μm) (Figures 1.1-1.3). Cancellous bone, however, does not contain true osteons—instead they consists of trabeculae, which are concentric lamellae arranged into plates and rods (Figures 1.3) and hemi-osteons[64]. At the center of every osteon is a longitudinally oriented central or Haversian canal—characteristic of the Haversian system or secondary osteon—that distributes neurovascular structures throughout the cortex[50,56,65] (Figure 1.1 and Figure 1.3). The neurovascular supply is also distributed throughout the cortex via transversely oriented Volkmann canals[65] (Figure 1.1 and Figure 1.3). Radiating outward from the central Haversian canal of every osteon are numerous concentric lamellar rings[50,56]. The lamellar rings are perforated with small holes called lacunae[47,49,50] (Figure 1.3). Within the lacunae there may be active osteocytes (mature bone cells; see next section on *Bone Physiology*). Interconnecting each lacuna are tiny channels called canaliculi which allow for cellular communication between osteocytes within the bone and to bone lining cells which line the periosteum and endosteum[49] (Figure 1.3).

Cortical and trabecular tissues are not naked—their surfaces are enveloped in protective and cytogenic membranes. All bones have 3 bone surfaces: outer periosteum, inner endosteum, and a distal cortical-trabecular divisional endocortex (Figure 1.1)—in the shaft of long bones, the endocortex and endosteum can be used synonymously. The outer surface of bone is encased in a double layered membrane called the periosteum[47,49] (Figure 1.1 and Figure 1.3). The outer layer of the periosteum is a fibrous layer composed of dense connective tissue, which contains blood vessels (to nourish the bone) and nerve endings (sp. nocioceptors)[47]. The outer fibrous layer of the periosteum is anchored to the bone by collagenous fibers (called Sharpey's fibers) that penetrate into the cortex and provide support for musculotendinous insertions[47,49] (Figure 1.1 and 1.3). The inner layer of the periosteum, however, is an osteogenic cellular layer that contains

chondroblastic and osteoblastic progenitor cells[47,50]. Immediately beneath the periosteum and inside the endocortex are the outer and inner circumferential lamellae, respectively—parallel lamellar rings that follow the perimeter of long bones—developed from these osteogenic cellular membranes of the inner periosteum and the endosteum[47] (Figure 1.3).

Distally dividing the cortical and trabecular bone tissues is the endocortical surface (endocortex) (Figure 1.1). The endocortex is a transitional zone having intermediate geometrical and topological attributes between the cortex and trabecular tissues[66]. Identifying the endocortex from trabecular bone is challenging, especially when the cortex has large, irregularly shaped pores and is highly trabecularized.

The inner surface of long bone is lined by a thin, membranous sheath called the endosteum[47,50] (Figure 1.1). The endosteum is in direct contact with the medullary cavity and bone marrow[47], and the membrane is lined with bone lining cells[50,56]. The endosteum and the bone marrow are primarily supplied with blood from the vessels traversing the nutrient foramina[50] (Figure 1.1). While we have a distinct description of the endosteum, it is difficult to differentiate trabeculae from the bone marrow at distal bone regions.

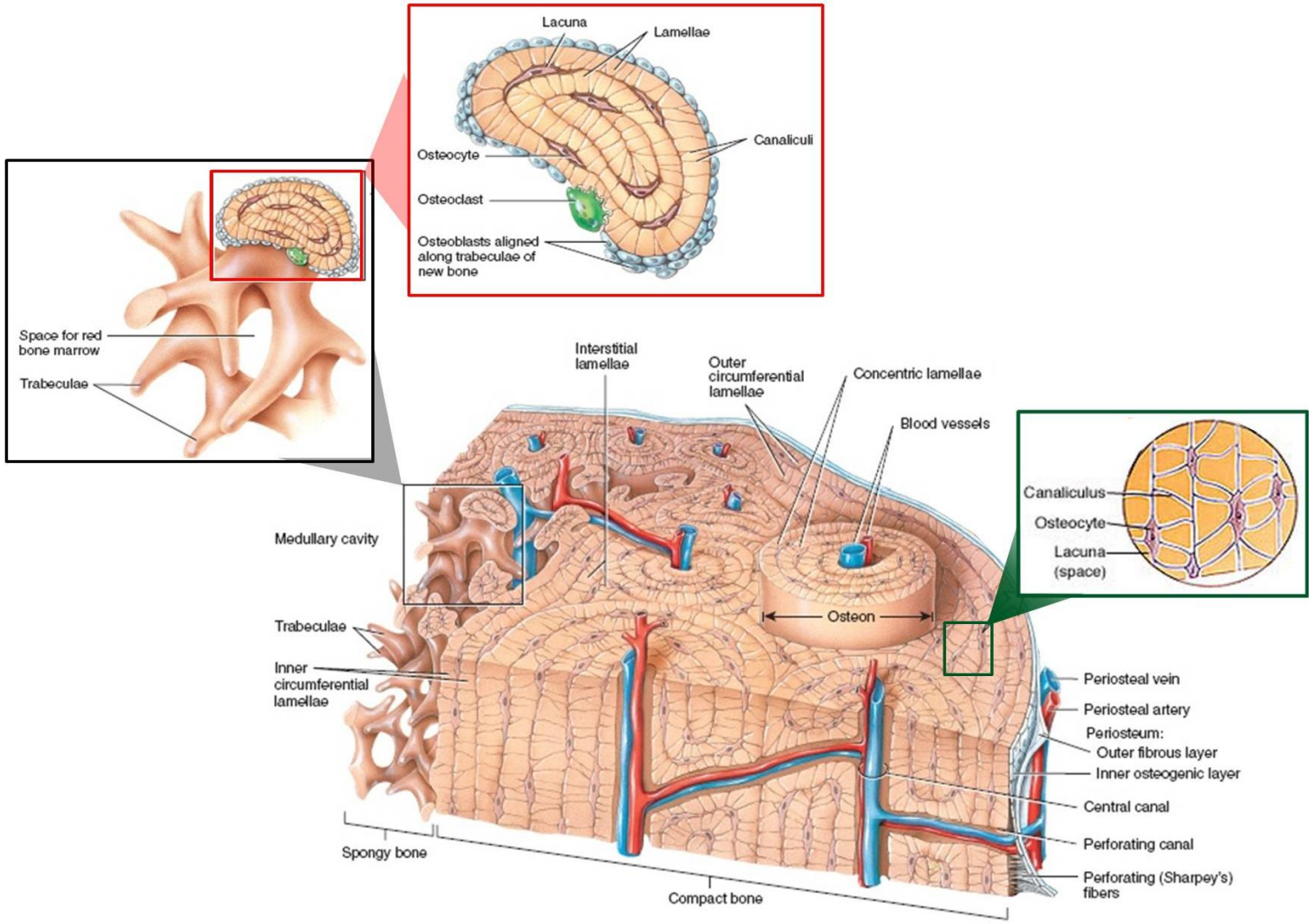

Figure 1.3. Cortical and trabecular bone histology. *Central:* Illustration of the outer periosteum, middle cortical and inner trabecular bone tissues. Bone tissues have numerous osteons with concentric lamellar rings (Haversian system). Within the Haversian system are lacunae filled with an osteocyte and outwardly directed canaliculi (illustrated in right (cortical) and left (trabecular) insets). *Left:* Illustration of concentric lamellae comprising trabecular plates and rods. [*Modified from: http://higheredbcs.wiley.com, retrieved 01-MAY-2015*]

1.2.2 Material Properties of Bone Strength

In order for human long bones to function properly they must be strong, stiff and yet flexible (tough)—able to resist deformation and fracture (to make locomotion possible) and yet able to bend (in order to absorb energy associated with loading and movement)[67]. Accomplishing these contradictory roles is a function of bone's size, structure, and material properties. Bone material properties include: mineral composition (mainly inorganic hydroxyapatite (HA), $Ca_{10}(PO_4)_6(OH)_2$), type I collagen and water (organic), as well as the number, size, and location of any (micro)damage[26,56,68-70].

Bone strength and bone stiffness are often used synonymously as being the amount of force or stress[1] that can be applied to the bone, resulting in fracture[67,68]. Bone stiffness is determined by the mineralization of the matrix[67]; specifically, the concentration of inorganic hydroxyapatite (HA) crystals saturated within the collagen matrix[26]. Stiffness is defined as the mechanical behavior of the bone *structure*[11,62]. At the *tissue* level, stiffness is referred to as the modulus of elasticity (elastic modulus or Young's modulus)[11,62]. Mathematically, stiffness is the ratio of the stress (σ)[1] to strain (ε)[2] within the linear-elastic region of the loading phase (the slope of the linear region of the stress-strain curve)[11,62] (Figure 1.4). The mineralization of the bone matrix will increase bone stiffness and, theoretically, strength; however, it will also make the tissue brittle, reducing the energy to fracture[26,70] (Figure 1.4). Aged bone is more mineralized compared to young bone, resulting in an age-related decline in bone flexibility and a simultaneous increase in bone brittleness[70-72]; making bone easier to fracture[62].

Bone flexibility (ductility or toughness) is a function of the collagen component of bone and defines the required energy to cause a fracture[26,73]. Mathematically, bone toughness is

[1] Stress (σ) is the force per unit area of the structure that the force is applied (i.e., Force [N]/Area [m^2])[10].
[2] Strain (ε) is the ratio of the change in length to the original length of the object ([original length - deformed length]/original length)[10].

determined by the area under the stress-strain curve[68] (Figure 1.4). A tough bone is one where strain increases faster than stress does[74]. Increasing levels of collagen (or decreasing levels of bone mineralization) will allow the bone to undergo more deformation; that is, the bone will absorb more strain energy prior to fracture (i.e., bone is less stiff or more flexible)[26,73] (Figure 1.4). While not contributing a significant proportion to bone stiffness in the linear-elastic region, the collagen matrix has been proposed to have a greater role in the post-yield properties of bone tissue (non-linear plastic region) by minimizing the accumulation of microdamage and inhibiting the growth of already initiated microcracks[26,70]. Type I collagen fibers comprise 85-90% of the protein in bone[56]; however, bone's collagen content decreases with age, consequently increasing the mineralization of the bone, which in turn facilitates microcrack initiation and accumulation, resulting in fracture with less plastic deformation[70,75,76].

Within the linear-elastic region of the stress-strain curve, load applied to bone will deform the bone allowing the bone to return to its original shape and size once the load is removed, according to Hooke's Law[11,62,67,68]. The collagen within the bone will facilitate this reversible deformation, allowing for the absorption of the loading energy (i.e., toughness)[67,68]. However, if the applied load exceeds the bone's ability to elastically deform (i.e., yield failure), the bone will undergo plastic deformation—permanently changing the shape of the bone (non-linear plastic region)[11,62,67,68] (Figure 1.4). The permanent change in the shape of bone is associated with the development of microdamage; the function of which is to allow for the release of energy and prevent fracture or ultimate failure[26,67]. However, if the applied load is enough to exceed both the linear-elastic and non-linear plastic regions, the bone will completely fracture (ultimate failure or failure load; Figure 1.4)[11,62,67,68].

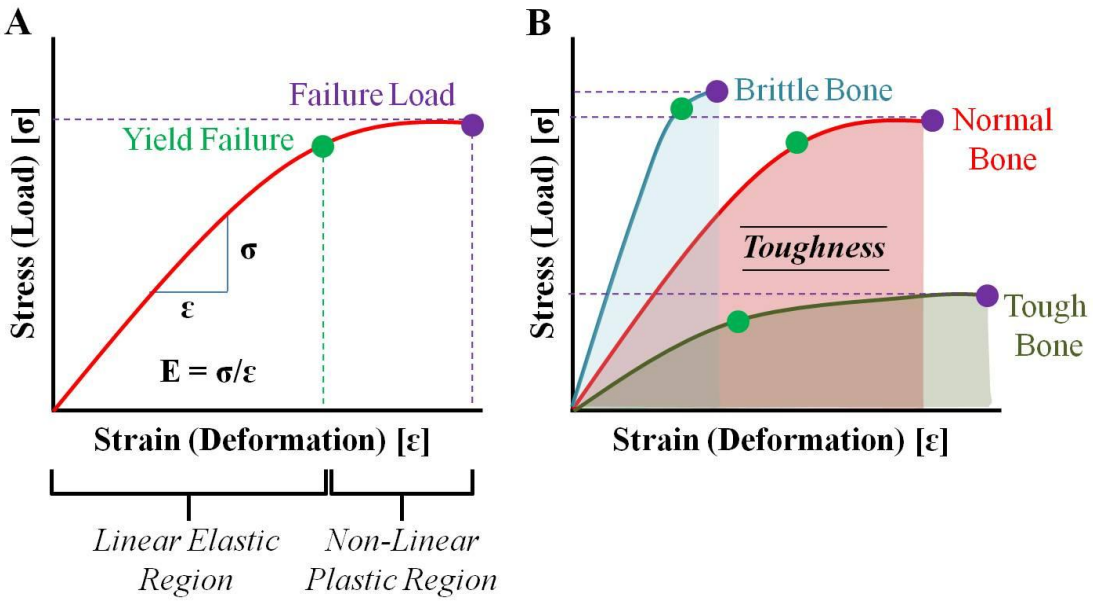

Figure 1.4. Graphical illustration of the stress-strain (tissue level) or load-deformation (structure level) curve. a) Slope of the line in the linear-elastic region indicates bone stiffness where loading does not permanently deform the bone. The non-linear plastic region follows yield failure (*green circle*), where the bone undergoes permanent deformation under load. Continued application of load exceeding plastic deformation results in fracture (failure load; *purple circle*). b) Graphical illustration of differences among brittle, normal, and tough bone. Bone toughness is defined as the area-under-the-curve. **Notice:** the non-linear plastic region (or post-yield strain) decreases as bone becomes more brittle, indicating that brittle bone absorbs less energy prior to fracture.

1.2.3 Forces and Osteoporotic Fracture

Forces acting on long bones come from all directions and the skeletal system must adapt to these loads in order to resist fracture. The composite nature of bone allows it to withstand compressive and tensile loads, as well as bending and torsion moments[62]—if the bone or region is adapted to these mechanical environments[74,77]. For instance, osteoporotic fragility fractures most commonly occur at the distal radius[18,48]. Fractures at long bone metaphyseal regions occur more readily than at the diaphyseal regions because the bone metaphyses are mainly adapted to compression about the longitudinal axis of the bone[74,77]. Long bone metaphyses adapt to compression because the adjacent joint (wrist) protects the metaphysis from large shearing, bending, and torsional loads[74,77]. This is unlike long bone (radius) diaphyses, which are

repeatedly loaded in, and thereby adapted to, compression, bending, and torsional loads from the muscles[74,77]. However, when a fall occurs, the combined bending, shearing, and torsional loads from impact are more likely to create a fracture in the metaphysis of the impacting limb because it is the region that is least adapted to these loading environments[74,77].

1.2.4 Bone Physiology

The word "skeleton" comes from the Greek word "skeletos" which means "dried up" suggesting that bone is an inanimate object[78]; however, the skeleton is anatomically complex as well as physiologically dynamic. Being a dynamic tissue, bone continually adapts to its internal and external environment in order to produce a structure that is capable of supporting the functional needs of the body—processes known as modeling and remodeling[47,79-81]. There are 3 cells within the basic multi-cellular unit (BMU) that are imperative in orchestrating the remodeling process: osteoblasts (mononucleate bone forming cells), osteoclasts (multinucleate bone resorbing cells), and osteocytes (mature bone cells responsible for intercellular communication and mechanosensation)[81,82] (Figure 1.5).

1.2.4.1 Bone Modeling

Bone's ability to maintain its shape and adapt its geometry and material properties to meet mechanical demands is a function of modeling and is indicative of the strong influence that applied external forces have on bone[79-81]. Bone modeling is a process where bone formation is not preceded by bone resorption and bone shifts its position in space[47,49,83,84]. Bone modeling occurs during development of the skeleton as well as in adult life; however, in adulthood modeling occurs less frequently[49]. During this process, the BMU will respond to mechanical loading by adding material to the periosteal surface (periosteum) and resorbing material from the endosteal surface (endosteum); thereby increasing the medullary cavity, maintaining cortical

thickness, and increasing bone's resistance to bending[59,79-81,85]. Overall, once the ground matrix is laid down, bone forming cells begin the mineralization process. The matrix becomes mineralized through the deposition of HA crystals.

1.2.4.2 Bone Remodeling

Bone remodeling is a phenomenon that involves the removal of bone followed by the deposition of new bone (i.e., bone reconstruction)[84]. This phenomenon occurs in 5 phases: activation, resorption, reversal, formation, and resting[49,82]. The first phase of remodeling involves the activation of the BMU. This signal can take several forms varying from direct mechanical strain to hormonal signals (e.g., parathyroid hormone, PTH)[49]. During the resorption phase, the osteoclasts remove bone using an acid secretion to dissolve the inorganic mineral and lysosomal enzymes to digest the organic matrix, thereby creating an erosion cavity in the bone[49] (Figure 1.5). This step takes approximately 2-4 weeks to complete[49,82]. The second step, reversal, is where the osteoclasts are finished resorbing the bone and undergo apoptosis (programmed cellular death). Following osteoclast apoptosis, osteoblasts begin synthesizing bone matrix to fill in the erosion cavity with new bone—the formation phase[49,82] (Figure 1.5). During the bone formation process, some osteoblasts are trapped in the ground matrix and become osteocytes, others differentiate into flattened bone lining cells that cover the bone surfaces[49]. The formation phase takes approximately 2-4 months to complete[49,82]. The final phase is a resting period that will continue until a new remodeling cycle begins (Figure 1.5). One remodeling cycle takes approximately 6 months to complete[49,65,82].

The 5 phases of remodeling are equivalent regardless of location, however, the phenotypic characteristics are tissue-dependent[82]. In trabecular bone, bone remodeling occurs directly on the bone surface creating saucer-shaped erosion cavities called Howship's lacunae or

hemi-osteons that are subsequently filled in[49,64,82] (Figure 1.5). In cortical bone, however, resorption proceeds headed by a cutting cone filled with osteoclasts that actively dissolve cortical bone matrix[65,86] (Figure 1.5). Immediately following the cutting cone is the closing cone which is filled with osteoblasts that are depositing bone matrix—thereby closing the resorption cavity and creating a new secondary osteon[65,86] (Figure 1.5).

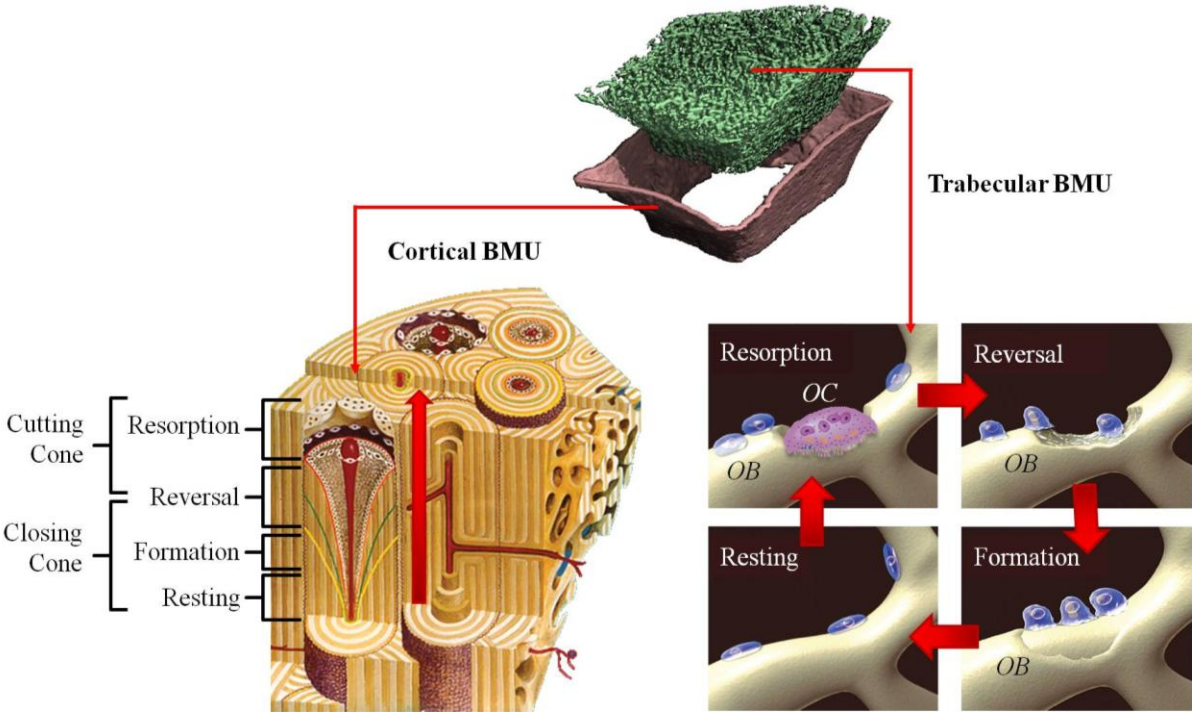

Figure 1.5. Illustration of the remodeling process. Note that the same process occurs differently in the cortical bone (left) and trabecular bone (right). *Left*: Cortical bone basic multi-cellular unit (BMU) showing the cutting cone through the bone's Haversian canal (red arrow indicates direction of cone movement). *Right*: Trabecular bone BMU showing the osteoclasts (OC; purple) and osteoblasts (OB; blue) resorbing and adding bone, respectively, to the trabecular surface. [*Modified from: www.Medscape.org, retrieved on 14-APR-2015*].

1.2.4.3 Bone Remodeling in Aging and Osteoporosis

Remodeling turns over internal bone and is required to replace dead or damaged bone tissue and gives bone the ability to adapt to different loading conditions and to respond to metabolic changes[56,86,87]. As described above, modeling facilitates changes of bone in space (i.e., periosteal and endosteal expansion increasing bone bending strength). At the completion of

growth, however, periosteal apposition slows and bone damage will be removed without a change in bone's volume (i.e., maintenance)—that is, the coupling of the cells in the BMU are in balance[68,81]. However, when the activities of these cells are out of balance, skeletal pathologies result. For instance, around midlife women enter menopause[3] where estrogen levels drastically drop, increasing osteoclast activity[88,89]. *Ex vivo* research suggests that the increased osteoclast activity (beyond osteoblast activity) leads to reduced bone mass, deteriorated micro-architecture, and compromised structural integrity; over time resulting in osteoporosis and, when a fall happens, fractures occur[68,81].

The rate of BMU remodeling within the cortical and trabecular tissues depends, in part, on the exposed surface area. Traditionally it was believed that trabecular bone has a higher surface area facilitating higher BMU activity[51]. According to cross-sectional and cadaveric research, the increased osteoclast activity associated with old age will compromise trabecular micro-architecture through the thinning and loss of trabeculae leading to fractures in bone containing large amounts of trabeculae (i.e., distal ends of long bones and vertebrae)[51] (Figure 1.2 and Figure 1.6). Mechanically, bone is 2-5 times weaker when the trabecular number is reduced compared to when the trabeculae are thinned; this is because the trabecular plates and rods are present, yet thinned, and able to continue supporting the cortex during loading[59,67,68,90] (Figure 1.6). Cortical bone, however, has many Haversian and Volkmann canals, the lining of which provides a surface for BMU activity[51]. Considering cortical bone comprises the majority of the skeleton (i.e., ~80%), it has a larger absolute surface area for bone remodeling compared to trabecular bone (Figure 1.2 and Figure 1.7). With age, BMUs acting on the cortical surface have been suggested to increased cortical porosity—a process commonly referred to as cortical

[3] Menopause is a natural event for women around age 50 years and is defined as a 12 month period where women no longer have a menstrual period and marks the end of ovulation and reproductive capability[85].

trabecularization[51,52,91]. According to cadaveric research, higher cortical porosity is associated with decreased bone strength and toughness[59,67] (Figure 1.7). These age-related changes to the bone remodeling process manifest in the deterioration of cortical and trabecular micro-architecture leading to reduced bone strength with age (Figure 1.2, Figure 1.6 and Figure 1.7). These manifestations in the micro-architecture were captured using cross-sectional and cadaveric data. Prospectively monitoring natural postmenopausal changes in bone micro-architecture are needed in order to understand how bone strength changes with age and optimize fracture prevention techniques.

The factors underpinning bone strength are not completely understood and therefore fracture prediction and prevention is not fully achieved. As a result, current therapeutic techniques rely on the use of medication to slow the deterioration of bone micro-architecture elicited by the BMU. For instance, bisphosphonates have been reported as the most widely used treatment for osteoporosis and prevention of osteoporotic fracture by reducing osteoclast activity and minimizing bone remodeling[92]. Because estrogen deficiency plays an important role in the development of osteoporosis, another common therapy used in osteoporosis treatment and fracture prevention is hormone replacement therapy[89,92]. Both therapies have been reported to maintain or increase bone mineral density and reduce fracture risk with short term use[92,93]. However, there is limited information pertaining to how these therapies effect bone micro-architecture. Research indicates that bisphosphonates are beneficial for preserving trabecular micro-architecture *in vivo*[93,94]; however, there is a lack of *in vivo* evidence characterizing the effects of hormone replacement therapy (i.e., estrogen) on micro-architectural changes in cortical and trabecular bone tissues.

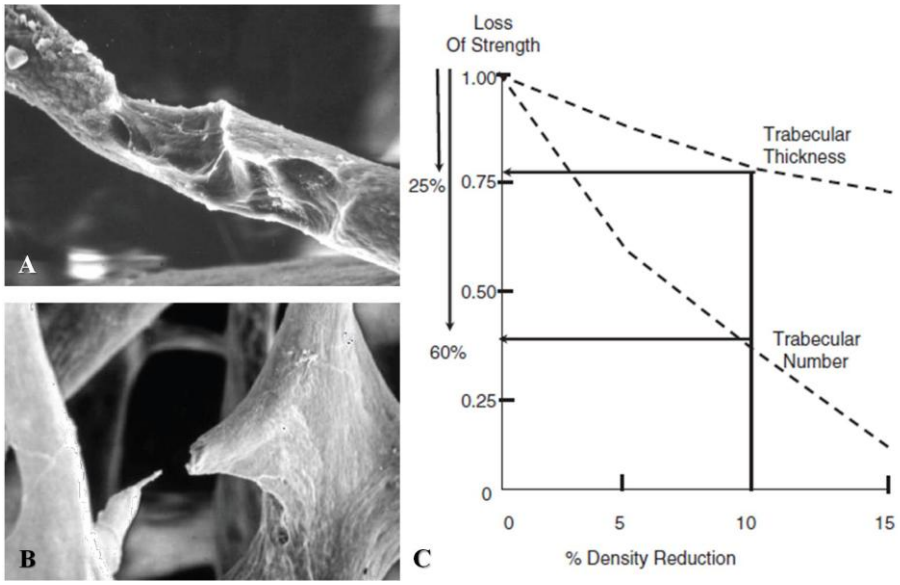

Figure 1.6. Images from scanning electron microscopy illustrating trabecular bone a) thinning and b) perforation (leading to loss in trabecular number). The graph at the right c) illustrates the reduction in bone strength as a function of loss in trabecular thickness (25% reduction in strength) and trabecular number (60% reduction in strength). [*Modified from Seeman (2013). J Gerontol A Biol Med Sci.*[59]*; Seeman (2008). JBMR*[67]].

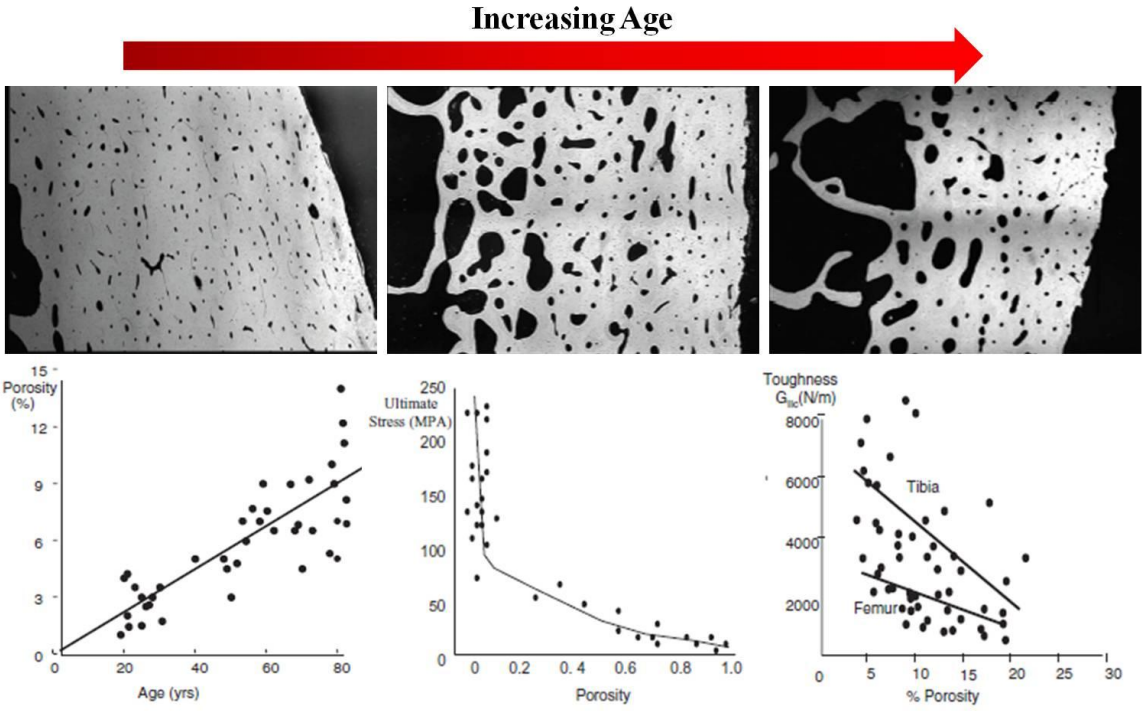

Figure 1.7. *Top:* Histomorphometric images of cortical bone sections from cadaveric bone shafts illustrating increased cortical porosity with age (age increases to the right). *Bottom Left:* Graph illustrating cortical porosity increases with age. *Bottom Middle*: Graph illustrating that ultimate stress (and therefore bone strength) decreases as a function of increased cortical porosity. *Bottom Right*: Graph illustrating that bone toughness decreases with increase cortical porosity. [*Modified from Zebaze et al. (2010). The Lancet*[51]*; Seeman et al (2008).JBMR*[67]].

1.3 Osteoporosis and Related Fractures

1.3.1 Epidemiology and Impact

Osteoporosis and related fractures are global public health concerns that currently affect 200 million people worldwide[95] and are a major cause of mortality, morbidity, chronic pain, and loss of independence[96]. What is concerning is that the prevalence of osteoporosis and related fractures are projected to increase by approximately 50% by 2025, as a result of the aging population[97].

Osteoporosis and related fracture incidence are detrimental to the individual and the health care system[97]. For instance, Budhia and colleagues (2012)[98] reported that the medical costs, to the individual who sustained an osteoporotic fracture, ranged from 1.6 - 6.2 times higher than that of their non-fracture counterparts. Further, in 1995 the national health care costs related to osteoporotic fractures amounted to approximately $8.6 billion US[98]. In 2005, however, the medical cost of osteoporosis and related fractures had increased to between $13.7 - 20.3 billion US[97]. As a result of the aging population, it has been predicted that the prevalence of osteoporosis will increase from 10 million to more than 14 million people by 2020 in the United States alone, and will amount to more than $25.3 billion US in medical costs as a result of fragility fractures[97]. Therefore, further research into the factors underpinning bone strength is warranted in order to circumvent these projected figures from becoming a reality.

1.3.2 Disease Characteristics

Osteoporosis is a chronic and multifactorial bone disease typically diagnosed after the occurrence of a low-trauma fracture[21]. Morphologically, osteoporosis is characterized by the reduction of bone mass and the deterioration of cortical and trabecular bone micro-architecture[15] (Figure 1.2, Figure 1.6, Figure 1.7). Biomechanically, osteoporosis is identified

by altered bone mechanical properties—such as: brittle behaviour of bone, decreased bone toughness, low compressive fracture force[99,100] (Figure 1.4, Figure 1.6 and Figure 1.7). Clinically, osteoporosis is diagnosed from bone mineral mass (bone mineral content, BMC) per unit area—a measure called areal bone mineral density (aBMD)[101]. BMC and aBMD are important factors in bone strength as identified by small increases corresponding to large increase in bone tissue stiffness[19,20]. For instance, a 10% increase in adult aBMD at the femoral neck can reduce the risk of a hip fracture by 50%[22]. However, the use of BMC and aBMD do not predict osteoporotic related fractures on an individual basis[102,103]. Incorporating estimates of bone geometry and micro-architecture may better predict fractures on an individual basis[5,29,30,32,40,41,104-107].

1.3.3 Assessment Techniques

1.3.3.1 Dual-energy X-ray Absorptiometry (DXA)

Presently, dual-energy x-ray absorptiometry (DXA) is the clinically recommended tool for diagnosing osteoporosis[21]. DXA acquires a 2D projection of BMC (g) in a defined area (cm^2)[101]. Using DXA, osteoporosis has been *operationally* defined based on aBMD, where the average BMC of each pixel is divided by the projection area (g/cm^2)[21,101,108]. According to the World Health Organization (WHO), osteoporosis is *clinically* defined as an aBMD that lies 2.5 standard deviations or more below the average value for healthy 30 year old women (i.e., T-score of $\leq$-2.5 SD)[21]. DXA can perform measures on the whole body, however, aBMD measures at the femoral neck are used in the diagnosis of osteoporosis because they have been reported to be more strongly related to common osteoporotic fracture types[96,103].

While DXA is considered the clinical tool for diagnosing osteoporosis, it significantly under predicts osteoporotic fractures at an individual level[102,103]. For instance, 20-60% of

individuals that have sustained an osteoporotic related fragility fracture have been pronounced osteopenic by DXA (i.e., T-score between -1.0 and -2.4 SD), and not osteoporotic[21,23,24]. It is evident that these fractures are not completely related to aBMD, and that the loss of bone strength is more likely the result of deteriorated bone micro-architecture[25]. Kazakia and colleagues (2011)[25] reported that participants with identical DXA-derived aBMD at the distal radius had significant variations in their cortical and trabecular micro-architecture at the same site (Figure 1.8). Therefore, DXA's ability to measure areal bone properties and the inability to separately measure cortical and trabecular bone properties[37,101,108] prevents DXA from acquiring any information of bone geometry and micro-architecture—biomechanically important properties of bone strength that are independent of aBMD[5,29,30,32,40,41,104-107].

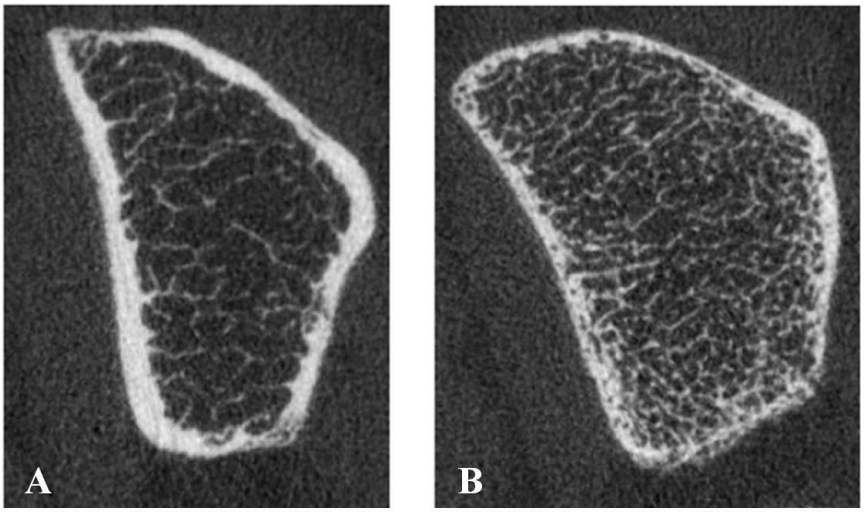

Figure 1.8. HR-pQCT (XtremeCT) scans of the distal radius illustrating identical DXA derived aBMD and T-score values however variations in selected micro-architectural and biomechanical indices. [*Modified from Kazakia et al (2011)*[25]].

		A	B
Ultra Distal Radius (UDR) aBMD	*(g/cm²)*	0.28	0.28
UDR T-Score	--	-1.7	-1.7
Cortical vBMD	*(mg HA/cm³)*	919	781
Trabecular vBMD	*(mg HA/cm³)*	60	151
Trabecular Number	*(1/N)*	0.86	1.80
Trabecular Separation	*(mm)*	0.683	0.196
Cortical Porosity	*(%)*	5	24
Cortical Load Fraction	*(%)*	67	34

1.3.3.2 Peripheral Quantitative Computed Tomography (pQCT)

Advances in bone research have shifted the focus of bone strength beyond 2D measures of bone mass (as measured by DXA) to measure 3D bone density (volumetric BMD, vBMD), geometry and micro-architecture[107,109]. Recent developments in imaging technology have yielded high-resolution peripheral quantitative computed tomography (HR-pQCT). HR-pQCT is a novel 3D imaging modality with an *in vivo* resolution of 82 µm, rendering this scanner capable of separately measuring cortical and trabecular bone vBMD, geometry, and bone micro-architecture *in vivo* in humans. Before the advent of HR-pQCT, measuring bone micro-architecture was accomplished by means of histomorphometry, either *ex vivo* or invasively *in vivo* using small bone biopsies of the iliac crest[39,110].

Beyond density, geometry and micro-architectural outcomes, HR-pQCT can provide estimates of bone strength through the application of an engineering-based computational technique known as finite element (FE) modeling or FE analysis. Using structural and material components of bone (i.e., geometry, micro-architecture, tissue stiffness, etc.), FE modeling will simulate mechanical testing to failure, provide metrics of tissue stiffness and bone strength (ultimate failure load), as well as estimates of internal stress and strain distribution. While direct mechanical testing of bone to failure is the gold standard to determine bone strength, the destructive nature of this technique renders it is unacceptable for use *in vivo*. Therefore, FE modeling is the best known tool to non-invasively estimate bone strength *in vivo*.

There are numerous studies available validating different linear and non-linear FE models with HR-pQCT on long bones[7,111-115]. Linear FE models define the stress-strain relationship within the elastic region of bone—that is, the region prior to yield failure[11]. Non-linear FE models, however, define the stress-strain relationship within the plastic region of bone[11]. Aged bone is brittle relative to the more compliant young bone resulting in limited or no plastic region

prior to ultimate failure[100] (Figure 1.4). Therefore, a linear model may be sufficient for estimating failure load in an elderly population (linear FE models association to compressive failure testing: R^2=0.66-0.95[7,111,112,116]).

Although HR-pQCT is an advanced *in vivo* technique for capturing 3D bone properties and strength estimates, it is limited to measuring the distal sites of the peripheral skeleton and is unable to measure the hip and vertebral column. However, the distal radius is an important site for scientific investigation because fragility fractures at the distal radius are a sentinel for future osteoporotic fracture at other sites[117,118]. Further, regarding density measures (the metric used to diagnose osteoporosis), research has reported that HR-pQCT derived density at the tibia are correlated with DXA-derived hip aBMD (r=0.51-0.70)[106]—another weight bearing skeletal site—suggesting that HR-pQCT may be a competent imaging modality for density-based osteoporosis assessments. Importantly, HR-pQCT derived outcomes have been reported to outperform DXA-derived outcomes in discerning postmenopausal women with and without a fracture[39,40,44] (Figure 1.9). These data suggest that HR-pQCT (combined with FE modeling) at the distal radius and tibia provide important insights into densitometric, geometric, and micro-architectural factors underpinning bone strength and may be a new method for monitoring skeletal changes in postmenopausal women—a population most in need of monitoring.

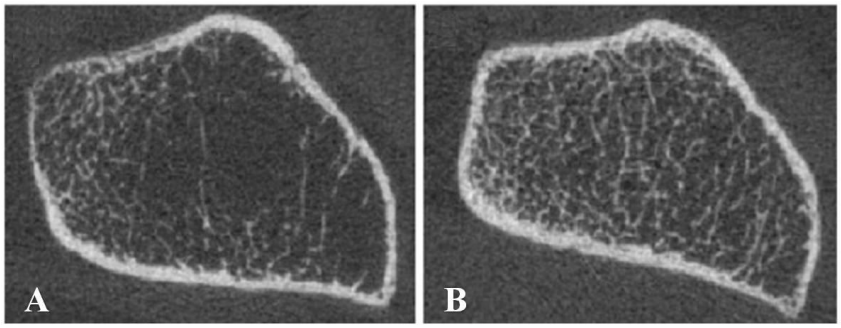

		A: Fracture	B: Control
UDR aBMD	*(g/cm²)*	0.32	0.36
Geometry			
Total Area	*(mm²)*	295.9	264.7
Cortical Area	*(mm²)*	55.0	58.9
Cortical Thickness	*(mm)*	0.84	0.99
Micro-architecture			
Cortical			
Cortical Porosity	*(%)*	11.5	10.2
Cortical Load Fraction	*(%)*	95	86
Trabecular			
BV/TV	(%)	7.8	12.7
Trabecular Number	*(1/N)*	1.24	1.83
Trabecular Separation	*(mm)*	0.840	0.492

Figure 1.9. HR-pQCT scans of the distal radius comparing participants with low-trauma forearm fracture to age-matched non-fracture controls regarding DXA-derived aBMD at the ultra distal radius (UDR) and selected HR-pQCT measures of bone geometry, micro-architecture, and biomechanical indices. [*Modified from Nishiyama et al (2012)*[40]].

1.3.4 Risk Factors for Osteoporosis and Related Fractures

It is well established that age and sex play a significant role in the development of osteoporosis. Specifically, the risk of developing osteoporosis increases with age[119,120] and women are more inclined to develop the disease relative to men[119,121]. Beyond age and sex, the development of osteoporosis is linked to genetics[119,122], inadequate peak bone mass accrued during puberty and young adulthood[119,121], poor lifestyle choices (physical inactivity, poor nutrition)[27,120], hormonal status (e.g., amenorrhea, use of certain birth contraceptives)[119,120], onset of menopause and resultant decline in estrogen[119,120], as well as long term use of certain medications (e.g., cortisone)[120,123]. Osteoporosis itself is a manageable disease, however, if not

diagnosed and/or treated properly the compounded influence of other age-related conditions (e.g., sarcopenia, peripheral neuropathy, etc.) can increase the risk of osteoporotic fragility fractures[120]. Fragility fractures are a detrimental outcome of osteoporosis that typically result from a fall[124].

It is well documented that falls are a problem for older adults and that the cause is multifactorial in nature[125]. Approximately 1-in-3 community dwelling individuals over the age of 65 years will succumb to at least one fall that results in physical injury (fracture, soft tissue damage, loss of physical function) and/or psychological damage (fear of falling, loss of independence)[126-130]. Forearm or wrist fractures are a common consequence of falls, especially in those individuals with low bone strength[131]. The most common scenario, and consequently the worst-case scenario, associated with osteoporotic fractures at the forearm or wrist is falling onto the hand of the outstretched forearm from low fall heights (e.g., standing height falls)[132,133]. Further, research has shown that previous fractures increase the risk for subsequent fractures at multiple skeletal sites[134-136]. Therefore, fall prevention is important to reduce fracture risk[28,137-141].

1.4 Evidence of Skeletal Change with Age

It is important to understand how bone mass, geometry and micro-architecture change with increasing age as this could elucidate new and important causative mechanisms, as well as preventative and/or treatment options for osteoporosis. The majority of information regarding bone mass and density changes with age come from DXA-based studies. It is generally accepted that aBMD declines at a rate of 1-2% per year (depending on site) around menopause[142,143].

Further, this accelerated rate of bone loss has been reported to continue for 5-10 years following menopause and gradually decline thereafter[144].

Despite the plethora of DXA research available, certain aspects of bone loss in postmenopausal women remain unclear. For instance, DXA does not capture aspects of geometry or micro-architecture and thereby offers limited information regarding bone strength estimates. Peripheral QCT evidence has indicated an annual 0.5-2% decline in cortical and trabecular bone vBMD at both radius and tibia[145-147]. However, there is still limited evidence regarding changes in bone geometry, micro-architecture, and strength with age. HR-pQCT has been used to describe these age-related changes using cross-sectional data. Yet, characterizing change from cross-sectional studies introduces error resulting from genetic and environmental differences (e.g., nutrition status, health related habits, socioeconomic status, etc.). Longitudinal studies are required to determine how bone geometry, micro-architecture and strength change with age and to minimize the effect of these confounding errors. Specifically, longitudinal research using HR-pQCT is necessary in order to establish how bone micro-architecture changes with age.

1.4.1 Cross-sectional HR-pQCT Research

1.4.1.1 Radius

Various cross-sectional studies regarding age-related differences in bone properties at the distal radius report similar cross-study findings among women aged 20 to 99 years of age[29,32,57]. Specifically, these cross-sectional studies suggest lower total (23-36%)[29,32], cortical (11-24%)[29,32,57], and trabecular (23%)[29] bone mineral densities from 20 to 99 years. Further, this research described lower trabecular bone volume fraction (23-27%)[29,32,57], which relates to lower trabecular number (13-21%)[29,32,57] and trabecular thickness (2-18%)[29,32,57], as well as the greater trabecular separation (27-34%)[29,32,57] (Figure 1.10). There is also an age-related difference in cortical thickness (29-52%)[29,32,57] in favor of young adults (Figure 1.10). Based on

these cross-sectional observations, it has been suggested that the thinning of the cortex is a result of elevated age-related cortical porosity (176%)[32]. This research also reports a 57% lower ultimate stress and a 46% lower age-related failure load from 20 to 99 years[32].

1.4.1.2 Tibia

At the tibia, cross-sectional studies suggested lower total (25-37%)[29,32], cortical (13-32%)[29,32], and trabecular (19%)[29] bone mineral densities from 20 to 99 years. Regarding trabecular micro-architecture, research indicated lower trabecular bone volume fraction (18-19%)[29,32], trabecular number (10-12%)[29,32], and trabecular thickness (6-8%)[29,32] in favor of young adults (Figure 1.10). Further, trabecular separation (16-21%) was lower among women aged 20 to 99 years[29,32] (Figure 1.10). There was also an age-related difference in cortical micro-architecture, specifically, lower cortical thickness (24-28%)[29,32] with an higher cortical porosity (259%)[32]. This research also indicates that there is a 49% lower ultimate stress and a 35% lower age-related failure load from 20 to 99 years[32].

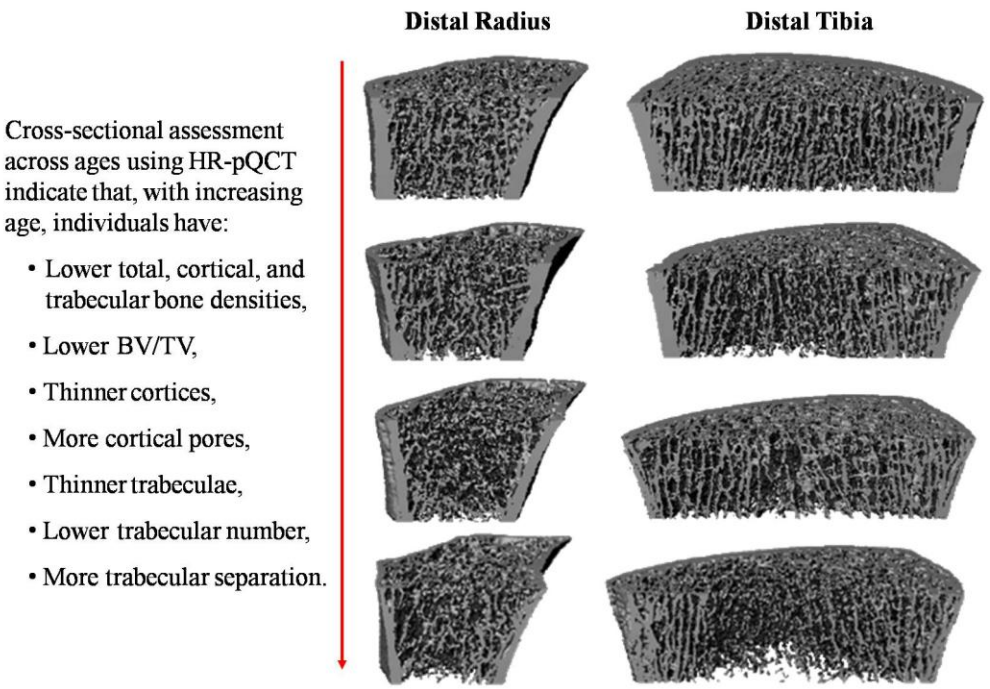

Figure 1.10. 3D reconstructed images from HR-pQCT illustrating age-related changes in bone density and micro-architecture at the distal radius (*left*) and tibia (*right*) based on cross-sectional research across age (21-82 years). [*Modified from Boutroy et al (2005)[29]*].

While this research provided unique information pertaining to the effect of the age-related changes on bone micro-architecture, it begs the question of whether these same differences would be seen if the same cohorts were followed longitudinally.

1.4.2 Longitudinal HR-pQCT Research

Prospectively following a group of people over time is the only way to capture true changes in bone. However, these studies are costly and have a yearly participant attrition rate which makes it difficult to acquire unbiased longitudinal data[148]. To date, there is only one prospective study using HR-pQCT to investigate micro-architectural changes in peri-menopausal women not related to intervention effects[14]. However, the authors described this research as being 'preliminary' as they measured 17 postmenopausal women (53±3 years) using a prototype HR-pQCT scanner with an isotropic resolution of 165 µm[14]. Laib and colleagues (1998)[14] measured these women at baseline, 6 months and again 1 year later. They report an average *annual decrease* in trabecular density (-3.4%), trabecular number (-1.2%), and cortical thickness (-2.0%); they also report an average *annual increase* in trabecular separation (+1.2%)[14]. Authors concluded that the number of participants included in the study was too small to accurately judge the sensitivity of the HR-pQCT to measure the structural indices of the trabecular bone tissue. Therefore, there is a need to determine whether the annual changes are similar using the standard HR-pQCT scanner (isotropic resolution: 82 µm) and with a larger sample of postmenopausal women—the population most in need of bone micro-architectural monitoring.

1.5 Monitoring Skeletal Change

1.5.1 Measurement Precision

In its most general definition, precision is the ability of a measurement to be consistently reproduced under the same conditions. Additionally, the amount that the repeated measurements change is the precision error. Generally, changes in skeletal tissue can be detected with non-invasive imaging techniques after 6 months—the average length of the bone remodeling cycle[82]. Therefore, precision (reproducibility) of an imaging technique is dependent on the time interval between repeated measurements, with short-term precision errors being generally smaller than long-term precision errors because true skeletal change can be expected to occur over longer periods of time (i.e., >6 months)[9,12]. Consequently, high precision (low precision error) is essential to reliably monitor small bone changes over time, changes due to drug therapy or intervention, and to compare minute differences between groups of people[9,12].

1.5.2 Precision Information in Research and Clinically

What is real, meaningful change? Is change a statistically significant difference between follow-up measurements, or is the measured difference a factor of the technique's measurement error? How do researchers and clinicians know if actual skeletal change has occurred and that this difference is beyond the (precision) error of the technique? For researchers and clinicians, it is important to know what magnitude of measured change is required to be sure the participant or patient has responded to intervention or treatment versus being non-responsive to either. Once precision is estimated it can be used in conjunction with a selected level of statistical confidence to determine the least significant change (LSC) and the monitoring time interval (MTI)—tools that will facilitate the answering of these questions.

1.5.2.1 Least Significant Change

The International Society for Clinical Densitometry (ISCD) recommends estimating the LSC to determine if true skeletal change has occurred beyond precision error[149]. The LSC is determined in relation to measurement precision errors and a statistical confidence value[9]. LSC provides a percentage outcome that can be used with baseline measures to determine the magnitude difference required to have change in follow-up measures. Currently, the only available LSC data for HR-pQCT estimate LSC values using long-term precision from postmenopausal women[46]. These results need to be interpreted with caution because long-term precision determined using follow-up data 1 year from baseline incorporate both precision error and non-linear skeletal changes into the precision estimate thereby obfuscating actual user precision and confounding the difference required between measures to have change[12,150].

1.5.2.2 Monitoring Time Interval

Using the ratio of LSC and the median annual percent change provides the MTI—an estimate of the time (in years) required between baseline and follow-up measures that is necessary to capture change[9,10,151]. The use of MTIs are important when planning or developing longitudinal or follow-up studies because their use will allow follow-up measures to be performed within the optimal window for capturing true skeletal change, as well as minimizing patient radiation exposure and costs associated with repeated scanning in prospective studies. To date, there are no MTIs available for HR-pQCT outcomes.

1.6 Summary

1. Osteoporosis and related fractures manifest in older age—especially after menopause in women. There is evidence that bone mass/density, geometry, and micro-architecture are important for bone strength. However, the exact skeletal measures underpinning bone

strength are currently unknown; therefore, it remains unclear what measures should be monitored with aging.

2. Menopause is associated with a rapid drop in estrogen. Cross-sectional evidence has indicated that low estrogen levels are associated with higher osteoclast activity, speeding the remodeling process, and exacerbating micro-architectural deterioration. Bisphosphonates and hormone replacement therapy (e.g., estrogen) have been shown to reduce remodeling and positively affect bone mass (BMC) and aBMD. Research indicates that bisphosphonates preserve trabecular micro-architecture, however, it remains unknown how hormone replacement therapy affects micro-architecture.

3. Research indicates that bone mass and density are important outcomes to prevent osteoporosis and related fracture; however, the majority of osteoporotic fractures occur in women diagnosed with osteopenia. This indicates that other factors beyond bone mass and density are responsible for bone strength and thereby fracture prevention. There is evidence that suggests bone geometry and micro-architecture are vital for bone strength, independent of bone mass and density. High-resolution imaging techniques are required in order to capture information regarding bone micro-architecture.

4. Cross-sectional *ex vivo* research indicates that bone becomes more mineralized and loses collagen content with age—resulting in bone that can withstand less strain prior to fracture and has little or no post-yield deformation before failure. Research also indicates that a linear-elastic model is accurate in predicting failure of this type of bone. However, the *in vivo* repeatability of these models remains unknown.

5. The effect of aging on cortical and trabecular micro-architecture in postmenopausal women is unclear. Cross-sectional evidence indicates that cortical and trabecular bone micro-architecture deteriorates with increasing age. There is need for longitudinal studies using non-invasive, high-resolution imaging tools to monitor bone micro-architecture in postmenopausal women to gain a better understanding of how bone changes with age.

6. Understanding how bone density, geometry, and micro-architecture change with age can improve osteoporosis prevention, diagnosis, and treatment options. However, it is unclear what time interval and what amount of difference between follow-up measures is required to actually capture skeletal change, beyond measurement error (precision)—particularly for bone micro-architecture.

7. Previous research suggests that the age-related increase in remodeling (especially after menopause) results in an overall loss of bone mass and deteriorated micro-architecture. It is unclear whether this deterioration would affect the precision for bone micro-architectural outcomes. Understanding the affect of menopause on micro-architectural precision is important when planning studies and interpreting information from studies interested in monitoring changes in micro-architectural outcomes in postmenopausal women.

1.7 Research Questions and Objectives

The overall goal of this thesis was to investigate precision for all HR-pQCT outcomes, establish the least significant change (LSC) and monitoring time interval (MTI), as well as characterize bone changes in density, geometry, and micro-architecture using HR-pQCT. In order to accomplish these goals I needed to determine precision of bone micro-architecture and strength

outcomes, estimate the LSC and the annual change of these outcomes. Using HR-pQCT images, in combination with FE modeling, I aimed to answer the following research questions:

1. What is the precision of HR-pQCT (standard) outcomes of density, geometry, and micro-architecture in postmenopausal women and young adults?
2. Can postmenopausal women and young adults be measured by HR-pQCT with comparable precision?
3. Does manual modification of the endocortical contour in the analysis of cortical bone micro-architecture affect precision or outcome values in postmenopausal women or young adults?
4. What is the precision of bone strength estimates derived from 3 commonly used HR-pQCT integrated FE models? Which of the 3 models is more precise?
5. What are the minimal differences in bone area, density, and micro-architecture between follow-up measures required in order to be 95% confident that change has occurred in postmenopausal women?
6. What is the minimum amount of time required between follow-up measures in order to be 95% confident that the minimal differences are attained in postmenopausal women?
7. How does bone micro-architecture change over one year in postmenopausal women?

To answer the questions posed in this study, our objectives were to:

1. To define and compare *in vivo* precision errors and outcomes for HR-pQCT derived:
    a) density, geometry, and micro-architecture in postmenopausal women and young adults.
    b) cortical bone micro-architecture in 2 groups (postmenopausal women and young adults) using 2 different cortical bone evaluation methods (automatically generated endocortical contours and manually modified endocortical contours).

c) estimates of bone strength from 3 FE models: i) single tissue model (STM), ii) dual tissue model (DTM), and iii) scaled model based on bone mineral density (E-BMD).

2. To define the LSC and MTIs for HR-pQCT-derived bone area, density, and micro-architecture in postmenopausal women.
3. To characterize annual changes in bone area, density, and micro-architecture at the distal radius and tibia using HR-pQCT in postmenopausal women.

1.8 Chapter Scope

Chapter 2 presents three *in vivo* precision studies for HR-pQCT-derived bone density, geometry, cortical and trabecular micro-architecture, as well as FE estimates of bone strength. Specifically, chapter 2 addresses whether HR-pQCT precision for bone micro-architecture can be measured comparably between postmenopausal women and young adults. Chapter 2 also answers whether manual modification of the endocortical contour affects cortical micro-architectural precision and/or outcomes in both age groups. The final section in chapter 2 defines the precision for three FE models and determines which is most precise. Chapter 3 describes the minimum differences between follow-up measures required in order to be confident change has occurred (LSC) as well as the minimum amount of time required between follow-up measures in order to be confident minimal differences are attained (MTI) in postmenopausal women for bone density, geometry and micro-architecture. Chapter 4 characterizes one year change in bone density, geometry, and micro-architecture in postmenopausal women. Chapter 5 reviews study findings and offers suggestions for future research.

2 STUDY 1: HR-PQCT PRECISION

SYNOPSIS: Measurement reproducibility is essential to reliably monitor bone micro-architectural changes over time. Methodological limitations and selective outcome reporting have merited further investigation into HR-pQCT precision of bone density, geometry, micro-architecture, and FE-derived estimates of bone strength. Therefore, the overall aim of this study was to determine precision in these outcomes for the standard HR-pQCT evaluation technique, the advanced dual-threshold analysis for cortical bone micro-architecture using 2 evaluation methods, and 3 different FE-models.

2.1 Area, Geometry, and Micro-architecture[4]

2.1.1 Introduction

Osteoporosis is a multi-factorial disease characterized by low bone mass and the deterioration of bone micro-architecture resulting in bone fragility and a subsequent increase in propensity to fracture[15]. Dual-energy x-ray absorptiometry (DXA) is used for assessing areal bone mineral density (aBMD, mg/cm^2) to diagnose osteoporosis[101,152]. However, the majority of fragility fractures occur in women whose DXA-derived aBMD and related T-scores are above the osteoporosis diagnostic threshold[24,153,154]. Some of these fractures are unrelated to aBMD and are likely due to the deterioration of bone micro-architecture and bone strength which planar 2-dimensional (2D) DXA measures cannot detect. This premise is supported by evidence from women with equal DXA-derived aBMD at the ultradistal radius but substantially different bone micro-architectural properties and strength estimates acquired using high-resolution peripheral

[4] **Published as:** Kawalilak CE, Johnston JD, Olszynski WP, Leswick D, Kontulainen SA (2014). Comparison of short term in vivo precision of bone density and micro-architecture at the distal radius and tibia between postmenopausal women and young adults. *Journal of Clinical Densitometry, 17*(4): 541-517.

quantitative computed tomography (HR-pQCT)[25]. Micro-architectural properties at distal bone sites are able to differentiate postmenopausal women who have had a fragility fracture from their non-fracture counterparts[38-41,44,106,155,156]. Therefore, the use of *in vivo* 3-dimensional (3D) high-resolution imaging techniques may improve osteoporosis diagnostics and fracture risk assessment, as well as offer a monitoring tool for micro-architectural deterioration in postmenopausal women.

Measurement reproducibility is essential to reliably monitor bone micro-architectural changes over time, changes due to drug therapy or intervention, and to compare difference between groups of people[9,12]. HR-pQCT *in vivo* precision errors, in terms of coefficient of variation ($CV\%_{RMS}$), have been reported to vary between 0.1-5% for selected standard outcomes in cortical and trabecular tissues at the distal radius and tibia[5,29,157]. However, the majority of *in vivo* precision studies using HR-pQCT have been completed with young and middle-aged adults[29,157]. It has been suggested that precision errors derived from young adults may underestimate errors in older adults, including clinically relevant postmenopausal women[149,158]. For example, older adults may have more difficulty remaining still during scanning (e.g., tremors), and optimum positioning may be difficult to achieve due to reduced range of motion. In addition, age-related deterioration in bone micro-architecture may challenge the repeatability in HR-pQCT analysis. Evidence from one HR-pQCT study suggested comparable precision errors between young adults and older females (minimum cut-off age: 40 years)[5]. However, measurements from older females were repeated on the same day[5], which has been shown to enhance the pQCT repeatability[159]. Notwithstanding, there is a need for comparison data from older postmenopausal women to confirm if menopausal status influence precision errors of HR-pQCT derived bone properties measured at least 24 hours apart. Finally, previous HR-pQCT

precision studies reported a selection of standard outcome variables. For example, precision of trabecular meta and inner densities are unknown. The objective of our study was to assess whether postmenopausal women could be scanned using HR-pQCT with comparable precision to young adults. We hypothesized that postmenopausal women would have higher precision errors (i.e., poorer repeatability) when compared to young adults.

2.1.2 Methods

2.1.2.1 Participants

The first group of was a random sub-sample of 34 postmenopausal women from the Saskatoon cohort of the Canadian Multi-centre Osteoporosis Study (CaM*os*) (Table 2.1)[160]. Postmenopausal status was assessed using a questionnaire (Table 3.1). We obtained osteoporosis status based on femoral neck (FN) T-scores from the Saskatoon CaM*os* database (Table 2.1)[96], and compared osteoporosis status in our sample to the literature to substantiate that the bone health in our sample was representative to postmenopausal women[160-162]. The second, comparison group was a convenient sample of 15 female and 15 male volunteers (Table 2.1). We combined the sexes to form an "ideal group" of young adults with optimal bone properties for comparison with the postmenopausal women. There was no effect of sex on precision in young adults (*data not shown*). Participant consent was attained prior to the study. This study was approved by the University of Saskatchewan Biomedical Research Ethics Board.

2.1.2.2 HR-pQCT Imaging

All participant had their non-dominant arm and ipsilateral leg immobilized in the manufacturer provided cast prior to imaging in order to acquire the correct limb position and to prevent gross participant movement[163]. After comfortably positioning the participant's limb in the scanner, a 2D anterior-posterior scout view scan was used to set the reference line and define the region of

interest (Figure 2.1). High-resolution pQCT (XtremeCT; Scanco Medical AG, Brüttisellen, Switzerland) was used to acquire 110 parallel CT slices over a 9.02 mm region of the distal radius and distal tibia (Figure 2.1). The radius and tibia regions of interest were 9.5 mm and 22.5 mm, respectively, proximal to the reference line placement (Figure 2.1). The field of view was reconstructed over a 1536 x 1536 matrix using an isotropic resolution of 82 μm. The effective dose was <4 μSv and the measurement time was approximately 2.8 minutes for each scan[163].

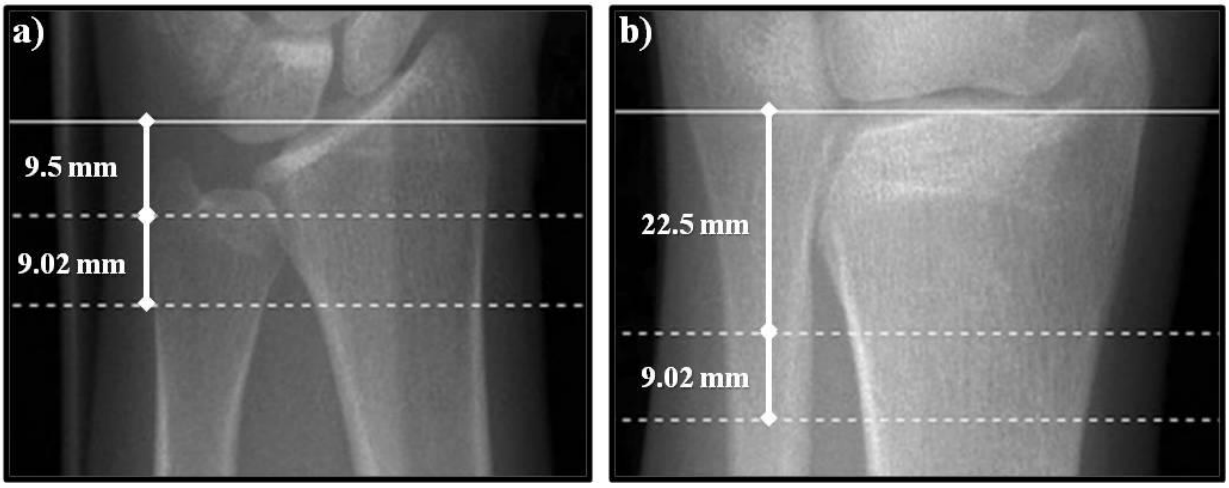

Figure 2.1. Standard HR-pQCT anterior-posterior scout view and location of the scan for a) distal radius and b) distal tibia. Solid line indicates the reference line location. Dashed lines represent the scanned volume of interest.

2.1.2.3 HR-pQCT Analysis

One trained operator (CK) scanned, graded, and analyzed all images. The postmenopausal women had follow-up measures a minimum of 1 week (9.9 ± 3.7 days) after the first measurement, while the young adults had follow-up measures a minimum time period of 1 day (24.0 ± 4.8 hours) from the first scan. All images were grading for quality according to a 5 point scale defined by the manufacturer and reported in a previous publication[164]. Upon detection of motion artifacts (e.g., streaking or broken cortices) a repeat scan was performed. Images graded as quality 4 and 5 were excluded from the study. At the radius, 5 scans from the older adult

group and 1 scan from the young adult group were removed because of excessive movement artifact. We also excluded an additional 2 older adult radius scans due to a skeletal defect noted by the study radiologist (DL). At the tibia, 2 scans were removed in postmenopausal women because of movement artifact. In total, 27 older adult radius scans and 29 young adult radius scans, as well as 32 older adult tibia scans and 30 young adult tibia scans were included in the study.

Image analysis was completed according to the manufacturer's standard *in vivo* evaluation protocol to acquire cortical and trabecular bone density, area, and micro-architectural values. Specifically, the periosteum of the radius and tibia was contoured from the soft tissue using a semi-automatic edge-finding algorithm in a slice-by-slice manner. Where the contour strayed from the periosteal boundary, the contour line was manually corrected. The cortex was separated from the trabecular bone using a coarse Gaussian filter to smooth the image and filter out thin structures. Using support and sigma values of 3 and 2, respectively, the image was binarized and a 7x7x7 voxel-based filter block was applied to fully isolate and define the cortex[42]. Mean cortical thickness (*CtTh*; µm) was calculated as the mean cortical volume divided by the mean periosteal surface area[14,25]. Cortical area (mm^2) and trabecular area (mm^2) were defined as the area of pixels included in the segmented cortical and trabecular compartments, respectively. Total bone density (mg HA/ cm^3) was determined as the average mineral density within the bone volume defined by the outer bone contour. Similarly, cortical and trabecular bone densities (mg HA/ cm^3) were defined as the average mineral density within cortical and trabecular bone volumes, respectively. Trabecular density was farther subdivided into 'Meta' (between) and 'Inner' trabecular bone densities. These densities were defined as the average mineral density within the 40% (*Meta*) and 60% (*Inn*) of the trabecular bone region.

Trabecular bone volume fraction (*BV/TV*, %) was defined as the trabecular density divided by the assumed mineral density of fully mineralized bone (i.e., 1200 mg HA/cm^3)[14,25]. A Laplace-Hamming filter (epsilon 0.5; cut-off frequency 0.4) was applied to enhance the edges of the trabeculae in order to compensate for HR-pQCT resolution constraints and associated partial volume effects, which limited HR-pQCT to measure individual trabeculae (spatial resolution: 105 µm)[165,166]. After binarization and the application of the Laplace-Hamming filter, a ridge detection method and distance transform were used to define the trabecular number (*TbN*, 1/mm)[14,167]. Trabecular thickness (*TbTh*, µm), trabecular separation (*TbSp*, µm), and the standard deviation of the trabecular separation (*Tb1/NSD* or *TbSpSD*; trabecular heterogeneity, µm) were calculated using the bone volume fraction and trabecular number based on plate model assumptions (theoretical basis previously described in detail[14]).

2.1.2.4 Statistical Analysis

We assess the precision of HR-pQCT derived bone outcomes using both coefficients of variation (CV%) and root-mean-squared coefficients of variation (CV%$_{RMS}$), as recommended by Glüer et al. (1995) and presented below

$$CV\% = \left(\frac{\sum_{j=1}^{m} \frac{SD}{\overline{x}_j}}{m}\right) x\ 100\% \tag{2.1}$$

$$CV\%_{RMS} = \sqrt{\sum_{j=1}^{m} \frac{CV\%_j^2}{m}} \tag{2.2}$$

where *SD* was the standard deviation between the two measurements, $\overline{x}_j$ was the mean of the two measurements, and *m* was the number of participants in the analysis. Using the above measures of repeatability, together with sufficient number of participants to acquire 27 degrees of freedom, allow us to achieve 90% confidence in our precision error estimates[12]. The two measures (i.e., CV% and CV%$_{RMS}$) were included because CV% is calculated for each individual, while the

$CV\%_{RMS}$ is a geometric mean and therefore only one value is provided for each outcome. In order to make statistical comparisons between the two groups we needed more than one value; hence all statistical comparisons were completed using CV%.

We also provided information on precision in absolute terms using the 95% limits of agreement (95% LOA). The 95% LOA was previously defined by Bland and Altman (1986) and presented below:

$$95\%\ LOA = \bar{d} \pm (1.96\ xSD_{meas}) \quad (2.3)$$

where $\bar{d}$ was the average measurement bias, and SD_{meas} was the standard deviation of the differences between the two measurements[8].

To determine the distribution of our dataset, we calculated the z-score for skewness and kurtosis for the precision error and 95% LOA for all standard outcome variables for both the young adult and older adult groups. The variables with skewness or kurtosis z-scores greater than 1.96 had a non-parametric distribution. We performed 13 Mann Whitney *U*-tests (with Bonferroni adjustments for multiple comparisons) to compare the CV% between young adults and postmenopausal women for each standard outcome variable. Significance was set to $P<0.004$.

2.1.3 Results

Mean standard outcome variables at baseline and follow-up scans are presented in Table 2.2 for the group of postmenopausal women, and Table 2.3 for the young adult group. The $CV\%_{RMS}$ and 95% LOA are also presented in Tables 2.2 and 2.3 for the postmenopausal women and the group of young adults, respectively. The standard outcome variables did not differ between the groups (Table 2.4).

Table 2.1. Participant demographics (mean ± SD); including the number (N) and proportion (%) of: participants with osteopenia or osteoporosis.

		Postmenopausal	**Young adults**	
		Females	*Males*	*Females*
Age	(years)	74 ± 7	25 ± 4	26 ± 8
Height	(cm)	160.1 ± 5.7	179.5 ± 4.1	166.5 ± 4.6
Weight	(kg)	72.4 ± 12.9	88.5 ± 4.1	71.4 ± 12.4
Osteopenia	N (%)	20 (63%)	--	--
Osteoporosis	N (%)	5 (16%)	--	--

Table 2.2. Mean (±SD) of the baseline and follow-up scans, mean (±SD) of both measurements, precision error ($CV\%_{RMS}$), and the lower and upper bounds for the 95% limits of agreement (LOA) for the CaM*os* Saskatoon cohort of postmenopausal women at a) distal radius and b) distal tibia.

		Baseline	**± SD**	**Follow-up**	**± SD**	**Mean**	**± SD**	**$CV\%_{RMS}$**	**95% LOA** *Lower*	*Upper*
a) Radius (n=27)										
Area										
Cortical	(mm^2)	37.9	± 13.9	37.9	± 14.2	37.9	± 14.0	2.9	-1.6	1.6
Trabecular	(mm^2)	242.4	± 46.2	242.3	± 46.3	242.3	± 46.2	0.4	-1.2	1.5
Density										
Total	(mg HA/cm^3)	245.1	± 54.8	245.3	± 55.6	245.2	± 55.2	1.4	-5.3	4.9
Cortical	(mg HA/cm^3)	774.3	± 101.8	771.7	± 103.7	773.0	± 102.6	1.1	-9.5	14.7
Trabecular	(mg HA/cm^3)	131.0	± 34.4	131.3	± 34.1	131.2	± 34.3	1.2	-2.9	2.3
Meta	(mg HA/cm^3)	188.0	± 31.2	189.0	± 31.6	188.5	± 31.3	1.6	-5.5	3.6
Inner	(mg HA/cm^3)	91.7	± 39.1	92.5	± 38.3	91.6	± 38.7	2.1	-2.5	2.9
Micro-architecture										
CtTh	(μm)	522.1	± 199.2	522.9	± 204.2	522.5	± 201.5	3.1	-21.5	20.1
BV/TV	(%)	10.9	± 2.9	10.9	± 2.9	10.9	± 2.9	1.2	-0.2	0.2
TbN	(1/mm)	1.8	± 0.4	1.8	± 0.3	1.8	± 0.4	6.0	-0.2	0.1
TbTh	(μm)	60.9	± 11.0	60.3	± 10.7	60.6	± 10.6	5.4	-4.8	5.9
TbSp	(μm)	522.9	± 139.3	514.8	± 129.4	518.8	± 132.2	6.1	-41.5	57.8
TbSpSD	(μm)	277.0	± 156.7	281.1	± 158.0	279.1	± 156.6	6.5	-31.3	23.1

b) Tibia (n=32)

Area									
Cortical	(mm^2)	85.3	± 26.6	84.9	± 26.3	85.1	± 26.4	1.1	-1.0	1.9
Trabecular	(mm^2)	622.7	± 102.6	623.3	± 102.6	623.0	± 102.6	0.1	-1.9	0.7
Density									
Total	(mg HA/cm^3)	244.9	± 48.1	244.0	± 47.5	244.5	± 47.8	0.9	-2.5	4.2
Cortical	(mg HA/cm^3)	776.2	± 77.0	776.3	± 75.6	776.2	± 76.3	0.3	-3.4	3.2
Trabecular	(mg HA/cm^3)	155.8	± 41.5	155.4	± 40.8	155.6	± 41.4	1.3	-2.6	3.3
Meta	(mg HA/cm^3)	224.5	± 38.1	224.2	± 37.3	224.3	± 37.6	1.1	-3.5	4.0
Inner	(mg HA/cm^3)	109.2	± 46.7	108.7	± 46.0	108.9	± 46.3	1.9	-2.2	3.1
Micro-architecture									
CtTh	(µm)	812.5	± 260.1	807.8	± 255.5	810.2	± 257.7	1.4	-13.1	22.4
BV/TV	(%)	13.0	± 3.5	12.9	± 3.4	13.0	± 3.4	1.3	-0.2	0.3
TbN	(1/mm)	1.7	± 0.4	1.7	± 0.3	1.7	± 0.3	6.7	-0.2	0.2
TbTh	(µm)	78.0	± 17.7	77.8	± 17.0	77.9	± 17.0	6.2	-6.1	6.5
TbSp	(µm)	550.8	± 177.6	549.4	± 168.0	550.1	± 170.9	6.8	-50.8	53.6
TbSpSD	(µm)	299.3	± 232.0	302.4	± 235.1	300.9	± 233.3	6.2	-24.3	18.2

Table 2.3. Mean (±SD) of the baseline and follow-up scans, mean (±SD) of both measurements, precision error ($CV\%_{RMS}$), and the lower and upper bounds for the 95% limits of agreement (LOA) for the young adult group at a) distal radius and b) distal tibia.

		Baseline	± SD	Follow-up	± SD	Mean	± SD	$CV\%_{RMS}$	95% LOA *Lower*	95% LOA *Upper*
a) Radius (n=29)										
Area										
Cortical	(mm^2)	62.5	± 18.6	61.4	± 18.0	62.0	± 18.3	3.1	-1.5	3.8
Trabecular	(mm^2)	274.5	± 60.1	275.4	± 60.3	274.9	± 60.2	0.6	-3.7	1.8
Density										
Total	(mg HA/cm^3)	328.1	± 50.5	324.7	± 49.1	326.4	± 49.7	1.6	-4.3	11.1
Cortical	(mg HA/cm^3)	866.6	± 53.1	861.1	± 57.3	863.9	± 54.8	1.2	-10.6	21.4
Trabecular	(mg HA/cm^3)	192.7	± 46.4	191.9	± 45.7	192.3	± 46.0	0.9	-2.0	3.6
Meta	(mg HA/cm^3)	248.9	± 44.8	248.0	± 44.7	248.4	± 44.8	0.8	-2.2	4.0
Inner	(mg HA/cm^3)	154.0	± 48.2	153.3	± 47.1	153.6	± 47.6	1.4	-2.7	4.0
Micro-architecture										
CtTh	(µm)	796.9	± 180.0	782.8	± 172.3	789.8	± 175.6	3.3	-19.8	48.1
BV/TV	(%)	16.0	± 3.9	16.0	± 3.8	16.0	± 3.8	0.9	-0.2	0.3
TbN	(1/mm)	2.2	± 0.3	2.2	± 0.3	2.2	± 0.3	5.7	-0.2	0.2
TbTh	(µm)	72.8	± 12.7	73.0	± 12.0	72.9	± 11.9	5.9	-6.8	6.5
TbSp	(µm)	391.1	± 67.6	393.2	± 62.3	392.2	± 63.0	5.7	-36.7	32.6
TbSpSD	(µm)	154.7	± 31.9	156.5	± 30.7	155.6	± 30.1	8.0	-20.3	16.7
b) Tibia (n=30)										
Area										
Cortical	(mm^2)	151.4	± 40.0	150.6	± 39.0	151.0	± 39.5	0.9	-1.5	3.2
Trabecular	(mm^2)	626.7	± 132.9	627.4	± 133.3	627.0	± 133.1	0.2	-2.5	1.1
Density										
Total	(mg HA/cm^3)	350.8	± 56.8	349.6	± 55.7	350.2	± 56.2	0.7	-2.6	5.1
Cortical	(mg HA/cm^3)	918.9	± 34.3	918.5	± 33.5	918.7	± 33.8	0.4	-5.3	6.0
Trabecular	(mg HA/cm^3)	212.8	± 48.4	212.1	± 47.6	212.4	± 48.0	0.8	-1.8	3.3
Meta	(mg HA/cm^3)	275.7	± 45.0	275.1	± 44.7	275.4	± 44.8	0.6	-1.8	3.0
Inner	(mg HA/cm^3)	170.1	± 51.8	169.3	± 50.7	169.7	± 51.2	1.4	-2.3	4.1

Micro-architecture										
CtTh	(µm)	1382.0	± 285.8	1377.0	± 278.5	1379.5	± 282.0	0.9	-15.8	25.8
BV/TV	(%)	17.7	± 4.0	17.7	± 4.0	17.7	± 4.0	0.9	-0.2	0.3
TbN	(1/mm)	2.1	± 0.4	2.0	± 0.4	2.0	± 0.4	4.0	-0.3	0.3
TbTh	(µm)	86.0	± 14.9	86.7	± 14.3	86.4	± 14.5	3.8	-5.3	3.9
TbSp	(µm)	413.3	± 96.7	417.3	± 91.6	415.2	± 93.4	4.0	-28.8	20.4
TbSpSD	(µm)	178.3	± 52.1	181.0	± 50.0	180.0	± 50.7	5.0	-14.6	9.2

Table 2.4. Median difference (young adults - postmenopausal women) for the percent coefficient of variation (CV%) between the group of postmenopausal women and the young adult group with their corresponding *P*-values for the a) distal radius, and b) distal tibia.

		CV% Median Difference	*P*-value
a) Radius (n=56)			
Area			
Cortical	(mm^2)	-0.5	0.264
Trabecular	(mm^2)	0.2	0.071
Density			
Total	(mg HA/cm^3)	-0.1	0.543
Cortical	(mg HA/cm^3)	0.0	0.383
Trabecular	(mg HA/cm^3)	0.0	0.481
Meta	(mg HA/cm^3)	-0.2	0.021
Inner	(mg HA/cm^3)	-0.4	0.090
Micro-architecture			
CtTh	(μm)	0.0	0.810
BV/TV	(%)	-0.1	0.508
TbN	(1/mm)	-0.2	0.762
TbTh	(μm)	1.0	0.905
TbSp	(μm)	-0.2	0.898
TbSpSD	(μm)	0.9	0.264
b) Tibia (n=62)			
Area			
Cortical	(mm^2)	-0.2	0.661
Trabecular	(mm^2)	0.0	0.729
Density			
Total	(mg HA/cm^3)	0.0	0.377
Cortical	(mg HA/cm^3)	-0.1	0.146
Trabecular	(mg HA/cm^3)	-0.2	0.066
Meta	(mg HA/cm^3)	-0.3	0.004
Inner	(mg HA/cm^3)	0.0	0.467
Micro-architecture			
CtTh	(μm)	-0.4	0.004
BV/TV	(%)	-0.3	0.070
TbN	(1/mm)	-1.4	0.070
TbTh	(μm)	-0.7	0.223
TbSp	(μm)	-1.0	0.121
TbSpSD	(μm)	-0.9	0.657

***** *Significant differences at P<0.004*

2.1.5 Discussion

Our objective was to assess whether postmenopausal women could be measured with comparable precision as young adults. Contrary to our hypothesis, there were no statistically significant differences between the postmenopausal women and young adults for standard outcome variables using HR-pQCT. These data indicate that postmenopausal status does not significantly affect the precision errors in skeletal parameters assessed using densitometric techniques as was previously suggested[149,158].

This study is the first to provide precision results for all standard outcome variables produced using HR-pQCT in postmenopausal women and young adults. Overall, our precision was comparable with those previously published for young and middle aged adults[5,29,157]. Also consistent with previous findings[5,29,157], the area and density precision errors appeared to be lower in the tibia compared to the radius. This may be due to challenges associated with locating the radius landmark for reference line placement, whereas the tibia had a consistently well-defined landmark. This is evident by the higher agreement in common region between baseline and follow-up scans in the tibia (i.e., 97%), relative to the radius (i.e., 93%). Further, the precision error appeared smaller for area and density measures ($CV\%_{RMS}$: 0.2-3.1), relative to the micro-architectural parameters ($CV\%_{RMS}$: 0.9-8.0). This trend was consistent between the distal radius and tibia in both young adults and postmenopausal women. This is likely due to the accumulation of error associated with limited resolution and inherent errors in the equations used for determining micro-architectural parameters.

Postmenopausal status did not affect the precision error for the majority of the standard outcome variables obtained using HR-pQCT. This may be the result of careful consideration to participant positioning within the cast and scanner, as well as attention to the placement of the reference line at follow-up measures and a conscientious effort during the analysis process.

Further, the manufacturer's image registration algorithm has previously been shown to reduce precision error[14,168]. The image registration algorithm uses a common region to match the average total cross-sectional area for all slices in the first measurement with all repeated measurements on that participant[14,157,168]. This is evident from the mean common region for total area measures between baseline and follow-up scans for the young adult radii and tibiae were 93±5% and 97±2%, respectively, and for the postmenopausal women radii and tibiae were 93±4% and 97±2%, respectively.

The assessment and monitoring of densitometric and micro-architectural properties, and related errors in repeated measurements, in postmenopausal women are clinically relevant due to the high risk of osteoporotic fractures in this population. Based on the observed 95% LOA, similar magnitude of change in the HR-pQCT derived standard outcome variables is required in both young adults and postmenopausal women. However, the rate and magnitude of change in bone micro-architecture likely depends on the age, sex and musculoskeletal health status of the participants. Therefore, the 95% LOA, based on short-term precision error, may over- or under-estimate the ability to monitor changes in participants with slower or faster rate of change in bone micro-architecture, respectively. Consequently, prospective follow-up data of bone micro-architectural changes is needed to confirm our findings.

Our study design had certain strengths that merit consideration. First, we compared precision errors in postmenopausal women to short-term precision errors observed with a "best case" sample of young adults, including both females and males. Second, we not only repositioned our participants between measurement times, but we also separated their repeat measurements by a minimum of 24 hours. This is important because underestimation of precision error in pQCT measurements has been reported when precision was calculated using

scans repeated on the same day[159]. Third, we had sufficient number of participants in both groups to attain a minimum of 27 degrees of freedom and calculated precision error based on root-mean-squared averages. Meeting this requirement permits 90% confidence in measurement precision[12,149]. Finally, 16% of our postmenopausal women had osteoporosis and 63% had osteopenia, based on their femoral neck T-scores. These proportions are comparable to the osteoporosis reference standards from North America, Europe, Australia and Japan[161,162], thereby making our data generalizable to postmenopausal women in these regions.

There are some limitations associated with this study that warrant discussion. First, while we studied a representative sample of postmenopausal women, skeletal precision may vary according to duration of menopause, time from menopause, and disease status (e.g., osteoporosis); this merits further investigation into population-specific precision studies. Second, osteoporosis status was not accounted for in the analysis because of the small number of participants with osteoporosis in our study (n=5). Third, the contouring algorithm is semi-automatic and the majority of the scans required manual correction of the periosteal contour line. This was especially true in the postmenopausal women whose cortex appeared more porous relative to the young adult group. However, the analysis for both groups was conducted carefully by a single operator, on a slice-by-slice manner, to reduce the error associated with the manual correction.

In summary, short-term precision errors in HR-pQCT-derived standard bone outcomes are comparable in postmenopausal women and in young adults.

The standard HR-pQCT evaluation algorithm provides a detailed description of trabecular micro-architecture but, beyond cortical thickness, it does not provide information on cortical bone micro-architecture. In order to evaluate the micro-architecture of the cortex (e.g.,

cortical porosity) the dual-threshold contour technique must be used to isolate the cortex. While this algorithm is relatively new, it has been widely accepted and utilized in research across all age groups. However, the precision of cortical bone micro-architecture provided by the dual-threshold technique is not fully known and there are some methodological questions that remain.

2.2 Cortical Bone Micro-architecture[5]

2.2.1 Introduction

Osteoporosis is a major public health problem in older adults[97,169]. It is a disease characterized by the loss of bone mass and the deterioration of bone micro-architecture, resulting in increased fracture risk, particularly in postmenopausal women[15,33]. Distal radius fractures are reported as being the most common fracture type occurring in postmenopausal women in North America and Europe[33,170-172].

Despite long bone ends (epiphyses and metaphyses) being predominantly comprised of trabecular bone, the thin cortical shell contributes to whole bone strength[170,173] bearing a significant proportion of the load[174]. Bone's mechanical properties have been associated with cortical bone micro-architecture[104]. High cortical porosity, in particular, has been negatively associated with elastic modulus (tissue stiffness), failure load (strength), toughness (resilience), and impact energy-absorption capacity of bone[71,173,175,176]. From their cross-sectional cadaveric comparison, McCalden and colleagues reported that 76% of the observed age-related decline in bone strength was accounted for by cortical porosity[75]. Further, in postmenopausal women with low-impact fractures, there is evidence of higher cortical porosity when compared to non-fracture controls[43,177-179]. For these reasons, cortical bone micro-architecture is an important target to monitor when assessing osteoporosis and treatment effects.

Precise measurement of cortical bone micro-architecture is fundamental when monitoring skeletal changes and treatment effects. Therefore, consideration must be given to the precision of the evaluation protocols used to obtain cortical micro-architectural outcomes. One method of

[5] **Published as**: Kawalilak CE, Johnston JD, Cooper DML, Olszynski WP, Kontulainen SA (2015). Role of endocortical contouring methods on precision of HR-pQCT-derived cortical micro-architecture in postmenopausal women and young adults. *Osteoporosis International. E-pub ahead of print.*

cortical micro-architecture evaluation, using high-resolution peripheral quantitative computed tomography (HR-pQCT), is the advanced cortical bone evaluation tool which uses a dual-thresholding to identify the periosteal (outer) and endocortical (inner) surfaces of the cortex[5,105]. The dual-threshold method is a semi-automatic process which requires manual modification of the contour lines when they appear to deviate from the periosteal and endocortical surfaces[105]. Cadaveric (*ex vivo)* evidence from the distal tibia suggested that modification of the endocortical contour line affects cortical bone outcomes[180]. However, it remains unknown whether manual modification of the endocortical contour line affects precision and outcomes of cortical bone properties *in vivo*. If automatic contouring can offer similar precision and outcomes as modified contouring, this will lead to time savings and reduced costs as modified contouring can be a laborious process.

The first objective of this study was to define *in vivo* precision errors (coefficient of variation root-mean-squared, $CV\%_{RMS}$) and least significant change (LSC) for cortical bone micro-architecture in postmenopausal women and young adults using 2 different cortical bone evaluation methods (automatic endocortical contour, AUTO and modified endocortical contour, MOD). The second objective was to compare precision errors and bone outcomes obtained with both methods within and between the groups.

2.2.2 Methods

2.2.2.1 Participants

The first group was a random sub-sample of 34 postmenopausal women (74±7 years) from the Saskatoon cohort of the Canadian Multi-centre Osteoporosis (CaM*os*) Study[1,160]. Postmenopausal status was assessed using a questionnaire; osteoporosis status was based on femoral neck (FN) T-scores obtained from the Saskatoon CaM*os* database[96]. The second group

of volunteers was a convenient sample of young adults (15 females and 15 males; mean age ± standard deviation (SD): 26±7 years)[1]. Participant consent was attained prior to the study. This study was approved by the University of Saskatchewan Biomedical Research Ethics Board.

2.2.2.2 HR-pQCT Imaging

Prior to imaging, all participants had their non-dominant arm and ipsilateral leg immobilized in a fiberglass cast provided by the manufacturer[1]. HR-pQCT (XtremeCT; Scanco Medical AG, Brüttisellen, Switzerland) was used to acquire a standard 9.02 mm region of interest (110 parallel CT slices) with an 82 μm isotropic voxel size at the distal radius and tibia[163]. The scan time was <2.8 minutes and the effective dose was <4 μSv per scan[4].

2.2.2.3 HR-pQCT Image Analysis

One investigator (CK) scanned, graded, and analyzed all HR-pQCT images. The group of postmenopausal women had follow-up measures at least 1 week (9.9±3.7 days) after the first measurement. The young adult group had follow-up measures with a minimum time period of 1 day (24±4.8 hours) from the first scan. All images were graded for quality according to the manufacturer's 5 point scale[1,164]. Images graded as quality 4 and 5 were excluded from the study[1]. In total: 27 postmenopausal radii, 29 young adult radii, 32 postmenopausal tibiae, and 30 young adult tibiae were included in the study.

Image analysis was completed according to the manufacturer's standard evaluation and the manufacturer-provided advanced cortical micro-architecture evaluation protocols (Scanco Module 64-bit IPL V5.08b). Briefly, the standard image evaluation was used to define the periosteum of the radius and tibia by separating bone from soft tissue using a semi-automatic edge-finding algorithm in a slice-by-slice manner, as described elsewhere[1,4]. Subsequently, we used the automated dual-threshold method for cortical micro-architecture evaluation to segment

the endocortical surface[5,181]. The periosteal contour was imported from the standard evaluation process while the endocortical contour was automatically created using a series of morphological operations (i.e., dilation and erosion) to separate the trabecular and cortical volumes of interest (VOI)[5].

All images underwent two methods for cortical micro-architecture evaluations. The first method (automated contour method, AUTO) used the automatic dual-threshold method to define the endocortical contour line (Figure 2.2 *solid line*). The second method (modified contour method, MOD) started with the automatically generated endocortical contour line, which was then qualitatively inspected for quality assurance and manually modified (via mouse) when the contour visually deviated from the apparent endocortical margin (Figure 2.2 *dashed line*). Cortical micro-architecture evaluation was completed using two methods for each bone site (radius and tibia), for each group (young adult and postmenopausal women), at both times points (baseline and follow-up). AUTO took approximately 5 minutes to complete; MOD took up to 3 hours per radius and up to 5 hours per tibia, depending on degree of cortical porosity. The following outcomes were included in this investigation: cortical porosity (CtPo, %), cortical pore volume (CtPoV, mm^3), cortical pore diameter (CtPoDm, mm), cortical bone total volume (CtTV, mm^3), cortical bone volume (CtBV, mm^3), cortical bone mineral density (mean mineralization of the cortical VOI; CtBMD, mg HA/cm^3), and cortical thickness (CtTh, mm).

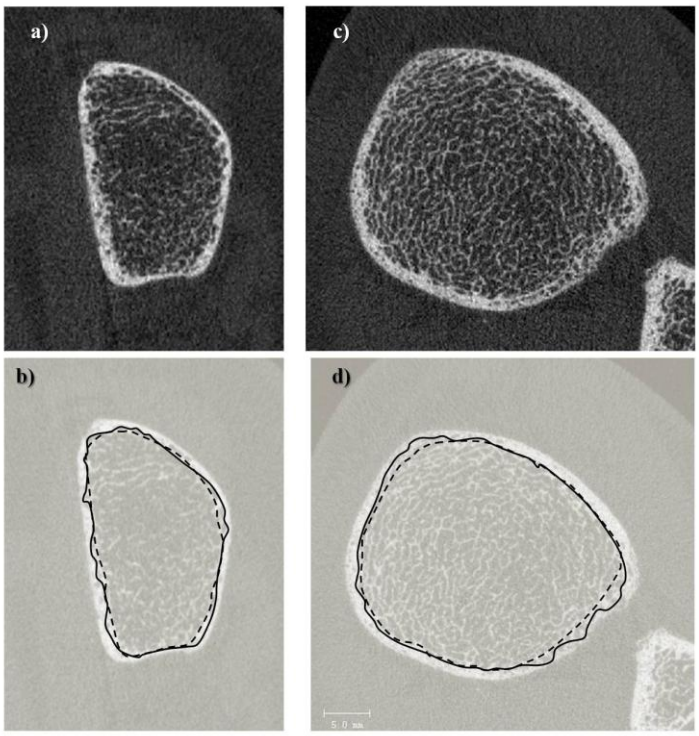

Figure 2.2. HR-pQCT scan illustrating the radius (a, *no contour*) and tibia (c, *no contour*) with the automatic contour (b and d: *solid line*) and the modified contour (b and d: *dashed line*) for the group of postmenopausal women.

2.2.2.4 Statistical Analysis

To determine the distribution of our dataset, we calculated the skewness z-score for all variables for both the automatic contour and the modified contour methods in the postmenopausal women and young adults. The variables with skewness z-scores greater than 1.96 had a non-parametric distribution and were normalized using log transformation.

We assessed the precision of HR-pQCT derived cortical micro-architecture outcomes by calculating coefficients of variation root-mean-squared ($CV\%_{RMS}$) for each outcome[1,12]. Reliable monitoring of skeletal changes and treatment effects requires information regarding the minimum difference between baseline and follow-up measures that is necessary for measuring real change beyond measurement error. As indicated by the International Society for Clinical Densitometry (ISCD), the LSC is the recommended method for determining true skeletal change with 95% confidence[9,149]. We determined the LSC in relation to measurement precision errors using the following equation[9]:

$$LSC_{(1x1)} = Z \times CV\% \sqrt{\frac{1}{n_1} + \frac{1}{n_2}} = 1.96 \times CV\%_{RMS} \sqrt{\frac{1}{1} + \frac{1}{1}} = 2.77 \times CV\%_{RMS} \quad (2.4)$$

Where the *'(1x1)'* indicates that we performed 1 measurement at each baseline (*'n_1'*) and follow-up (*'n_2'*) visit, and the Z-score corresponds a two-tailed 95% confidence level (i.e., 1.96)[10].

Within each group, we compared mean CV% and cortical bone outcomes between the two methods using repeated-measures analysis of variance (ANOVA) with Bonferroni correction for multiple comparisons. We compared mean CV% and cortical bone outcomes (evaluated using automatic and modified contour methods) between the postmenopausal women and group of young adults using multivariate ANOVA with Bonferroni adjustment for multiple comparisons. Significance was set to $P<0.05$. All statistical analyses were performed using IBM SPSS commercial statistics software (PASW, Version 21 for Windows, SPSS Inc., Chicago, IL, USA).

2.2.3 Results

Cortical bone micro-architecture $CV\%_{RMS}$ (precision errors) for AUTO and MOD for both groups are summarized in Figure 2.3. Mean (±SD) for outcome variables and LSC are presented in Table 2.5 for both contour evaluation methods and for both groups. For both contour methods, both measurement sites, and for both age groups, the LSC values were higher for CtPo, CtPoV and CtPoDm (range: 10.6-45.0%, Table 2.5) and lower for CtTV, CtBV, CtBMD, and CtTh (range: 0.9-9.1%, Table 2.5).

There were no significant differences in precision errors between AUTO and MOD methods in either group; however, precision errors differed between the groups (Figure 2.3). When using AUTO at the distal tibia, precision error for cortical BMD was 0.2% *higher* for the postmenopausal women (P=0.022) (Figure 2.3). When using MOD at the distal radius, precision

error for cortical porosity and cortical pore volume was, respectively, 9.3% (P=0.024) and 7.5% (P=0.039) *lower* in postmenopausal women relative to the young adults (Figure 2.3). At the distal tibia precision error for cortical thickness was 0.8% *higher* for the postmenopausal women compared to the young adults (P=0.009) (Figure 2.3). All other cortical micro-architectural outcome variables did not differ between the two age groups for either evaluation method (Figure 2.3).

Pertaining to cortical bone micro-architectural outcomes, in postmenopausal women there were between-method differences for every variable, except cortical thickness at the distal radius (P=0.902) (Table 2.5). For postmenopausal women, MOD resulted in *higher* cortical porosity (Radius: 48.6%; Tibia: 31.2%), pore volume (Radius: 54.3%; Tibia: 41.9%), pore diameter (Radius: 14.3%; Tibia: 16.7%), total volume (Radius: 10.8%; Tibia: 15.9%), and bone volume (Radius: 6.7%; Tibia: 11.5%) in addition to *lower* cortical density (Radius: -5.5%; Tibia: -7.5%) at both measurement sites (Table 2.5). Also, at the distal tibia in postmenopausal women MOD yielded, on average, -0.02 mm (-1.7 %) *thinner* cortices (P<0.028) (Table 2.5). In the young adult group we found no significant differences between the contour methods across all outcomes (Table 2.5).

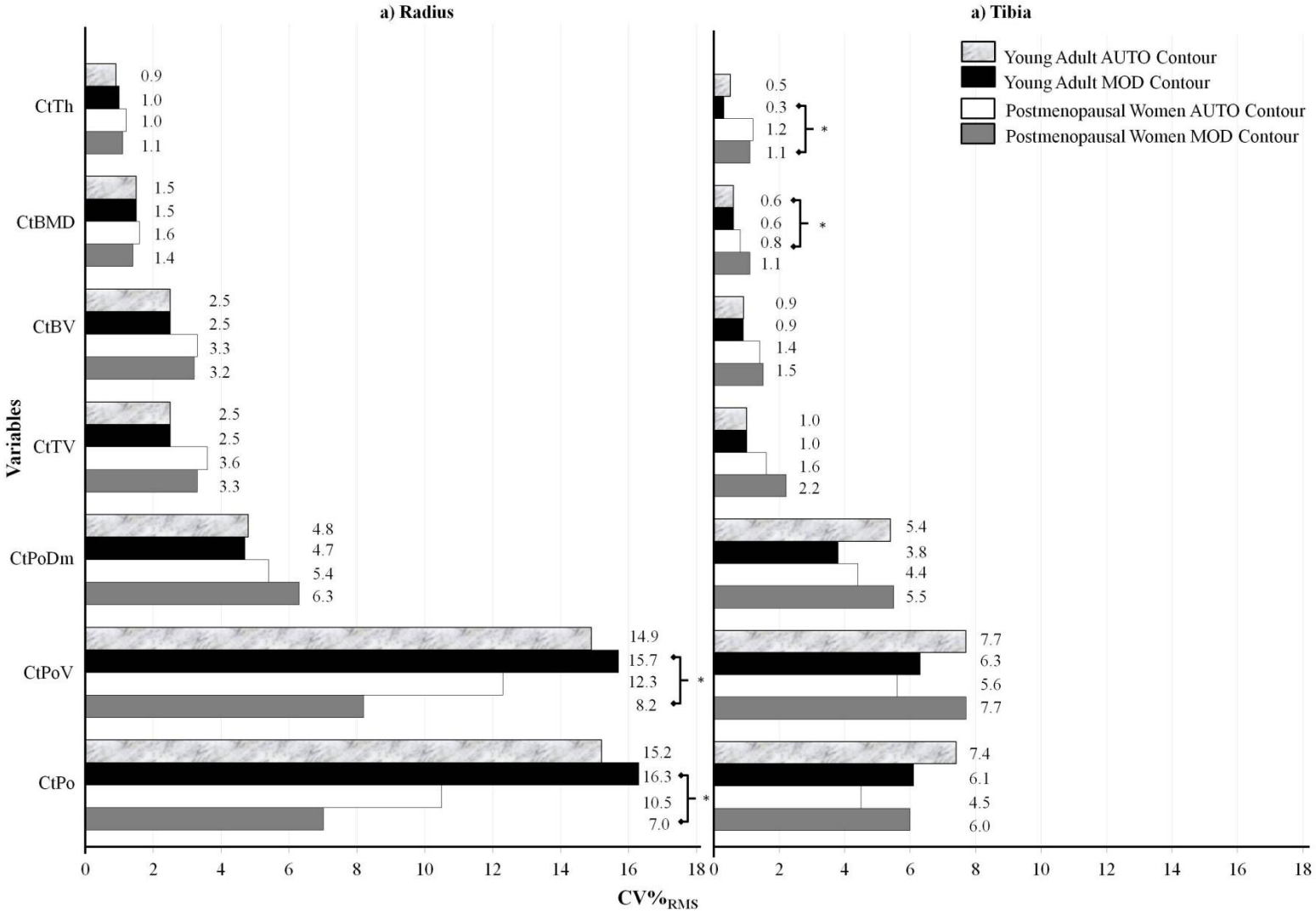

Figure 2.3. Root-mean-square precision errors (CV%) for cortical micro-architecture variables for both contouring methods as well as the group of young adults and postmenopausal women at the a) distal radius, and b) distal tibia. Cortical micro-architecture outcomes include: cortical porosity (CtPo, %); cortical pore volume (CtPoV, mm^3); cortical pore diameter (CtPoDm, mm); cortical bone total volume (CtTV, mm^3); cortical bone volume (CtBV, mm^3); cortical bone mineral density (CtBMD, mg HA/cm^3);and cortical thickness (CtTh, mm). * *Indicates significant differences.*

Table 2.5. Mean (±SD) of baseline and follow-up measurements, Least Significant Change (LSC), mean outcome difference between evaluation methods (*MOD-AUTO*), the significance value of log transformed outcomes between evaluation methods for a) postmenopausal women and b) young adult group at i) distal radius and ii) distal tibia.

		Automatic Contour (AUTO)			Modified Contour (MOD)				
a) Postmenopausal Women									
i) Radius (n=27)		**Mean**	**±SD**	**LSC (%)**	**Mean**	**±SD**	**LSC (%)**	**Mean Outcome Difference Between Evaluation Methods**	***P*-value***
CtPo	(%)	3.6	± 1.0	29.0	7.0	± 3.7	19.5	3.4 ± 2.9	**<0.001**
CtPoV	(mm^3)	13.2	± 3.7	34.0	28.9	± 15.4	22.8	15.6 ± 13.6	**<0.001**
CtPoDm	(mm)	0.18	± 0.02	15.1	0.21	± 0.04	17.4	0.03 ± 0.02	**<0.001**
CtTV	(mm^3)	375.6	± 90.9	9.8	421.2	± 94.2	9.1	45.6 ± 43.1	**<0.001**
CtBV	(mm^3)	368.8	± 86.4	9.1	393.5	± 84.8	8.8	24.7 ± 19.5	**<0.001**
CtBMD	(mg HA/cm^3)	918.1	± 77.2	4.5	867.8	± 101.3	4.0	-50.3 ± 38.6	**<0.001**
CtTh	(mm)	1.187	± 0.060	2.7	1.189	± 0.068	3.0	0.002 ± 0.032	0.902
ii) Tibia (n=32)									
CtPo	(%)	9.7	± 3.4	12.6	14.1	± 5.3	16.6	4.4 ± 3.5	**<0.001**
CtPoV	(mm^3)	77.9	± 33.7	15.4	134.1	± 58.7	21.4	56.2 ± 38.1	**<0.001**
CtPoDm	(mm)	0.20	± 0.02	12.3	0.24	± 0.05	15.3	0.04 ± 0.5	**<0.001**
CtTV	(mm^3)	803.6	± 200.3	4.6	955.2	± 198.0	6.1	151.6 ± 85.4	**<0.001**
CtBV	(mm^3)	734.8	± 178.4	3.8	830.4	± 177.4	4.2	95.6 ± 85.4	**<0.001**
CtBMD	(mg HA/cm^3)	841.4	± 71.5	2.3	778.7	± 92.7	3.2	-62.7 ± 40.5	**<0.001**
CtTh	(mm)	1.17	± 0.08	3.3	1.15	± 0.06	3.1	-0.02 ± 0.07	**0.028**
b) Young Adults									
i) Radius (n=29)									
CtPo	(%)	2.19	± 1.67	42.0	2.16	± 1.37	45.0	-0.03 ± 0.40	0.188
CtPoV	(mm^3)	14.2	± 17.4	41.3	13.5	± 13.0	43.5	-0.8 ± 5.1	0.319
CtPoDm	(mm)	0.151	± 0.010	13.2	0.152	± 0.010	13.1	0.001 ± 0.005	0.432

CtTV	(mm^3)	567.2	± 155.3	7.0	564.3	± 144.3	6.8	-2.9	± 18.7	0.564
CtBV	(mm^3)	556.3	± 141.9	7.0	554.1	± 134.4	6.9	-2.2	± 13.7	0.403
CtBMD	(mg HA/cm^3)	963.76	± 53.12	4.1	963.79	± 51.23	4.3	0.03	± 4.24	0.882
CtTh	(mm)	1.130	± 0.056	2.6	1.126	± 0.055	2.7	-0.004	± 0.009	0.063
ii) Tibia (n=30)										
CtPo	(%)	4.5	± 1.8	20.6	4.3	± 1.5	16.8	-0.2	± 1.2	0.440
CtPoV	(mm^3)	58.8	± 36.5	21.4	53.9	± 27.0	17.5	-4.8	± 22.3	0.492
CtPoDm	(mm)	0.185	± 0.019	15.0	0.183	± 0.024	10.6	-0.002	± 0.018	0.474
CtTV	(mm^3)	1223.3	± 287.5	2.8	1202.8	± 253.3	2.7	-20.5	± 84.6	0.194
CtBV	(mm^3)	1165.8	± 256.8	2.6	1149.9	± 232.8	2.6	-15.9	± 63.0	0.178
CtBMD	(mg HA/cm^3)	981.6	± 38.7	1.7	983.7	± 37.4	1.7	2.1	± 15.9	0.479
CtTh	(mm)	1.068	± 0.026	1.5	1.067	± 0.018	0.9	0.001	± 0.009	0.473

**Assessed using repeated measures ANOVA comparison of logarithm transformed data with Bonferroni adjustment for multiple comparisons*

2.2.4 Discussion

Our primary objective was to define *in vivo* precision errors and LSC for cortical bone micro-architecture in 2 groups (postmenopausal women and young adults) using 2 different cortical bone micro-architecture evaluation methods (automatic endocortical contour, AUTO; modified endocortical contour, MOD). Results suggest that precision errors appear higher for micro-architectural outcomes requiring higher resolution. For instance, cortical porosity had a CV% range between 7 and 16%, while cortical bone mineral density had a CV% range of 1-2%. These precision errors, especially those from the AUTO method, appeared to be similar to those previously reported[5].

Our percent LSCs were also comparable to those previously published[5]. For example, the percent LSC at the distal radius of postmenopausal women for cortical pore volume was 34% (AUTO) and 23% (MOD), while Burghardt et al. reported 33% (combined AUTO & MOD)[5]. For ease of interpretation, percent LSCs can be used to determine (with 95 % confidence) that the observed change is clinically meaningful[149]. For example, in postmenopausal women, the minimum difference required to measure change in cortical pore volume would be 4.5 mm^3 (AUTO) and 6.6 mm^3 (MOD). This LSC is 2-3 times higher than previously reported (2.2 mm^3)[5] likely due to larger pore volumes in our cohort of older postmenopausal women ($CtPoV_{PM\text{-}Radius[4]}$: 9.1 mm^3; $CtPoV_{AUTO}$: 13.2 mm^3, $CtPoV_{MOD}$: 28.9 mm^3).

Precision Errors Comparison: AUTO and MOD

In terms of our secondary objectives, CV% precision errors did not differ between AUTO and MOD endocortical contour methods. That is, user-error associated with endocortical contour manipulation did not appear to affect repeatability for cortical bone micro-architecture. Importantly, this suggests that the endocortical contour line can be manually modified, in both

postmenopausal women and young adults, with similar repeatability as the automatically generated contour line.

Precision Errors Comparison: Postmenopausal Women and Young Adults

Our precision comparison between the group of postmenopausal women and young adults found no differences for the AUTO method, except for cortical BMD. Specifically, postmenopausal women had slightly higher (0.2%) precision error (i.e., lower repeatability) for distal tibial cortical BMD. In contrast, when using MOD, postmenopausal women had lower precision errors for cortical porosity (-9%) and cortical pore volume (-8%) at the radius and a 1% higher precision error for cortical thickness at the tibia. These results highlight challenges associated with automatically separating cortical from trabecular bone[182]. Specifically, in postmenopausal women, trabecularized cortices with large irregular cortical pores make it difficult to know what to include as cortical versus trabecular bone[4,51]. Previous research indicates that trabecularized cortical remnants are thicker and less organized compared to the trabecular bone network; however, the resolution of HR-pQCT is not sufficient enough to capture such subtleties[51,180]. Though, quantitative assessment of cortical micro-architecture will improve with advancements in HR-pQCT technology (e.g., XtremeCT II with 61µm voxel size) and with new techniques to optimize image analysis.

Cortical Outcomes Comparison: AUTO and MOD

In the group of postmenopausal women all cortical micro-architectural outcomes (except cortical thickness at the distal radius) differed between AUTO and MOD. The manually modified endocortical contour line at both the distal radius and tibia included a higher amount of bone and void (i.e., higher cortical bone volume and total volume), which resulted in a higher percentage of cortical pores, greater pore volume and diameter, leading to lower cortical BMD measures.

This is logical because with higher total volume more bone and void (pores) are included within the cortical envelope. Essentially, the manually modified contouring resulted in larger trabecularized cortex when compared to automatic contouring. This issue seems to pertain to more porous cortices since there were no differences in cortical bone micro-architecture outcomes between AUTO and MOD in young adults.

By comparing our results to previous findings using Synchrotron Radiation μCT (SR-μCT), manual modification of the endocortical contour appears to capture cortical properties more accurately than the automatic contour method, particularly when analyzing thin cortices with large and irregularly shaped cortical pores (as in postmenopausal women). These findings are supported by Ostertag and colleagues who reported differences in site-matched cortical micro-architecture outcomes from intact cadaveric tibiae between HR-pQCT and SR-μCT[180]. A comparison of *in vivo* HR-pQCT results from the distal tibiae of our postmenopausal women to those obtained with SR-μCT by Ostertag et al[180] suggests that the modified contour method with HR-pQCT images generate outcomes comparable to the data produced by SR-μCT. For instance, the average cortical pore diameter obtained from SR-μCT was 0.28 mm[180], which is closer to the modified contour method (0.24 mm) than the automatic method (0.20 mm). Jorgenson and colleagues recently reported a good agreement between HR-pQCT and SR-μCT derived cortical bone micro-architecture (R^2=0.977-0.983)[183]. It is unknown whether these results would be similar at the clinically relevant distal radius and this should be addressed in future research. However, it is worthwhile noting that while manual contouring may provide comparable results relative to higher resolution imaging (i.e., SR-μCT), these benefits may not outweigh the time required to obtain them. Therefore, it may be more feasible to use the AUTO

method with minor modification to the endocortical contour line where obvious and gross contour defects occur.

Study strengths pertain to study design and randomly selected study sample. First, repeat measurements of participants were obtained on separate days with a minimum of 24 hours between scans. This approach minimized precision error underestimation found when precision is calculated using scans repeated on the same day or without repositioning[159]. Second, we had sufficient number of participants in both groups to attain a minimum of 27 degrees of freedom required to achieve 90% confidence in our precision error estimate[12,149]. Third, based on femoral neck T-scores, 16% of our postmenopausal women had osteoporosis and 63% had osteopenia. These proportions are comparable to the osteoporosis reference standards from North America, Europe, Australia and Japan[161,162], thereby making our data generalizable to postmenopausal women in these regions.

Study limitations pertain to sample size. While our study included a random sample of older postmenopausal women, skeletal precision may vary according to disease status (e.g., osteoporosis vs osteopenia); this merits further investigation into population-specific precision studies. Further, our sample size was based on precision analysis and likely limited in our secondary comparisons of small between-method differences observed in young adults.

In summary, precision errors of cortical bone micro-architecture from high-resolution pQCT ranged from 1-16% did not differ between automatic or manually modified endocortical contour methods in postmenopausal women or young adults. Precision results suggest that both the automatic and manually modified endocortical contour method provide similar repeatability. In postmenopausal women, manual modification of endocortical contours led to generally higher

cortical bone properties when compared to the automated method, while no between-method differences were observed in young adults.

Bone mineral density, geometry and micro-architecture all provide indirect estimates of bone strength. However, when assessing fracture risk it would be advantageous to provide estimates in terms of force—particularly the force required to create a fracture. While the most direct way to determine this fracture force would be to break a bone, it is not ideal. Therefore, computer-based fracture simulation programs incorporating bone mineral density, geometry, and micro-architecture as well as bone material properties into bone strength estimates would be optimal. Finite element models are such programs

2.3 Bone Strength Estimates[6]

2.3.1 Introduction

Osteoporosis and related fractures are global public health concerns that currently affect 200 million people worldwide[95] and are a major cause of mortality, morbidity, chronic pain, and loss of independence[96]. Distal radius fractures are the most common fracture type occurring in postmenopausal women in North America and Europe[33,170-172]. Importantly, individuals who have suffered a distal radius fracture have greater risk of future osteoporotic wrist, hip and spine fractures[117,136,184]. Information regarding bone's ability to resist fracture (i.e., bone strength) and the factors underpinning bone strength are important in estimating wrist fracture risk.

Fractures occur when the load applied to bone exceeds bone's strength[185]. The gold standard to determine bone strength is direct mechanical testing to failure[112,186]; however, because of the destructive nature of this process, it is only done *ex vivo*. Finite element (FE) modeling is an engineering technique that can be applied to simulate mechanical testing in bone using inputted geometry, micro-architecture, and tissue material properties from computed tomographic (CT) images[6,112]. FE modeling has recently been integrated with high resolution peripheral quantitative computed tomography (HR-pQCT) to provide estimates of distal radius and tibia bone strength, tissue stiffness, as well as tissue-level stresses and strains[6].

Currently, there are 3 main types of (linear) FE models available using HR-pQCT: 1) homogeneous single-tissue model (STM) which models the distal radius or tibia as being comprised of empty voids and bone tissue with the same material stiffness (i.e., elastic modulus, E) for both cortical and trabecular bone[112]; 2) homogeneous dual-tissue model (DTM) which separates cortical and trabecular bone (as well as voids) using different E's for each bone

[6] **Manuscript submitted as:** Kawalilak CE, Kontulainen SA, Lanovaz JL, Amini MA, Johnston JD (2015). *In vivo* precision of three HR-pQCT-derived finite element models of the distal radius and tibia in postmenopausal women. *Bone*.

tissue[44]; and 3) a scaled model which links imaged bone mineral density (BMD) with E for each voxel via density-modulus E-BMD relationships[7].

Validation studies demonstrate close correlations between experimental findings and FE-derived bone failure load or ultimate stress (STM: R^2=0.66-0.94; E-BMD: R^2=0.95)[7,111,112,116] and stiffness (STM: R^2=0.97; E-BMD: R^2=0.98)[7]. These promising results offer great potential for HR-pQCT-derived FE assessments of wrist fracture risk in populations prone to osteoporotic fractures, such as postmenopausal women. While the validity of the STM and E-BMD models have been investigated, there is little known about the repeatability (or precision) of all three FE models (i.e., STM, DTM, and E-BMD).

In order to detect and monitor small changes in bone strength over time and assess intervention/treatment effects, high measurement precision is fundamental[9,12]. Other than the time period between repeat scans[159], factors that may affect precision at distal bone sites include: limb and reference line repositioning (quantified as scan common region)[10,166], and the degree of movement artifact (scan quality)[166,187]. To date, two precision studies report reproducibility for the STM of HR-pQCT-derived FE outcomes using cadaveric forearms[188] and young adults[157]. Cadaveric precision errors, reported as percent coefficient-of-variation (CV%), were 2.9% and 2.6% for stiffness and failure load, respectively[188]. Short-term *in vivo* precision errors, reported as root-mean-squared coefficient-of-variation ($CV\%_{RMS}$), were 2.0% and 2.5% for average von Mises stress at the radius and tibia, respectively[157]. Other commonly reported variables include apparent modulus, and percent load carried by the cortical and trabecular bone (*for DTM*) (Table 2.6)[7,30,32,40,44,94,111,112,155,157,166,174,188-192]; however, precision for these outcomes is unknown. Further, it remains unknown whether outcomes of the commonly used FE models are comparably repeatable—especially in postmenopausal women.

The primary objective of our study was to define and compare *in vivo* precision errors across 3 FE models (STM, DTM, scaled E-BMD) at the distal radius and tibia in postmenopausal women. Secondary objective was to determine the associations regarding time between follow-up scans, scan quality, and common region on precision errors of all outcomes for each of the 3 FE models.

2.3.2 Methods

2.3.2.1 Participants

Measurements were completed on a sample of 34 postmenopausal women (74±7 years) from the Saskatoon cohort of the Canadian Multi-centre Osteoporosis (CaM*os*) Study[1]. Postmenopausal status was assessed using a questionnaire[160]. Osteoporosis status was based on femoral neck (FN) T-scores obtained from the Saskatoon CaM*os* database[1,96]. Participant consent was attained prior to the study. This study was approved by the University of Saskatchewan Biomedical Research Ethics Board.

2.3.2.2 HR-pQCT Imaging

Repeat measurements were performed with an average 1 week (9.9±3.7 days) between baseline and follow-up. As per standard protocol, all participants had their non-dominant arm and ipsilateral leg immobilized in the manufacturer-provided cast during scanning[1]. At the distal radius and tibia, a standard 9.02 mm region of interest (110 parallel CT slices) was obtained using HR-pQCT (XtremeCT; Scanco Medical AG, Brüttisellen, Switzerland) with an isotropic voxel size of 82 μm[4]. The scan time was <2.8 minutes and the effective dose was <4 μSv per scan[4].

Table 2.6. Current literature using HR-pQCT finite element (FE) modeling for uniaxial compression simulations in elderly human; illustrating the type of FE model used, elastic modulus (E) used in the model, the reported outcomes, and the sites measured per study. Literature listed in chronological order by year.

Reference	FE Model[a]	Elastic Modulus (E)	Outcomes Reported	Site Measured
Pistoia et al. Bone **2002**; 30(6): 842-848.	STM	10 GPa	1. Failure Load (N)	Cadaver Radius
MacNeil et al. Med Eng and Phys **2007**; 29: 1096-1105.	STM	10 GPa	1. Reaction Load (N) 2. Strain Energy Density 3. Average von Mises Stress (MPa)	Cadaveric Radius (Cube Sample)
MacNeil et al. Med Eng and Phys **2008**; 30: 792-799.[b]	STM	Calculated[c]	1. Elastic Modulus ($CV\%_{RMS}$)[b] 2. Reaction Force ($CV\%_{RMS}$)[b] 3. Average von Mises Stress ($CV\%_{RMS}$)[b] 4. Strain Energy Density ($CV\%_{RMS}$)[b]	*In vivo* Radius and Tibia
MacNeil et al. Bone **2008**; 42: 1203-1213.	STM E-BMD	6829 MPa $E_{element} = 15004 \times (\rho/1200 \text{ mg HA/cm}^3)^{1.7}$	1. Apparent Bone Strength (Ultimate Stress) (GPa)	*In vivo* Radius
Boutroy et al. JBMR **2008**; 23(3): 392-399.	DTM	Cortical: 20 GPa Trabecular: 17.5 GPa	1. Stiffness (kN/mm) 2. % Load Carried by Each Tissue[d] 3. Average von Mises Stress for Each Tissue[d] (MPa)	*Iv vivo* Radius and Tibia
Mueller et al. Bone **2009**; 44: 364-371.	STM	10 GPa	1. Strength (N) 2. Stiffness (N/mm)	Cadaveric Radius

Dalzell et al. Osteoporos Int **2009**; 20: 1683-1694.	STM	10 GPa	1. Stiffness (N/mm) 2. Failure Load (N)	*In vivo* Radius and Tibia
Varga et al. J Biomech **2009**; 42: 1726-1731.	DTM	Cortical: 16.5 GPa Trabecular: 2974.0 MPa	1. Failure Load (N) 2. Stiffness (N/mm)	Cadaveric Radius
Burghardt et al. JBMR **2010**; 25(12): 2558-2571.	DTM	Cortical: 10 GPa Trabecular: 10 GPa	1. Stiffness (N/mm) 2. Apparent Modulus (N/mm^2) 3. Failure Load (N) 4. % Load Carried by Cortex	*In vivo* Radius and Tibia
Vilayphiou et al. Bone **2010**; 46: 1030-1037.	DTM	Cortical: 20 GPa Trabecular: 17 GPa	1. Failure Load (N) 2. Stiffness (kN/mm) 3. % Load Carried by Each Tissue[d] 4. Average von Mises stress for Each Tissue[d] (MPa)	*In vivo* Radius and Tibia
Varga et al. Bone. **2010**; 47: 982-988.	STM	15 GPa	1. Stiffness (kN.mm) 2. Failure Load (kN)	Cadavers Radius
Vilayphiou et al. JBMR **2011**; 26(5): 965-973.	DTM	Cortical: 20 GPa Trabecular: 17 GPa	1. Failure Load (N) 2. Stiffness (kN/mm) 3. % Load Carried by Each Tissue[d] 4. Average von Mises stress for Each Tissue[d] (MPa)	*In vivo* Radius and Tibia
Macdonald et al. JBMR **2011**; 26(1): 50-62.	STM	6829 MPa	1. Stiffness (N/mm) 2. Apparent Bone Strength (Ultimate Stress) (MPa) 3. Failure Load (N) 4. % Elastic Strain Energy Carried by Each Tissue[d]	*In vivo* Radius and Tibia

Varga et al. Biomech Model Mecahnobiol **2011;** 10: 431-444.	DTM	Cortical: 15 GPa Trabecular: 15 GPa	1. Stiffness (kN/mm) 2. Failure Load (kN) 3. Apparent Modulus (kN/mm^2) 4. % Load Carried by Each Tissue[d]	Cadaver Radius
Rizzoli et al. Osteoporos Int **2012**; 23: 305-315.	DTM E-BMD	Cortical: 20 GPa Trabecular: 17 GPa $E_{element}$ = 15004 x (ρ/900 mg HA/cm^3)$^{1.1}$	1. Failure Load (N) 2. Stiffness (kN/mm) 3. Average von Mises stress for Each Tissue[d] (MPa)	*In vivo* Radius and Tibia
Nishiyama et al. Osteoprosis Int **2012**; 24(5): 1733-1740	STM	6829 MPa	1. Apparent Bone Strength (Ultimate Stress) (MPa) 2. % Load Carried by Each Tissue[d]	*In vivo* Radius and Tibia
Ellouz et al. Bone **2014**; 63: 147-157	DTM	Cortical: 20 GPa Trabecular: 17 GPa	1. Stiffness (kN/mm) 2. Average von Mises stress (MPa) for Each Tissue[d] 3. % Load Carried by Each Tissue[d]	*In vivo* Radius and Tibia

[a] ***STM*** *= Single Tissue Model;* ***DTM*** *= Dual Tissue Model;* ***E-BMD*** *= Scaled model based on bone mineral density*

[b] *Results of this study only report long-term and short-term precision errors (CV%), but outcome values not reported.*

[c] *Elastic modulus (E) was calculated in this study based on the reaction force required to induce 1% strain over the average area of the slices within the section.*

[d] *"Each tissue" refers separately to the cortical and trabecular tissues.*

2.3.2.3 HR-pQCT Image Analysis

All images were graded for quality according to the manufacturer's 5 point scale[1,164]. Five radius and 2 tibia images with a quality of 4 or 5 were excluded from the study. In total, 27 radii and 32 tibiae were included in this current investigation.

Image analysis was completed according to the manufacturer's standard evaluation and dual-threshold evaluation protocols (Scanco Module 64-bit IPL V5.08b). Briefly, standard image evaluation was used to define the periosteal surface of the radius and tibia using a semi-automatic edge-finding algorithm in a slice-by-slice manner, as described elsewhere[1,4]. Modification of the periosteal contour line was done when it deviated from the outer bone surface. Once the standard evaluation was completed, the dual-threshold method was performed to separately define the cortical and trabecular bone tissues at both skeletal sites[5]. For the dual-threshold technique, the periosteal contour was imported from the standard evaluation image files and the endocortical contour was automatically created using a series of morphological operations (i.e., dilation and erosion) to separate the trabecular and cortical regions[5]. Modification of the endocortical contour line was done when it deviated from the endocortical surface, as previously described[2]. To separate bone from all other voxels (i.e., void, marrow, etc.), a set global threshold (400 mg HA/cm^3) was applied automatically by the software during image processing.

2.3.2.4 Finite Element (FE) Modeling

All 3 FE models (STM, DTM, E-BMD) had linear-elastic, isotropic material properties. They were generated and solved using the Image Processing Language (IPL; version 1.15) software provided by Scanco Medical. FE models were created by converting every voxel in the scanned volume of interest (VOI) into brick elements[6,193]. Image voxels in the VOI were converted to ~2.6 million brick elements at the radius and ~4.1 million brick elements at the tibia. Boundary

conditions were set to simulate a "high-friction" axial compression test applied to the distal surface of the bone VOI at 1% strain, with the proximal bone surface suppressed in all direction. High friction corresponds to the suppression of displacement in all directions at the proximal region of the bone, while displacement is suppressed in the *x* and *y* directions (but not *z* direction) at the distal region of the bone—where the bone is loaded in axial compression.

2.3.2.4.1 Single Tissue Model (STM)

The STM is a discrete homogeneous model where all the bone voxels are assigned to one tissue and given a user-defined E, in this case the standard E=10 GPa with Poisson's ratio = 0.3[6,112]. The segmented image file created from the standard outcome evaluation procedure (_SEG.AIM) was imported into the model. Segmentation, with manual contour correction, took ~30 minutes per radius or tibia. The STM solved in ~3 hours per radius scan and ~5 hours per tibia scan.

2.3.2.4.2 Dual Tissue Model (DTM)

The DTM is a discrete model with cortical and trabecular bone assigned their own tissues and given a user-defined E-value of 20 GPa (cortical tissue) and 17 GPa (trabecular tissue)[44,189]; Poisson's ratio was set to 0.3[6]. To identify cortical and trabecular bone tissue, the segmented image from the dual-threshold evaluation procedure were imported into the model (_COMBI.AIM). Segmentation, with manual contour correction, took $\leq$3 hours per radius image and $\leq$5 hour per tibia. The DTM solved in ~3 hours per radius scan and ~5 hours per tibia scan.

2.3.2.4.3 Density-Based (E-BMD) Model

The density-based E-BMD model is a scaled model where each element within the model was assigned E values based on the relative gray-value density of that element, as defined within the image[7,194]. Assigned E were based on the image-derived density (ρ) using a density-modulus equation (2.5) proposed by MacNeil and Boyd[7]:

$$E = 15{,}004\left(\frac{\rho}{1200}\right)^{1.7} \quad (2.5)$$

With this equation, individual E are scaled in relation to fully mineralized bone (ρ=1200 mg HA/cm^3) and the 15,004 and 1.7 terms have been derived from experimental testing[7]. Poisson's ratio was set to 0.3[6]. The unsegmented image file (.AIM) was imported into the model and a global threshold (400 mg HA/cm^3) was applied to remove the majority of the surrounding soft tissue. The scaled E-BMD model solved in ~5 hours per radius scan and ~10 hours per tibia scan.

The four primary outcomes for each model included: *bone stiffness* (kN/mm), calculated as the average reaction force divided by the applied displacement (0.0902 mm, corresponding to 1% strain with a 9.02 mm thick region); *apparent modulus* (MPa), calculated as reaction force divided by estimated cross-sectional area and a fixed known strain (1%); *average von Mises stress* (MPa); and *failure load* (kN), defined using the criterion developed by Pistoia et al[112] where fracture was assumed to occur when 2% of the bone tissue exceeded a critical (von Mises) strain limit of 7000 με. Of note, a critical strain limit of 3500 με was used with the DTM because E for cortical bone (E=20 GPa) was twice that used with the STM (E=10 GPa)[44]. We chose these 4 primary outcomes because they are the most commonly reported in the literature (Table 1) and common to all 3 FE models. Secondary outcomes included: the proportion of von Mises stress and the percentage of the ultimate failure load carried by the cortex and trabecular bone tissues (*DTM only*).

2.3.2.5 Statistical Analysis

We assessed the precision error of each outcome for all FE models by calculating root-mean-squared coefficients of variation (CV%) (equation 2.6)[1,12].

$$CV\%_{RMS} = \sqrt{\sum_{j=1}^{m}\left(\frac{\left(\frac{SD_j}{\bar{x}_j} x\ 100\%\right)^2}{m}\right)} \quad (2.6)$$

where SD_j was the standard deviation between the two measurements, x_j was the mean of the two measurements, and m was the number of participants in the analysis[12].

We compared individual CV% across the three FE models using multivariate analysis of variance (MANOVA) followed by pairwise comparison. MANOVA models were adjusted for multiple comparisons using Bonferroni correction. We performed Spearman correlation (ρ) to determine the associations regarding time between follow-up scans, scan quality, and common region on precision errors of all outcomes for each of the 3 FE models for the radius and tibia. Significance was set to $P<0.05$. All statistical analyses were performed using IBM SPSS commercial statistics software (PASW, Version 23 for Windows, SPSS Inc., Chicago, IL, USA).

2.3.3. Results

For each of the 3 FE models, mean (±SD) for outcome variables and CV% precision are summarized in Table 2.7 for the distal radius and in Table 2.8 for the distal tibia. For the primary outcomes at the distal radius, CV% precision for all models were <10% (Range STM: 2.8-5.3%; DTM: 3.0-5.4%; E-BMD: 2.6-8.7%). Generally, the lowest precision errors at the distal radius were noted for the STM, followed by the DTM, and then the E-BMD model (Table 2.7, Figure 2.4). At the distal tibia, the precision error for the primary outcomes was <5% (Range STM: 2.9-4.8%; DTM: 3.0-3.8%; E-BMD: 1.6-2.1%). The lowest precision errors for the primary outcomes at the distal tibia were for the E-BMD model, followed by the DTM, and then the STM (Table 2.8, Figure 2.5).

At the radius, precision for the main outcomes across all 3 FE models were different from one another (F=3.824, $P<0.001$). Apparent modulus differed between E-BMD model and STM (mean CV% difference$_{(\text{E-BMD} - \text{STM})}$: 3.4%, $P=0.010$), as well as between E-BMD and DTM (mean CV% difference$_{(\text{E-BMD} - \text{DTM})}$: 3.3%, $P=0.013$) (Figure 2.4, Table 2.7). Compared to STM and DTM, the scaled E-BMD model had significantly higher precision error for average von Mises stress (mean CV% difference$_{(\text{E-BMD} - \text{DTM/STM})}$: 3.3%, $P<0.001$) (Figure 2.4, Table 2.7). At the distal tibia, the precision for the main outcomes across all 3 FE models were not different from one another (F=1.511, $P=0.156$) (Figure 2.5, Table 2.8).

There were no associations regarding the time between follow-up scans and precision of main FE outcomes for any of the models at the radius and tibia ($P>0.05$). Similarly, there were no associations between scan quality and precision of main FE outcomes for any of the models at the radius and tibia ($P>0.05$). The only associations were for the E-BMD model between the common scan region and the precision of von Mises stress ($\rho=0.603$; $P=0.001$), apparent modulus ($\rho=-0.553$; $P=0.003$), and stiffness ($\rho=-0.422$; $P=0.028$) at the distal radius.

Table 2.7. Mean (±SD) of the baseline and follow-up scans, mean (±SD) of both measurements, root-mean-square precision error ($CV\%_{RMS}$) for stiffness, apparent stiffness, average von Mises stress, and failure load from 3 different FE models at the distal radius in postmenopausal women.

Radius (n=27)		**First Scan**	**± SD**	**Second Scan**	**± SD**	**Mean**	**± SD**	**$CV\%_{RMS}$**
Single Tissue Model (STM)								
Stiffness	*(kN/mm)*	57.2	± 11.7	56.1	± 11.7	56.6	± 11.7	3.4
Apparent Modulus	*(MPa)*	1296.3	± 340.2	1257.1	± 307.7	1276.7	± 320.6	5.3
Average von Mises Stress	*(MPa)*	5803.5	± 609.2	5695.5	± 585.3	5749.5	± 578.7	3.8
Failure Load	*(kN)*	2.835	± 0.543	2.784	± 0.547	2.809	± 0.543	2.8
Dual Tissue Model (DTM)								
Stiffness	*(kN/mm)*	106.8	± 22.3	105.2	± 22.3	106.0	± 22.2	3.3
Apparent Modulus	*(MPa)*	2428.5	± 652.3	2355.2	± 583.90	2391.9	± 611.6	5.4
Average von Mises Stress	*(MPa)*	108.1	± 12.2	106.2	± 11.5	107.2	± 11.5	3.8
Failure Load	*(kN)*	2.790	± 0.544	2.752	± 0.542	2.770	± 0.540	3.0
Cortical Bone								
Average von Mises Stress	*(MPa)*	153.5	± 7.9	152.2	± 7.4	152.8	± 7.5	1.5
% Minimum Load Carried	*(%)*	48.3	± 8.4	48.4	± 7.7	48.3	± 7.8	6.1
% Maximum Load Carried	*(%)*	77.6	± 9.0	77.8	± 8.9	77.7	± 8.8	2.2
Trabecular Bone								
Average von Mises Stress	*(MPa)*	76.6	± 12.1	74.4	± 11.9	75.5	± 11.4	6.7
% Minimum Load Carried	*(%)*	51.8	± 8.4	51.6	± 7.7	51.7	± 7.8	7.1
% Maximum Load Carried	*(%)*	22.4	± 9.0	22.2	± 8.9	22.3	± 8.8	9.5
Scaled E-BMD Model								
Stiffness	*(kN/mm)*	41.1	± 12.6	40.6	± 12.0	40.8	± 12.2	4.4
Apparent Modulus	*(MPa)*	595.2	± 215.1	583.7	± 184.1	589.4	± 196.0	8.7

Average von Mises Stress	*(MPa)*	13.2	± 4.0	13.0	± 3.4	13.1	± 3.6	7.1
Failure Load	*(kN)*	2.99	± 0.44	3.00	± 0.47	2.99	± 0.45	2.6

Table 2.8. Mean (±SD) of the baseline and follow-up scans, mean (±SD) of both measurements, root-mean-square precision error ($CV\%_{RMS}$) for stiffness, apparent stiffness, average von Mises stress, and failure load from 3 different FE models at the distal tibia in postmenopausal women.

Tibia (n=32)		**First Scan**	**± SD**	**Second Scan**	**± SD**	**Mean**	**± SD**	**$CV\%_{RMS}$**
Single Tissue Model (STM)								
Stiffness	*(kN/mm)*	172.7	± 33.7	173.1	± 34.1	172.9	± 33.7	3.7
Apparent Modulus	*(MPa)*	1896.8	± 375.2	1908.3	± 374.3	1902.5	± 372.0	4.0
Average von Mises Stress	*(MPa)*	6659.4	± 578.2	6680.9	± 543.1	6670.1	± 513.6	4.8
Failure Load	*(kN)*	8.234	± 1.524	8.248	± 1.540	8.241	± 1.525	2.9
Dual Tissue Model (DTM)								
Stiffness	*(kN/mm)*	316.1	± 60.9	317.2	± 61.8	316.6	± 61.0	3.4
Apparent Modulus	*(MPa)*	3477.5	± 685.3	3500.6	± 685.3	3489.1	± 680.7	3.8
Average von Mises Stress	*(MPa)*	120.6	± 10.2	120.9	± 9.4	120.7	± 9.3	3.8
Failure Load	*(kN)*	8.232	± 1.540	8.244	± 1.554	8.240	± 1.540	3.0
Cortical Bone								
Average von Mises Stress	*(MPa)*	166.4	± 5.4	166.6	± 5.6	166.5	± 5.5	0.8
% Minimum Load Carried	*(%)*	41.5	± 9.1	41.9	± 9.7	41.7	± 9.4	3.5
% Maximum Load Carried	*(%)*	61.6	± 9.9	61.8	± 10.2	61.7	± 10.0	2.1
Trabecular Bone								
Average von Mises Stress	*(MPa)*	97.9	± 11.6	97.8	± 11.4	97.9	± 10.8	5.9

% Minimum Load Carried	*(%)*	58.5	± 9.1	58.2	± 9.7	58.3	± 9.4	2.6
% Maximum Load Carried	*(%)*	38.4	± 9.9	38.2	± 10.2	38.3	± 10.0	3.5
Scaled E-BMD Model								
Stiffness	*(kN/mm)*	118.7	± 27.8	118.7	± 27.5	118.8	± 27.6	2.1
Apparent Modulus	*(MPa)*	910.6	± 223.7	912.8	± 224.9	911.7	± 224.0	1.8
Average von Mises Stress	*(MPa)*	16.7	± 3.3	16.8	± 3.2	16.7	± 3.2	2.0
Failure Load	*(kN)*	7.82	± 1.37	7.81	± 1.34	7.81	± 1.35	1.6

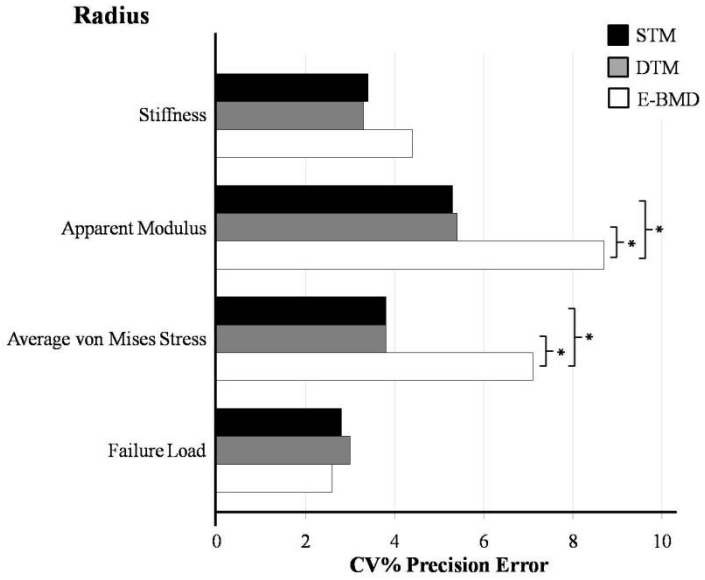

Figure 2.4. Comparison of root-mean-square precision errors (CV%) for tissue stiffness, apparent modulus, average von Mises stress, and failure load in postmenopausal women at the distal radius. * *Significant at P<0.05.*

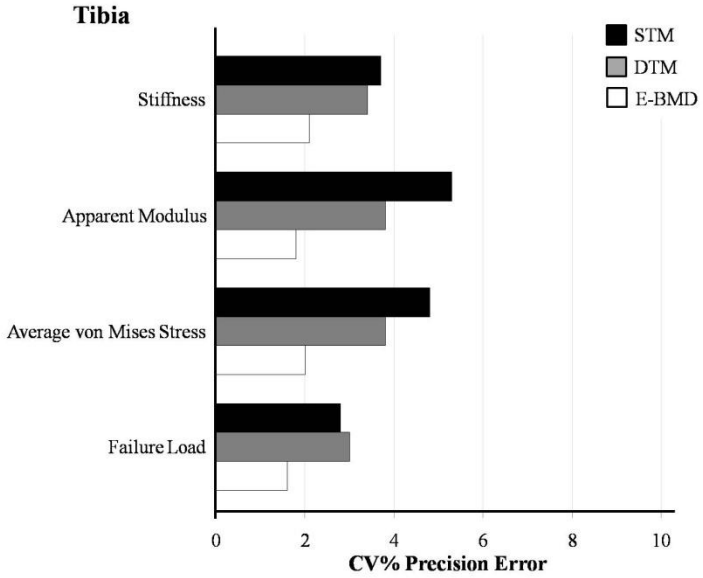

Figure 2.5. Comparison of root-mean-square precision errors (CV%) for tissue stiffness, apparent modulus, average von Mises stress, and failure load in postmenopausal women at the distal tibia.

2.3.4. Discussion

The primary objective of our study was to define and compare *in vivo* precision errors for 3 FE models (2 homogeneous and 1 scaled) using postmenopausal women. Precision error was significantly higher for apparent modulus and average von Mises stress using the scaled E-BMD model at the distal radius. At the distal tibia, however, all models had comparable outcomes. Reported *in vivo* precision errors at the radius for STM and DTM, but not E-BMD, were comparable to those reported in cadaveric forearms (CV%: Failure Load: 2.6%; Stiffness: 2.9%)[188] as well as previous *in vivo* precision at the radius ($CV\%_{RMS}$: Average von Mises stress: 2.0%)[157]. Our *in vivo* precision error at the tibia for average von Mises stress using E-BMD, but not STM or DTM, was more comparable to those previously reported ($CV\%_{RMS}$: 2.5%)[157].

The secondary objective of our study was to determine the associations regarding time between follow-up scans, scan quality, and common region on precision errors of all outcomes for each of the 3 FE models. Results indicated that the noted differences in precision errors at the radius were strongly associated with the common scan region. It is likely that this relationship was not found at the tibia because the common region was higher at this site. The common region for the distal radius was 93% (range: 81-99%) with an average absolute slice shift of 7.0 (SD 4.8) between successive scans, whereas at the distal tibia, the common region was 97% (range: 88-99%) with an absolute average slice shift of 2.9 (2.6)[1]. Previous research has suggested that even small rotation angles can lead to considerable variance in the scan region[166]. While the use of the CSA registration within the HR-pQCT software aids in the correction of axial misplacement between baseline and follow-up scans, it does not account for possible 3D misalignments in the limb within the cast[166]. The arm cast allows for the possibility of more rotation at the wrist, while it is easier to consistently place the leg within the leg cast. The compounded effect of reference line inconsistencies between successive scans also affects the

common region. This illustrates the importance of repositioning (both the limb in the cast and the reference line).

Superficially, the STM has the shortest total analysis time (i.e., image segmentation and FE analysis) per scan for both the radius (3.5 hours) and tibia (5.5 hours). The DTM and the E-BMD model, however, have approximately equal per scan analysis times at both sites (radius: 5 hours; tibia: 9-10 hours); though, the E-BMD model does not require invested manual time in the segmentation part of the analysis because it uses the unsegmented files—effectively resulting in overall time and cost savings.

Our study design and study cohort had strengths that warrant consideration. First, repeat measurements were separated by an average of 1 week—an important condition because underestimation of precision error has been reported when precision is calculated using scans repeated on the same day[159]. Second, our study contained enough repeat scans which provides the recommended 27 degrees of freedom necessary to establish reliable precision errors with an upper 90% confidence limit[12,149]. Third, the reported bone health status of our sample of postmenopausal women was comparable to their peers in North America, Europe, Australia and Japan[1,161,162], thereby suggesting our data to be generalizable to postmenopausal women in these regions.

Limitations associated with this study pertain to our study sample and sample size. First, although we studied older postmenopausal women, skeletal precision may vary according to duration of menopause, time from menopause, and disease status—this merits further investigation into population-specific precision studies. Second, our sample size, while sufficient to obtain the required degrees of freedom for accurate precision error estimates, limited assessing the possible role of osteoporosis status in the comparisons.

In summary, the STM and DTM models appeared more precise for modeling the distal radius whereas all methods provided comparable precision for modeling the distal tibia. Results suggest that the E-BMD model could be used when the common region between follow-up scans is high (≥93%), while STM or DTM should be considered when the common region is lower (<93%).

The precision of bone strength estimates has been defined using bone density, geometry, and micro-architecture indirectly through the use of the standard HR-pQCT evaluation (trabecular bone) and the dual-threshold technique (cortical bone), as well as through the application of FE modeling. Now the question become, "how can clinicians and researchers apply this precision information?" While the answer may seem simple—*precision information will assist when planning to monitor or when interpreting change within these outcomes*—there still remains the methodological question of *how?*

3 STUDY 2: MONITORING SKELETAL CHANGES

SYNOPSIS: How do researchers and clinicians know whether actual skeletal change has occurred for their patients'? Is meaningful change merely having statistically significant differences between follow-up measures? What is the time interval required to guarantee change can be captured without unnecessary testing to the patient? The aim of this study is to define the least significant change (LSC) and the monitoring time interval (MTI)—tools that will facilitate the answering of these questions.

3.1 LSC and MTI for HR-pQCT[7]

3.1.1 Introduction

The advent of high-resolution peripheral quantitative computed tomography (HR-pQCT) has enabled the measurement of 3D micro-architectural properties at the distal tibia and fracture-prone distal radius. Importantly, fragility fractures at the distal radius are a sentinel for future fragility fractures at other sites[117,118]. Further, because the tibia is a weight-bearing skeletal site, it may reflect bone strength at other weight-bearing sites, such as the hip and vertebrae[41]. As such, HR-pQCT is an important tool for advancing our understanding of osteoporosis-related bone deterioration and for providing new targets for investigations and strategies aiming to optimize osteoporotic fracture prevention.

Measuring and monitoring minute skeletal changes over time using any imaging modality requires a high degree of measurement precision or repeatability (i.e., low precision error) to ensure measurement sensitivity to capture changes and treatment effects[12]. There are several

[7] **Published as:** Kawalilak CE, Johnston JD, Olszynski WP, Kontulainen SA (2015). Least significant changes and monitoring time intervals for high-resolution pQCT-derived bone outcomes in postmenopausal women. *Journal of Musculoskeletal and Neuronal Interactions, 15*(2):190-196.

reports of HR-pQCT short-term precision in young adults[1,29,157], postmenopausal women[1,195], and mixed age cohort[13] (Table 3.1). Two studies reported long-term precision in young adults and postmenopausal women[46,157] (Table 3.1). The International Society for Clinical Densitometry (ISCD) recommends estimating the least significant change (LSC) to determine if true skeletal change has occurred[149]. LSC is estimated based upon measurement error (estimated via root-mean-squared coefficient of variation ($CV\%_{RMS}$) precision errors) and an adjusting Z-score derived from the selected level of statistical confidence (typically two-tailed 95% confidence, with a Z-score of 1.96 used in the equation $LSC = 2.77 \times CV\%_{RMS}$). LSC essentially serves as a quantitative metric for ensuring (with a certain level of statistical confidence) that observed differences or changes are sufficiently larger than precision errors associated with a technique. Currently, the only available LSC data for HR-pQCT reports estimated LSC values which ranged from 1-40% for bone micro-architectural outcomes at the distal radius and tibia[46]. These estimates, however, need to be interpreted with caution as the LSCs were calculated using long-term precision estimates from postmenopausal women with and without fractures and osteoporosis medication[12,150]. Long-term precision estimates determined using follow-up data 1 year from baseline incorporate both precision error and non-linear skeletal changes, thereby obfuscating the measurement's actual precision[12]. Further, measurement precision should be applicable to the group being studied, such as postmenopausal women without fracture history[12].

To facilitate the design of therapeutic interventions and longitudinal follow-up studies in postmenopausal women[94,196,197], information of the LSC, together with the information of median annual changes, can be used to estimate a monitoring time interval (MTI) between HR-pQCT measurement occasions[9,149]. MTIs provide a time estimate (in years) to reliably measure

bone change[9,10,151], thereby allowing follow-up measures to be performed within the optimal window for capturing true skeletal change, as well as minimizing patient radiation exposure and costs associated with repeated scanning in prospective studies. To our knowledge, there have been no reported MTIs for bone parameters using HR-pQCT in postmenopausal women.

The first objective of our study was to define the LSC using short-term precision data in postmenopausal women. Our second objective was to define MTIs for HR-pQCT derived bone area, density, and micro-architecture in postmenopausal women.

Table 3.1. Literature reporting *in vivo* precision using high-resolution peripheral quantitative computed tomography (HR-pQCT), with breakdown of precision dependent components including: type of precision, participant number and degrees of freedom, age, follow-up criteria, method used in determining precision error, and reported precision results.

	***In vivo* Precision**						
Reference	**Type of Precision**	**Participant Number (Degrees of Freedom)**[†]	**Age (years)**	**Follow-up Criteria**	**Method of Determining Precision Error**	**Precision Results**	
Boutroy et al (2005).[29]	Short-term Precision	15 F Radii and Tibiae (30)	21-47	3 Scans within 1 month[§]	Gluer et al (1995)[12]: $CV\%_{RMS}$	*Radius:* Densities: 0.9-1.5% Micro-architecture: 0.9-4.4%	*Tibia:* Densities: 0.9-1.5% Micro-architecture: 0.9-4.4%
Kazakia et al (2008).[13]	Short-term Precision	8 Radii[‡] (16) 7 Tibiae[‡] (14)	25-65 29-73	3 Scans[§]	Not Specified: CV%	BV/TV: 1.2% Micro-architecture: 1.0-5.8%	
MacNeil & Boyd (2008).[157]	Short-term Precision	14 M (14) 15 F (15)	20-37 20-40	2 Scans within 1 week	Not Specified: $CV\%_{RMS}$	*M -Radius:* Densities:0.3-0.7% Micro-architecture: 0.6-4.4% *F - Radius:* Densities: 0.4-0.5% Micro-architecture: 0.5-3.4%	*M - Tibia:* Densities: 0.2-0.5% Micro-architecture: 0.5-3.6% *F - Tibia:* Densities: 0.6-1.0% Micro-architecture: 0.8-4.0%
Kawalilak et al (2013).[Study 1]	Short-term Precision	*Young Adult*: 28 F Radii (28) 32 F Tibiae (32) *Postmenopausal Women:* 29 M and F Radii (29) 30 M and F Tibiae (30)	19-48 19-48 62-88 62-88	2 Scans on 2 separate days within 24 hours 2 Scans within 1 week	Gluer et al (1995)[12]: $CV\%_{RMS}$	*Young Adult Radius:* Area: 0.6-3.1% Densities: 0.8-1.6% Micro-architecture: 0.9-8.0% *Postmenopausal Radius:* Area: 0.4-2.9%	*Young Adult Tibia:* Area: 0.2-0.9% Densities: 0.4-1.4% Micro-architecture: 0.9-5.0% *Postmenopausal Tibia:* Area: 0.1-1.1%

						Densities: 1.1-2.1% Micro-architecture: 1.2-6.5%	Densities: 0.3-1.9% Micro-architecture: 1.3-6.8%
Wong et al (2014) (Part I).[195]	Short-term Precision	31 M and F Radii and Tibiae (31)	20-69	2 Scans repeated within same day	Gluer et al (1995)[12]: $CV\%_{RMS}$	*Radius:* Densities: 0.5-0.7% Micro-architecture: 0.7-4.8%	*Tibia:* Densities: 0.2-0.4% Micro-architecture: 0.4-4.1%
MacNeil & Boyd (2008).[157]	Long-term Precision	14 M (14) 15 F (15)	20-37 20-40	2 Scans within 4 months	Langton & Njeh (2004)[150]: SEE	*M -Radius:* Densities:0.3-0.7% Micro-architecture: 0.6-3.9% *F - Radius:* Densities: 0.3-0.5% Micro-architecture: 0.5-3.2%	*M - Tibia:* Densities: 0.3-0.5% Micro-architecture: 0.4-3.4% *F - Tibia:* Densities: 0.5-1.0% Micro-architecture: 0.8-3.8%
Wong et al (2014) (Part II).[46]	Long-term Precision	*All Participants:* 38 F Radii (38) 38 F Tibiae (38) *Non-fracture, Non-medicated:* 13 F Radii (13) 13 F Tibiae (13)	61-89 63-81	2 Scans repeated within 1 year	Gluer et al (1995)[12]: SEE	*All Participants Radius:* Densities: 1.9-2.5% Micro-architecture: 2.6-6.2% *Non-fracture, Non-medicated Radius:* Densities: 1.7-2.5% Micro-architecture: 1.7-6.8%	*All Participants Tibia:* Densities: 1.1-1.9% Micro-architecture: 2.0-7.7% *Non-fracture, Non-medicated Tibia:* Densities: 0.7-0.9% Micro-architecture: 1.0-8.1%

Abbreviations: ***M*** *= Male;* ***F*** *= Female;* $\boldsymbol{CV\%_{RMS}}$ *= Root-mean-squared percent coefficient of variation;* ***SEE*** *= Standard Error of the Estimates*

† *Degrees of Freedom = m·(n-1) where m=number of subjects, n = repeat measures; equation from Gluer et al. (1995)*[12]

§ *Time between scans not specified*

‡ *Sex not specified*

3.1.2 Methods

3.1.2.1 Participants

In 2011, 104 community-dwelling postmenopausal women (mean age ± standard deviation: 75±8 years), who were a part of the Saskatoon cohort of the Canadian Multi-centre Osteoporosis (CaM*os*) Study, enrolled to receive HR-pQCT measurements. Approximately 1 year later (410±54 days; 2012-2013), fifty-one women (78±7 years) returned for follow-up HR-pQCT measurements. There were no differences in osteoporosis status or HR-pQCT outcomes at baseline between the women who returned and those who did not return for follow-up measures (*Appendix A*). We excluded 18 women who were using hormone replacement therapy or bisphosphonates. Thirty-three women (77±7 years) were included in this study. Postmenopausal status was determined by a questionnaire and defined as not menstruating for at least 12 months[160]. Osteoporosis status was based on DXA-derived femoral neck (FN) T-scores obtained from the Saskatoon CaM*os* database (Table 3.2)[96]. Of the participants not using bone altering medication, 33% had normal FN T-Scores, 52% were osteopenic, and 15% had osteoporosis (Table 3.2). Participant consent was obtained prior to the study. This study was approved by the University of Saskatchewan Biomedical Research Ethics Board.

Table 3.2. Participant demographics including the number (n) and proportion (%) of participants with osteopenia or osteoporosis at the baseline.

(n = 33)	**Minimum**	**Maximum**	**Mean ± SD**
Age *(years)*	62	88	77 ± 7
Height *(cm)*	147.9	177.6	160.3 ± 5.9
Weight*(kg)*	54.5	101.5	73.5 ± 12.8
DXA Measures			
FN aBMD (g/cm^2)	0.4	1.1	0.7 ± 0.1
FN T-score	-3.5	2.0	-1.2 ± 1.1
Osteoporosis Status	**n (%)**		
Normal	11 (33%)		
Osteopenia	16 (49%)		
Osteoporosis	6 (18%)		

3.1.2.2 HR-pQCT Imaging

The non-dominant arm and ipsilateral leg of all participants were immobilized in the standard carbon fiber cast prior to imaging, as per the manufacturer's standard *in vivo* protocol. A scout view scan was used to set the reference line and define the volume of interest for each scan, further defined elsewhere[1]. Using HR-pQCT (XtremeCT; Scanco Medical AG, Brüttisellen, Switzerland) we obtained a 9.02 mm region of interest (110 parallel CT slices) located 9.5 mm (radius) and 22.5 mm (tibia) proximal to the reference line. Using the standard *in vivo* imaging protocol, an isotropic voxel size of 82 μm was used to collect our data. The effective dose was <4 μSv[1]. Measurement time was approximately 2.8 minutes for each scan[1].

3.1.2.3 HR-pQCT Image Analysis

One operator (CK) scanned, graded, and analyzed all images. Based on the 5 point image grading scale, all images with a quality of 4 and 5 were deemed unacceptable and removed from the study without further analysis[163,164]. We included scans of grade quality 1-3.

Image analysis was completed according to the manufacturer's standard *in vivo* evaluation protocol, described in detail elsewhere[1]. Briefly, we outlined the periosteal surface of the bone of interest (i.e., radius or tibia) to separate the bone from the surrounding soft tissue. A semi-automatic edge-finding algorithm was used to detect the periosteal bone surface and facilitated the contour iteration process from the first slice through the subsequent 109 slices in a slice-by-slice manner. For every slice the contour line was examined and adjustments were manually made to correct the line when it strayed from the periosteal surface of the bone. We analyzed standard HR-pQCT outcome variables[1]. Bone area outcomes were: cortical and trabecular area. Bone density outcomes were: total, cortical, and trabecular bone densities (including: meta and inner densities). Bone micro-architecture outcomes were: cortical thickness (*CtTh*), bone volume fraction (*BV/TV*), trabecular number (*TbN*), trabecular thickness (*TbTh*),

trabecular separation (*TbSp*), and trabecular heterogeneity (*TbSpSD*). The methods to define these outcome variables are described elsewhere[14,25,167,168,198].

3.1.2.4 Statistical Analysis

We determined the LSC, median annual percent change, and MTI. As the LSC calculation requires $CV\%_{RMS}$, short-term $CV\%_{RMS}$ precision errors were first obtained from repeated measures of the 32 postmenopausal women, reported earlier[1]. This sample size provided 32 degrees of freedom (DOF), which exceeded Glüer's recommendation of 27 DOF required to establish reliable precision errors with an upper 90% confidence limit less than 30% (e.g., if the precision error is 2%, we are 90% confident that the true precision error is less than 2.6%)[12]. $CV\%_{RMS}$ was calculated using the following equations:

$$CV\%_j = \left(\frac{SD_j}{\bar{x}_j}\right) x\ 100\% \quad (3.1)$$

$$CV\%_{RMS} = \sqrt{\sum_{j=1}^{m} \frac{CV\%_j^2}{m}} \quad (3.2)$$

Where *j* refers to an individual participant, SD_j is the standard deviation between the baseline and follow-up measurements (for that individual participant), $\bar{x}_j$ is the mean of these two measurements, and *m* is the total number of participants in the analysis[12].

LSC was then calculated as follows:

$$\mathrm{LSC}_{(1x1)} = \mathrm{Z\ x\ CV\%_{RMS}} \sqrt{\frac{1}{n_1} + \frac{1}{n_2}} = \ 2.77\ \mathrm{x\ CV\%_{RMS}} \quad (3.3)$$

Where *(1x1)* indicates that we performed 1 measurement at each visit (i.e., baseline and follow-up); Z-score corresponds a two-tailed 95% confidence level (Z=1.96), while $n_1$and n_2 are the number of measures performed at baseline (n_1=1) and follow-up (n_2=1), respectively[10].

The median annual percent change was determined using the median difference in bone measures between baseline and 1 year follow-up, expressed in relation to the baseline measurement.

MTI was defined as the ratio of LSC to median annual percent change, and specifies the period after which half the participants demonstrate a measured change exceeding the LSC[9,10,151]. We calculated MTI using the following equation, defined by Glüer[9]:

$$MTI = \frac{LSC}{Median\ Annual\ Percent\ Change} \quad (3.4)$$

3.1.3 Results

3.1.3.1 Least Significant Change (LSC)

At the distal radius, trabecular area, bone volume fraction, and all density measures had LSC values that were <6.0% (range: 1.1-5.9%; Table 3.3). LSCs for distal radius cortical area and micro-architecture (excluding bone volume fraction) were >8.0% (range: 8.1-18.2%; Table 3.3). At the distal tibia, all area and density measures, as well as cortical thickness and bone volume fraction had LSC values that were <5.5% (range: 0.3-5.3%; Table 3.3). Distal tibia micro-architecture measures (excluding bone volume fraction) had LSC values that were >17% (range: 17.4-19.0%; Table 3.3).

3.1.3.2 Monitoring Time Interval (MTI)

At the distal radius, all area and density measures exhibited MTIs >3.7 years (Table 3.3). MTIs for density measures ranged from 3.9 years (total density) to 29.5 years (inner trabecular density) (Table 3.3). MTIs for micro-architectural measures were ~2 years for trabecular number (TbN), thickness (TbTh), separation (TbSp) and heterogeneity (TbSpSD) (Table 3.3). The MTI for distal radius cortical thickness was 4.4 years.

At the distal tibia, all area measures exhibited MTIs of ~1 year (Table 3.3). MTIs for density measures ranged from 0.5 years (cortical density) to >7.8 years (all trabecular density variables) (Table 3.3). MTIs for micro-architectural measures were >6 years for trabecular number (TbN), thickness (TbTh), separation (TbSp) and heterogeneity (TbSpSD) (Table 3.3). The MTI for distal tibia cortical thickness was 1.3 years.

Table 3.3. Mean±SD of combined baseline and follow-up measures, median annual percent change, Least Significant Change (LSC; *2.77*CV%$_{RMS}$*), and the Monitoring Time Interval (MTI; *LSC/median change*) for the bone outcomes at the distal radius and distal tibia.

		Mean of Both Measures	± SD	Median Annual Percent Change (%)	LSC (%)	MTI (Years)
Radius (n=31)						
Area						
Cortical	*(mm^2)*	38.7	± 13.3	-1.1	8.1	7.4
Trabecular	*(mm^2)*	239.2	± 46.0	0.3	1.1	3.7
Density						
Total	*(mg HA/cm^3)*	248.7	± 55.1	-1.0	3.9	3.9
Cortical	*(mg HA/cm^3)*	771.6	± 84.2	-0.5	3.1	6.2
Trabecular	*(mg HA/cm^3)*	134.1	± 44.4	-0.2	3.4	17.0
Meta	*(mg HA/cm^3)*	188.8	± 39.4	-0.6	4.5	7.5
Inn	*(mg HA/cm^3)*	96.2	± 49.8	-0.2	5.9	29.5
Micro-architecture						
CtTh	*(μm)*	533.6	± 188.1	-2.0	8.7	4.4
BV/TV	*(%)*	11.2	± 3.7	0.0	3.4	∞
TbN	*(1/mm)*	1.8	± 0.5	-8.3	16.8	2.0
TbTh	*(μm)*	63.6	± 10.1	6.8	15.1	2.2
TbSp	*(μm)*	598.5	± 397.0	9.0	17.1	1.9
TbSpSD	*(μm)*	361.9	± 352.8	10.5	18.2	1.7
Tibia (n=32)						
Area						
Cortical	*(mm^2)*	78.3	± 27.5	-3.6	3.1	0.9
Trabecular	*(mm^2)*	644.7	± 100.9	0.3	0.3	1.0
Density						
Total	*(mg HA/cm^3)*	236.9	± 52.7	-1.4	2.5	1.8
Cortical	*(mg HA/cm^3)*	750.7	± 72.3	-1.7	0.8	0.5

Trabecular	*(mg HA/cm^3)*	158.8	± 39.0	-0.1	3.6	36.0
Meta	*(mg HA/cm^3)*	265.1	± 32.5	-0.4	3.1	7.8
Inn	*(mg HA/cm^3)*	110.4	± 45.0	0.1	5.3	53.0
Micro-architecture						
CtTh	*(μm)*	733.9	± 264.5	-3.1	3.9	1.3
BV/TV	*(%)*	13.3	± 3.3	0.0	3.6	∞
TbN	*(1/mm)*	1.8	± 0.4	2.0	18.8	9.4
TbTh	*(μm)*	76.8	± 15.3	-2.9	17.4	6.0
TbSp	*(μm)*	544.1	± 251.6	-2.1	19.0	9.0
TbSpSD	*(μm)*	342.7	± 437.5	-1.5	17.4	11.6

3.1.4 Discussion

The first objective of our study was to define the LSC using short-term precision data in postmenopausal women. These are the first reported LSCs using HR-pQCT measurements for postmenopausal women derived from short-term precision data with adequate degrees of freedom[1]. Generally, bone area and density measures, as well as bone volume fraction, tended to have lower LSCs (i.e., <6.0%) when compared to micro-architectural measures (LSCs >8.0%).

The second objective of our study was to define the MTI required to observe true change in bone properties in postmenopausal women using HR-pQCT. To our knowledge, these are the first MTIs for HR-pQCT derived bone properties. Obtained MTIs suggest that: a) changes in distal radius trabecular bone micro-architecture can be measured within ~2 years, and b) changes in distal tibial cortical area, density and thickness, as well as trabecular area, can be measured within ~1 year. Conversely, measuring change of distal radius cortical bone properties and distal tibia trabecular micro-architectural properties require longer monitoring times in postmenopausal women (>6 years).

Bone properties with short MTIs had either low precision errors (consequently low LSC) and/or large median annual changes; the opposite seemed to explain long MTIs. For instance, our

precision error (expressed as $CV\%_{RMS}$) for trabecular area at the radius was a low 0.4%[1], and though the median change was also low at 0.3% per year, the resulting MTI was 3.7 years. Alternatively, the MTIs for micro-architectural measures at the distal radius exhibited smaller MTIs of ~2 years for trabecular number (TbN), thickness (TbTh), separation (TbSp) and heterogeneity (TbSpSD). These short MTIs may be explained by the observed median annual changes ranging from -8 to 11%, despite of 4-7% precision error in the same outcomes[1]. Longer MTIs (especially for trabecular density and bone volume fraction) appeared to reflect a low (<1%) annual percent change observed in this cohort of older postmenopausal women. For example, bone volume fraction, which had an infinite MTI, was due to near zero median annual percent change. The longer MTIs may also be due to the image processing algorithms used with HR-pQCT to register (match) repeated scans, as well as scan quality. HR-pQCT uses area measures to matches image slices acquired at different time points. With this approach, images that have larger common region between measurement times will have more accurate representation of the true change because of the reduced influence of error (e.g., unequal slice comparison). Similarly, images that are graded as better quality will also have a more accurate representation of true change due to the reduced influence of movement artifacts and associated errors. Importantly, when compared to the distal radius, the distal tibia scans tended to be more easily landmarked resulting in more shared common region between baseline and follow-up images (radius common region mean: 91±7%; tibia common region mean: 96±2%) and had higher scan quality (radius scan quality grades: 1-3; tibia scan quality grades: 1-2)—likely explaining shorter MTIs for distal tibia outcomes.

This study has strengths and limitations that warrant some consideration. Study strengths pertain to participants pool from a population-based cohort of community-dwelling

postmenopausal women[160]. Given the proportionally similar osteopenia and osteoporosis bone health status within our sample relative to postmenopausal women in North America, Europe, Australia, and Japan[162], we anticipate that the observed bone changes and MTIs can be generalized to postmenopausal women of similar ages in these regions. Further, both LSC and median annual percent changes were derived from the same sample by the same operator using the same scanner, thereby minimizing measurement variability and resulting to accurate time interval predictions. With regards to study limitations, our findings were restricted to the monitoring of bone changes in a small sample of postmenopausal women over 1 year. Multiple measurement years in a larger sample may provide a more representative estimates of the annual rates of skeletal changes and associated MTIs[9]. Further, skeletal changes may vary according to the cohort's age, ethnicity, disease status, and sex; therefore, monitoring disease progression and skeletal changes associated with intervention will likely require population-specific MTIs[9].

The results of this HR-pQCT study suggest that, for the distal radius, MTIs of ~2 years duration are required in order to have skeletal changes exceeding the LSC for micro-architectural parameters (trabecular number, thickness, separation and heterogeneity). At the distal tibia, MTIs of ~1 year duration are required in order to have skeletal changes exceeding the LSC for cortical area, density and thickness, as well as trabecular area. HR-pQCT derived MTIs warrant consideration when designing and interpreting prospective studies and interventions in postmenopausal women.

To date, there are numerous HR-pQCT studies available characterizing the effect of age on skeletal mass, geometry, and micro-architecture using cross-sectional evidence[29-35], and only one prospective study to illustrate change[14]. However, Laib et al (1998)[14] used the prototype HR-pQCT scanner; therefore, it would be inappropriate to apply the provided LSC and MTIs to

this published change information. Consequently, there is need for a prospective follow-up study using the standard HR-pQCT in order to demonstrate the use of the above LSC and MTI statistics as they pertain to skeletal change. The following chapter will provide this necessary information.

4 STUDY 3: CHARACTERIZING SKELETAL CHANGES

SYNOPSIS: Understanding how bone density, geometry, and micro-architecture change with age can improve osteoporosis prevention, diagnosis, and treatment options. Research has provided us with DXA-derived measures of how bone density changes. However, there is still need for longitudinal research to characterize how bone geometry and micro-architecture change with age—especially in postmenopausal women. The aim of this study is to characterize changes in bone density, geometry, and micro-architecture in postmenopausal women over 1 year.

4.1 Characterizing Micro-architectural Changes Using HR-pQCT[8]

4.1.1 Introduction

Osteoporosis has been clinically defined as a multi-factorial disease characterized by low bone mass and the deterioration of bone micro-architecture, leading to bone fragility and a subsequent increase in fracture risk[15]. Areal bone mineral density (aBMD) measured using dual-energy x-ray absorptiometry (DXA) is the gold-standard imaging modality for diagnosing and monitoring osteoporosis[161]. However, 50-60% of fragility fractures are sustained by women who are above the World Health Organization (WHO) threshold for osteoporosis (i.e., they are classified as being 'normal' or 'osteopenic' by DXA-derived aBMD)[153,161,199]. This may partially be the related to DXA's inability to measure 3-dimensional (3D) micro-architectural properties of the cortical and trabecular bone[101,108,200].

[8] **Published as:** Kawalilak CE, Johnston JD, Olszynski WP, Kontulainen SA (2014). Characterizing micro-architectural changes at the distal radius and tibia in postmenopausal women using HR-pQCT. *Osteoporosis International, 25*(8): 2057-2066.

The advent of high-resolution peripheral quantitative computed tomography (HR-pQCT) has enabled measurement of 3D micro-architectural properties at peripheral bone sites (i.e., distal radius and tibia). While the distal radius and tibia are not clinically used to diagnose osteoporosis[120,201], they are clinically relevant. For instance, approximately 80% of all fragility fractures in postmenopausal women are non-vertebral in nature[202]. Moreover, fragility fractures at the distal radius are a sentinel for future fragility fractures at other sites[117,118]. A fragility fracture sustained at the distal radius will precede a vertebral fracture by an average of 5-7 years, and a hip fracture by an average of 10 years[117]. Further, because the tibia is a weight-bearing skeletal site it may better reflect bone strength at other weight-bearing sites, such as the hip and vertebrae[41]. Therefore, evidence of micro-architectural changes in cortical and trabecular bone properties at the distal radius and tibia in postmenopausal women will advance our understanding of bone deterioration beyond bone mass and provide new targets for investigations and strategies for optimizing osteoporotic fracture prevention.

Using cross-sectional data, HR-pQCT has been used to postulate and describe probable alterations in bone micro-architecture over time[29-33,51,203]. Only one prospective longitudinal study, however, has focused on age-related changes in bone micro-architecture at the distal radius in postmenopausal women[14]. This research was described as being 'preliminary' by the authors as they measured 17 postmenopausal women (53±3 years) using a prototype HR-pQCT with an isotropic resolutions of 165μm (60 slices per scan; 9.90 mm total scan thickness; image matrix: 512 x 512)[14]. This warrants investigation of micro-architectural changes using the standard HR-pQCT with an isotropic resolution of 82μm (110 slices per scan; 9.02 mm total scan thickness; image matrix: 1536 x 1536)[163], at both the distal radius and tibia in postmenopausal women; a population highly susceptible to osteoporotic fracture. In addition to the limited

prospective evidence of bone micro-architectural changes in postmenopausal women, evidence of micro-architectural changes in women receiving treatments influencing bone tissue, such as hormone replacement therapy (HRT), is warranted. Therefore, our first objective was to characterize annual changes in bone area, density, and micro-architecture at the distal radius and tibia using HR-pQCT in postmenopausal women. We hypothesized that observing bone loss and micro-architectural deterioration in both cortical and trabecular bone would occur in women not using any anti-resorptive medications (i.e., HRT or bisphosphonate). Based on the previous *ex vivo* cross-sectional findings[51,52,91], we anticipated that the majority of bone loss would be from cortical bone. Our secondary objective was to provide preliminary data of bone micro-architectural changes in women receiving hormone replacement therapy or bisphosphonate treatment.

4.1.2 Materials and Methods

4.1.2.1 Participants

In 2010, we recruited 147 community-dwelling postmenopausal women (mean age ± standard deviation, SD: 75±8 years) from the Saskatoon cohort of the Canadian Multi-centre Osteoporosis Study (CaM*os*)[160] to participate in a prospective investigation of musculoskeletal health[204]. In 2011, 104 women participated in the first follow-up and underwent baseline HR-pQCT scanning. Approximately 1 year later (2012-2013; mean time between measurements: 412±56 days), 51 women (77±7 years) returned for follow-up HR-pQCT measurements and were included in this study. Postmenopausal status was assessed using a questionnaire, as defined elsewhere[160]. Osteoporosis status was based on femoral neck (FN) aBMD obtained from the Saskatoon CaM*os* database[96] (Table 4.1). There appeared to be no difference in osteoporosis status between those women who returned for follow-up measures (aBMD ranges—normal: 27%; osteopenia: 57%;

osteoporosis: 16%) versus those who did not return (aBMD ranges—normal: 20%; osteopenia: 62%; osteoporosis: 11%). Participant consent was obtained prior to the study. This study was approved by the University of Saskatchewan Biomedical Research Ethics Board.

4.1.2.2 Medication Use

All participants filled out a questionnaire pertaining to their medication use for 12 months prior to their visit at study baseline and each follow-up. We recorded medications related to hormone replacement (e.g., conjugated estrogens tablets) and bisphosphonate therapies (e.g., risedronate, alendronate) based on reported medication use since 2009.

Table 4.1. Participants baseline demographics (mean±SD) categorized according to use of bone altering medication (no medication, hormone replacement therapy (HRT),or bisphosphonates), including DXA-derived osteoporosis status, number (n) of women in each category and the mean±SD of their areal bone mineral density (aBMD).

(N = 51)		**No Medication Use**		**HRT**		**Bisphosphonates**	
Variable	**Units**	**(n=33; 64%)**		**(n=8; 16%)**		**(n=10; 20%)**	
Age	(*years*)	77	± 7	81	± 7	76	± 8
Height	(*cm*)	160.3	± 5.9	158.3	± 7.4	158.6	± 3.9
Weight	(*kg*)	73.5	± 12.8	67.3	± 5.1	64.9	± 11.9
Osteoporosis Status							
Normal	*n (aBMD)*	11	(0.80±0.06)	3	(0.81±0.08)		--
Osteopenia	*n (aBMD)*	16	(0.70±0.11)	5	(0.69±0.16)	7	(0.67±0.04)
Osteoporosis	*n (aBMD)*	6	(0.54±0.05)		--	3	(0.54±0.02)

4.1.2.3 HR-pQCT Imaging

All participants had their non-dominant arm and ipsilateral leg immobilized in the standard carbon fiber cast prior to imaging, as per the manufacturer's standard *in vivo* protocol. Prior to scanning, a 2D anterior-posterior scout view scan was used to set the reference line and define the volume of interest, as defined elsewhere[1]. HR-pQCT (XtremeCT; Scanco Medical AG,

Brüttisellen, Switzerland) was used to acquire a 9.02 mm region (110 parallel CT slices) located 9.5 mm (radius) and 22.5 mm (tibia) proximal to the reference line placement. Using an isotropic resolution of 82 μm, the field of view was reconstructed over a 1536 x 1536 matrix. The effective dose was <4 μSv and the measurement time was approximately 2.8 minutes for each scan. Our measurement precision error for bone area is between 0.1-3.0%, for density measures is between 0.3-2.0%, and for micro-architecture parameters is between 1.2-6.5% at the distal radius and tibia, as described elsewhere[1]. The precision for cortical perimeter measures was 0.4% at both the distal radius and tibia.

4.1.2.4 HR-pQCT Analysis

One investigator (CK) scanned, graded, and analyzed all images. All images were graded for quality according to the 5-point scale defined by the manufacturer and reported previously[164]. Upon detection of motion artifacts (e.g., streaking or broken cortices), a repeat scan was performed. All images graded as quality 4 and 5 were removed without further analysis. All scans included in this analysis were of grades 1-3 for both the distal radius and distal tibia.

Image analysis was completed according to the manufacturer's standard *in vivo* evaluation protocol to acquire cortical and trabecular bone density, area, and micro-architectural values. We described the technique in detail elsewhere[1]. Briefly, the periosteal surface of the region of interest was contoured from the surrounding soft tissue using a semi-automatic edge-finding algorithm that morphed the contour to subsequent slices in a slice-by-slice manner over the entire volume-of-interest. The contour line was qualitatively inspected and corrected using manual manipulation when the line strayed from the periosteal surface. The baseline measures were automatically matched to follow-up measures by HR-pQCT software. The matching criterion is based on the total cross-sectional area within the contours of each measurement. In

the database, the total cross-sectional area for each contour on each slice is recorded and then the algorithm finds the best slice range that the average contoured area matches the follow up measurements. The average common regions for the distal radius measurements was 92% (±7%), and 96% (±2%) for the distal tibia measurements. The standard HR-pQCT outcomes represent an average of all slices in the common scan region and include area, density, and micro-architectural variables[14,25,167,168,198]. Area outcomes included: cortical and trabecular areas. Density outcomes included: total, cortical, and trabecular bone (including: meta and inner trabecular) densities. Micro-architectural outcomes included: cortical thickness (*CtTh*), trabecular bone volume fraction (*BV/TV*), trabecular number (*TbN*), trabecular thickness (*TbTh*), trabecular separation (*TbSp*), and trabecular heterogeneity (*TbSpSD*). In addition to the standard HR-pQCT outcomes, we report cortical perimeter (the outer boundary of the periosteal surface, mm). Further, we calculated bone mineral content (mg/mm) as the product of density and area for both cortical and trabecular compartments.

4.1.2.5 Statistical Analysis

To determine the distribution of our dataset, we calculated the z-score for skewness and kurtosis for all bone outcome variables. Z-score for skewness was calculated by dividing the skewness value by the standard error of skewness for each parameter, Z-score was calculated similarly for kurtosis[205]. The variables with skewness or kurtosis z-scores greater than 1.96 were deemed to have non-parametric distribution. The non-parametric parameters (i.e., TbSp and TbSpSD) were skewed to the right and therefore log transformed outcomes were used in the analysis.

We first used repeated measures analysis of covariance (ANCOVA) with Bonferroni adjustment for multiple comparisons to compare the change in bone parameters between baseline and follow-up and to assess possible interactions between time from baseline to follow-up and

covariates of age, height or weight. The only main effect was noted for the time from baseline to follow-up. Therefore, we assessed bone changes using analysis of variance (ANOVA), without covariates, and adjusted for multiple comparisons.

Using linear regression we assessed the relationship between absolute change in cortical and trabecular area at both sites in women without bone altering medication. We reported both equation and Pearson's correlation coefficient for each analysis. Significance was set to $P<0.05$. All statistical analyses were performed using IBM SPSS commercial statistics software (PASW, Version 21 for Windows, SPSS Inc., Chicago, IL, USA).

4.1.3 Results

We report mean age, height, weight, DXA-measured femoral neck aBMD (to describe osteoporosis status), and categorized participants according to reported history of hormone replacement and bisphosphonate therapy (Table 4.1). At the distal radius, there were a total of 43 scans analyzed; 31 from postmenopausal women not using medication, 6 were from women using HRT, and 6 were from women using bisphosphonates (Table 4.1). At the distal tibia, there were 50 scans analyzed; 32 from postmenopausal women not using medication, 8 were from women using HRT, and 10 were from women using bisphosphonates (Table 4.1).

We observed the following changes ($P<0.05$) in the distal radius. In women without bone altering medications, total density (-1.7%) and trabecular number (-6.4%) decreased while trabecular thickness (+6.0%), trabecular separation (+8.6%), and trabecular heterogeneity (+12.1%) increased (Table 4.2). Women using HRT had an increase in trabecular area (+1.3%), and decreases in cortical area (-6.5%), total density (-3.2%), cortical density (-2.8%), cortical content (-9.1%), and cortical thickness (-6.8%) (Table 4.2). In women using bisphosphonates, bone volume fraction (+3.8%) and trabecular density (+3.8%) increased, particularly in the inner

trabecular region (+5.5%) (Table 4.2). There was a negative relationship (r = -0.82) between cortical area and trabecular area change at the distal radius (Figure 4.1).

At the distal tibia, we observed bone changes only in women *not* using bone altering medications. Specifically, there were decreases in total density (-1.9%), cortical area (-4.5%), cortical density (-1.9%), cortical content (-6.3%), and cortical thickness (-4.4%), while trabecular area (+0.4%) increased and trabecular content did not change (Table 4.3, Figure 4.2). There was a negative relationship (r = -0.91) between trabecular area and cortical area change at the distal tibia (Figure 4.1).

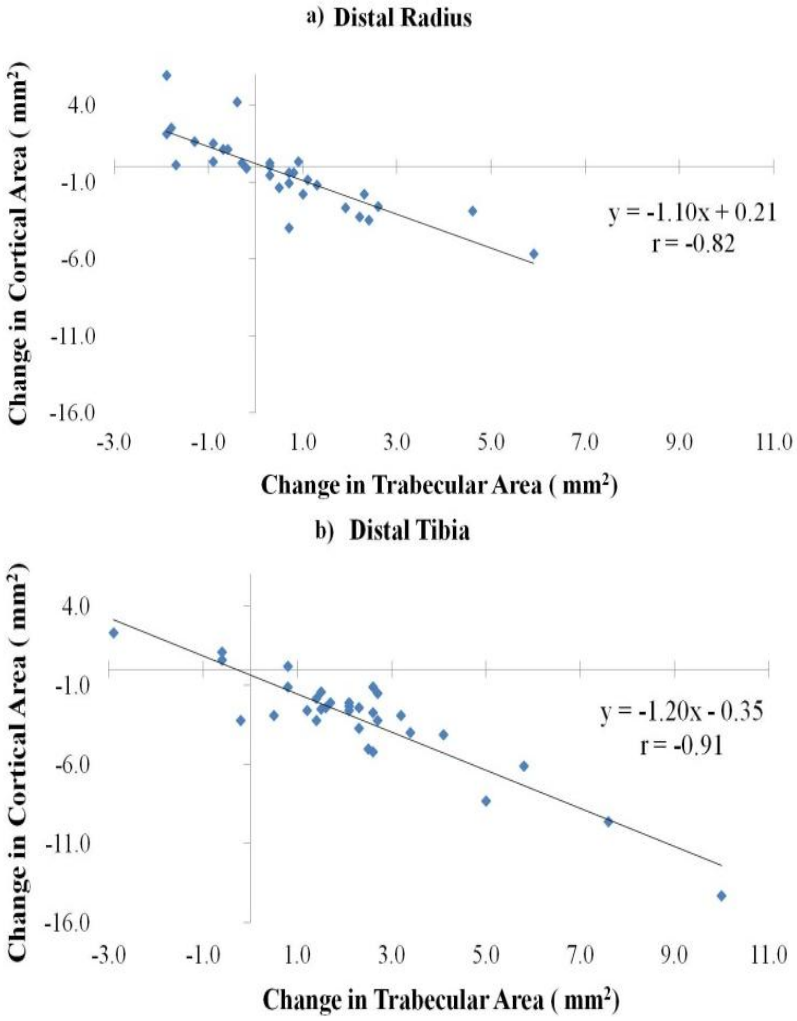

Figure 4.1. Relationship between absolute change in cortical and trabecular areas (mm^2) at a) the distal radius, and b) distal tibia.

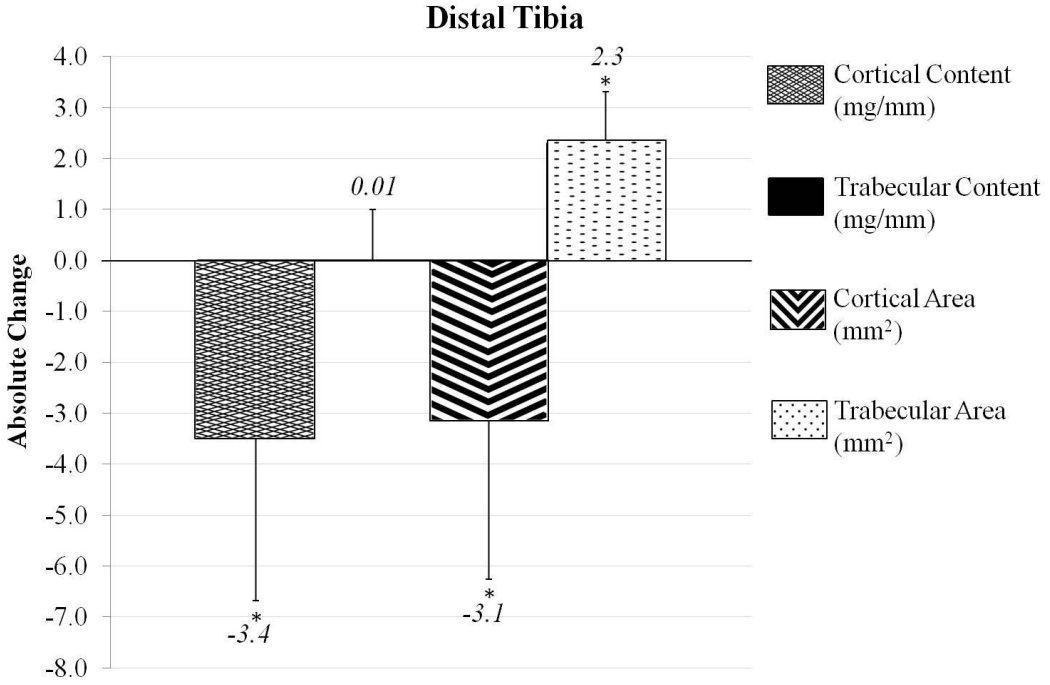

Figure 4.2. Absolute mean changes in cortical and trabecular bone mineral content (mg/mm) and area (mm^2) at the distal tibia. Error bars show SDs. *P<0.05.

Table 4.2. Mean (±SD) of the baseline and follow-up scans, mean annual change (percent), the lower and upper bounds for the 95% confidence interval, and *P*-value for the observed changes in the *distal radius* for those participants not taking medications, those participants using HRT, and those participants using bisphosphonates.

(N=43)		Baseline Scan	± SD	Follow-up Scan	± SD	Mean Annual Change (%)	95% Confidence Interval Lower	Upper	*P*-value
No Medication (n=31)									
Area									
Cortical	(mm^2)	38.9	± 13.3	38.4	± 13.2	-0.4 (-1.0)	-1.306	0.448	0.326
Trabecular	(mm^2)	238.9	± 46.2	239.5	± 45.8	0.6 (0.3)	-0.082	1.237	0.084
Perimeter									
Cortical	(mm)	71.95	± 4.78	71.89	± 4.82	-0.06 (-0.08)	-0.258	0.142	0.558
Density									
Total	(mg HA/cm^3)	250.8	± 55.2	246.5	± 55.0	-4.4 (-1.7)	-8.232	-0.536	**0.027**
Cortical	(mg HA/cm^3)	773.1	± 83.6	770.0	± 84.8	-3.1 (-0.4)	-10.061	3.945	0.380
Trabecular	(mg HA/cm^3)	135.5	± 44.2	132.6	± 44.6	-2.9 (-1.5)	-7.840	2.072	0.244
Meta	(mg HA/cm^3)	190.1	± 39.8	187.5	± 39.0	-2.5 (-1.1)	-6.550	1.530	0.214
Inn	(mg HA/cm^3)	97.7	± 49.0	94.6	± 50.6	-3.2 (-3.4)	-9.412	3.063	0.307
Content									
Cortical	(mg/mm)	31.0	± 13.0	30.6	± 12.9	-0.4 (-1.2)	-1.271	0.393	0.290
Trabecular	(mg/mm)	32.1	± 10.6	31.6	± 10.9	-0.5 (-1.2)	-1.670	0.625	0.360
Micro-architecture									
CtTh	(μm)	535.8	± 189.5	531.3	± 186.6	-4.5 (-0.5)	-0.018	0.009	0.499
BV/TV	(%)	11.3	± 3.7	11.0	± 3.7	-0.2 (-1.4)	-0.007	0.002	0.257
TbN	(1/mm)	1.8	± 0.5	1.7	± 0.5	-0.1 (-6.4)	-0.218	-0.065	**0.001**
TbTh	(μm)	61.9	± 10.0	65.3	± 10.2	3.4 (6.0)	0.001	0.006	**0.010**
TbSp[§]	(μm)	584.2	± 422.2	612.8	± 371.8	28.6 (8.6)	0.029	0.121	**0.002**
TbSpSD[§]	(μm)	352.3	± 368.1	371.4	± 337.4	19.1 (12.1)	0.042	0.161	**0.002**

HRT Use (n=6)									
Area									
Cortical	(mm^2)	49.0	± 16.3	46.3	± 16.6	-2.8 (-6.5)	-4.526	-1.007	**0.010**
Trabecular	(mm^2)	238.4	± 58.1	240.9	± 56.9	2.4 (1.3)	0.294	4.572	**0.033**
Perimeter									
Cortical	(mm)	74.07	± 6.70	73.95	± 6.69	-0.12 (-0.16)	-0.559	0.326	0.528
Density									
Total	(mg HA/cm^3)	282.0	± 93.2	273.3	± 90.6	-8.7 (-3.2)	-16.319	-0.981	**0.034**
Cortical	(mg HA/cm^3)	832.9	± 92.0	810.6	± 102.1	-22.3 (-2.8)	-39.037	-5.630	**0.018**
Trabecular	(mg HA/cm^3)	137.9	± 36.3	139.2	± 37.7	1.3 (0.8)	-4.344	6.978	0.576
Meta	(mg HA/cm^3)	191.5	± 34.6	192.0	± 36.9	0.5 (0.2)	-8.608	9.575	0.897
Inn	(mg HA/cm^3)	100.8	± 38.4	102.7	± 38.8	1.9 (1.7)	-2.037	5.771	0.274
Content									
Cortical	(mg/mm)	42.0	± 17.5	38.8	± 17.4	-3.2 (-9.1)	-4.613	-1.654	**0.003**
Trabecular	(mg/mm)	31.3	± 3.4	31.8	± 3.1	0.6 (2.0)	-2.039	0.839	0.333
Micro-architecture									
CtTh	(µm)	671.7	± 261.7	633.3	± 261.1	-38.3 (-6.8)	-0.062	-0.015	**0.008**
BV/TV	(%)	11.5	± 3.0	11.6	± 3.1	0.1 (0.7)	-0.004	0.006	0.597
TbN	(1/mm)	1.8	± 0.3	1.9	± 0.3	0.1 (7.5)	-0.266	0.482	0.490
TbTh	(µm)	63.0	± 11.6	59.8	± 11.1	-3.2 (-4.2)	-0.013	0.007	0.453
TbSp[§]	(µm)	497.7	± 85.7	471.3	± 93.3	-26.3 (-4.0)	-0.269	0.154	0.518
TbSpSD[§]	(µm)	228.3	± 62.9	224.5	± 80.3	-3.8 (-2.2)	-0.245	0.169	0.659
Bisphosphonates Use (n=6)									
Area									
Cortical	(mm^2)	35.0	± 11.4	34.7	± 10.1	-0.3 (-0.7)	-1.792	1.292	0.694
Trabecular	(mm^2)	229.8	± 30.0	230.6	± 28.4	0.8 (0.4)	-0.593	2.126	0.207
Perimeter									
Cortical	(mm^2)	77.12	± 3.48	77.03	± 3.67	-0.08 (-0.11)	-0.624	0.458	0.708

Density									
Total	(mg HA/cm^3)	240.9	± 34.0	242.4	± 27.8	1.5 (1.0)	-5.791	8.757	0.623
Cortical	(mg HA/cm^3)	773.1	± 95.8	768.7	± 84.4	-4.5 (-0.4)	-16.795	7.895	0.397
Trabecular	(mg HA/cm^3)	131.1	± 14.2	135.8	± 13.3	4.8 (3.8)	0.920	8.646	**0.024**
Meta	(mg HA/cm^3)	187.9	± 22.5	192.6	± 19.9	4.7 (2.7)	-0.443	9.776	0.066
Inn	(mg HA/cm^3)	91.7	± 11.4	96.7	± 11.8	5.0 (5.5)	1.493	8.441	**0.014**
Content									
Cortical	(mg/mm)	27.9	± 11.2	27.4	± 9.9	-0.6 (0.4)	-2.065	0.999	0.412
Trabecular	(mg/mm)	30.3	± 6.3	31.5	± 6.3	1.2 (4.1)	-6.019	9.186	0.615
Micro-architecture									
CtTh	(μm)	495.0	± 17.1	488.3	± 15.1	-6.7 (-0.3)	-0.029	0.016	0.484
BV/TV	(%)	10.9	± 1.2	11.3	± 1.1	0.4 (3.8)	0.001	0.007	**0.018**
TbN	(1/mm)	1.8	± 0.2	1.8	± 0.1	0.0 (1.3)	-0.201	0.221	0.908
TbTh	(μm)	60.7	± 5.8	62.7	± 86.0	2.0 (3.4)	-0.005	0.009	0.508
TbSp[§]	(μm)	497.2	± 57.0	489.3	± 34.5	-7.8 (-0.7)	-0.128	0.096	0.794
TbSpSD[§]	(μm)	212.7	± 24.9	217.7	± 14.3	5.0 (3.4)	-0.096	0.151	0.594

§ Non-parametric variables normalized using log transformation

Table 4.3. Mean (±SD) of the baseline and follow-up scans, mean annual change (percent), the lower and upper bounds for the 95% confidence interval, and *P*-value for the observed changes in the *distal tibia* for those participants not taking medications, those participants using HRT, and those participants using bisphosphonates.

(N=50)		Baseline Scan	± SD	Follow-up Scan	± SD	Mean Annual Change (%)	95% Confidence Interval Lower	Upper	*P*-value
No Medication (n=32)									
Area									
Cortical	(mm^2)	79.9	± 27.3	76.7	± 27.7	-3.1 (-4.5)	-4.259	-1.997	**<0.001**
Trabecular	(mm^2)	643.5	± 100.9	645.8	± 100.9	2.3 (0.4)	1.448	3.165	**<0.001**
Perimeter									
Cortical	(mm)	104.42	± 7.56	104.44	± 7.59	-0.02 (-0.03)	-0.182	0.238	0.787
Density									
Total	(mg HA/cm^3)	239.0	± 52.4	234.7	± 52.9	-4.3 (-1.9)	-6.126	-2.399	**<0.001**
Cortical	(mg HA/cm^3)	758.0	± 71.9	743.4	± 72.7	-14.6 (-1.9)	-18.829	-10.440	**<0.001**
Trabecular	(mg HA/cm^3)	159.1	± 38.7	158.5	± 39.2	-0.6 (-0.5)	-1.887	0.750	0.386
Meta	(mg HA/cm^3)	230.3	± 32.1	299.9	± 32.9	-0.4 (-0.2)	-2.048	1.205	0.601
Inn	(mg HA/cm^3)	110.7	± 44.7	110.0	± 45.2	-0.7 (-1.5)	-2.039	0.570	0.260
Content									
Cortical	(mg/mm)	62.1	± 26.0	58.7	± 26.0	-3.4 (-6.3)	-4.609	-2.266	**<0.001**
Trabecular	(mg/mm)	102.0	± 28.3	102.0	± 28.9	0.01 (-0.1)	-0.942	0.942	0.999
Micro-architecture									
CtTh	(μm)	748.1	± 262.6	719.4	± 266.3	-28.8 (-4.4)	-0.040	-0.018	**<0.001**
BV/TV	(%)	13.3	± 3.2	13.2	± 3.3	-0.1 (-0.5)	-0.002	0.001	0.369
TbN	(1/mm)	1.7	± 0.4	1.8	± 0.4	0.1 (2.8)	-0.024	0.103	0.214
TbTh	(μm)	77.8	± 15.4	75.7	± 15.2	-2.1 (-2.2)	-0.005	0.001	0.138
TbSp	(μm)	550.1	± 252.2	538.0	± 251.0	-12.1 (-1.7)	-0.059	0.015	0.228
TbSpSD	(μm)	342.7	± 424.6	342.6	± 450.4	-0.1 (-0.9)	-0.055	0.024	0.431

HRT Use (n=8)									
Area									
Cortical	(mm^2)	94.7	± 26.7	93.1	± 26.0	-1.6 (-1.1)	-6.344	3.194	0.460
Trabecular	(mm^2)	619.1	± 148.1	619.2	± 149.3	0.1 (0.0)	-3.407	3.632	0.942
Perimeter									
Cortical	(mm)	108.04	± 9.61	108.15	± 9.47	-0.11 (-0.10)	-0.079	0.304	0.208
Density									
Total	(mg HA/cm^3)	252.8	± 65.4	251.4	± 64.0	-1.4 (-0.3)	-7.513	4.813	0.620
Cortical	(mg HA/cm^3)	806.8	± 68.9	793.1	± 65.4	-13.6 (-1.6)	-27.607	0.332	0.054
Trabecular	(mg HA/cm^3)	148.8	± 34.5	149.7	± 33.8	0.8 (0.7)	-2.306	3.956	0.553
Meta	(mg HA/cm^3)	214.5	± 31.6	215.1	± 30.9	0.6 (0.3)	-3.533	4.658	0.755
Inn	(mg HA/cm^3)	104.2	± 36.5	105.3	± 36.0	1.0 (1.2)	-2.036	4.111	0.451
Content									
Cortical	(mg/mm)	77.9	± 27.6	75.2	± 26.7	-2.6 (-2.6)	-7.235	1.885	0.208
Trabecular	(mg/mm)	91.0	± 26.4	91.5	± 25.8	0.5 (0.7)	-1.242	2.192	0.534
Micro-architecture									
CtTh	(µm)	903.8	± 310.6	893.8	± 310.1	-10.0 (-0.8)	-0.052	0.032	0.592
BV/TV	(%)	12.4	± 2.9	12.5	± 2.8	0.1 (0.6)	-0.002	0.003	0.588
TbN	(1/mm)	1.7	± 0.2	1.8	± 0.3	0.0 (3.2)	-0.230	0.297	0.771
TbTh	(µm)	72.8	± 17.7	71.5	± 15.7	-1.3 (-0.4)	-0.013	0.010	0.800
TbSp	(µm)	516.3	± 70.4	509.3	± 81.9	-7.0 (-0.3)	-0.175	0.139	0.798
TbSpSD	(µm)	240.1	± 44.5	234.4	± 48.7	-5.8 (-1.7)	-0.171	0.112	0.633
Bisphosphonates Use (n=10)									
Area									
Cortical	(mm^2)	75.2	± 26.8	74.3	± 26.6	-0.9 (-1.6)	-2.723	0.903	0.286
Trabecular	(mm^2)	581.3	± 110.4	582.1	± 109.5	0.8 (0.2)	-0.918	2.518	0.319
Perimeter									
Cortical	(mm)	109.73	± 6.90	109.65	± 7.13	-0.08 (-0.07)	-0.336	0.176	0.498

Density									
Total	(mg HA/cm^3)	237.2	± 35.5	235.8	± 35.3	-1.4 (-0.6)	-4.985	2.185	0.400
Cortical	(mg HA/cm^3)	755.7	± 96.6	746.5	± 99.9	-9.2 (-1.3)	-19.781	1.421	0.082
Trabecular	(mg HA/cm^3)	151.2	± 21.3	151.9	± 22.4	0.7 (0.4)	-1.716	3.116	0.529
Meta	(mg HA/cm^3)	222.2	± 18.3	222.8	± 20.3	0.5 (0.2)	-3.486	4.526	0.776
Inn	(mg HA/cm^3)	102.9	± 24.4	103.8	± 24.7	0.9 (0.8)	-0.942	2.642	0.311
Content									
Cortical	(mg/mm)	59.0	± 25.6	57.7	± 25.3	-1.2 (-2.8)	-2.821	0.361	0.114
Trabecular	(mg/mm)	87.9	± 20.4	88.5	± 21.2	0.6 (0.5)	-0.551	1.791	0.261
Micro-architecture									
CtTh	(µm)	747.0	± 277.7	735.0	± 272.7	-12.0 (-1.9)	-0.029	0.005	0.140
BV/TV	(%)	12.6	± 1.8	12.7	± 12.9	0.1 (0.5)	-0.001	0.003	0.448
TbN	(1/mm)	1.6	± 0.2	1.7	± 0.2	0.1 (3.9)	-0.106	0.222	0.445
TbTh	(µm)	77.2	± 10.2	75.1	± 11.5	0.0 (-2.3)	-0.009	0.005	0.494
TbSp	(µm)	538.7	± 60.9	524.8	± 81.0	-13.9 (-2.3)	-0.128	0.066	0.485
TbSpSD	(µm)	255.4	± 50.5	248.5	± 53.8	-6.9 (-1.6)	-0.175	0.079	0.415

4.1.4 Discussion

Our primary objective was to characterize annual skeletal changes in bone area, density, and micro-architecture at the distal radius and distal tibia using HR-pQCT in postmenopausal women from a community-dwelling, population-based cohort living in Saskatoon, Canada. Women who did not use bone altering medication had 6-12% increase in trabecular thickness, separation, and heterogeneity together with a 6% decrease in trabecular number with no change in trabecular density at the distal radius. Observed changes suggest that small trabeculae were lost while partially resorbed cortical bone remnants were detected as new, thicker trabeculae. While we did not detect changes in bone mineral content within the cortical bone at the distal radius, cortical content decreased at the distal tibia. Trabecular bone density and content did not change at the tibia, while the 0.4% increase in trabecular area was accompanied by 2-6% decreases in cortical area, density, content, and thickness.

These findings, especially from the distal tibia, suggest that the majority of bone was lost due to intracortical remodeling adjacent to the trabecular bone and marrow. Based on the negative correlation between the changes in cortical and trabecular area, women with the greatest decreases in cortical area had the greatest increases in trabecular area at both sites. Altogether, these observations lend credence to the suggestion that with advancing age, resorption at the endocortex results in the appearance of cortical remnants resembling trabecular bone (i.e., trabecularization of the cortex)[51,52,91]. Observed changes agree with reported histomorphometric (*ex vivo*) data from the femur[51,52,91]. As the cortical bone is being resorbed the area of the cortex decreases while the trabecular area increases to incorporate the cortical remnants into the trabecular volume, which simultaneously results in an increase in the apparent trabecular thickness measured using HR-pQCT. Our results suggest that cortical thinning maybe more

apparent at weight-bearing bone sites (such as tibia) than non-weight bearing sites (such distal radius).

Study findings are consistent with others suggesting that the majority of bone loss in postmenopausal women is from cortical bone[51,58,91,206,207]. Using longitudinal pQCT measures at the distal tibia, Lauretani and colleagues reported that age-related medullary expansion at the tibia shaft was not balanced by periosteal apposition leading to cortical bone loss and thinning of the cortex[208]. These findings are consistent with our results showing no changes in the cortical perimeter at the distal radius or tibia over the 1-year follow-up. These observations are important because a thin cortical shell at the femoral neck and lumbar spine has been associated with lower tissue toughness and elasticity thereby compromising load-bearing capacity and increasing the probability of sustaining a fracture[209,210]. This evidence suggests that cortical bone should be targeted when monitoring osteoporosis treatments and fracture-prevention strategies. It further highlights the need for 3D imaging techniques to monitor both cortical and trabecular bone deterioration in fracture prone populations.

Our secondary objective was to describe micro-architectural changes over 1 year for those women using bone altering medication. Our findings at the distal radius of postmenopausal women using HRT showed similar results to that of the distal tibia in the non-medicated group of our cohort. That is, over 1 year there was approximately 1% increase in trabecular area with a simultaneous 3-9% decrease in cortical area, density, content, and thickness. These data suggest that despite the use of HRT, cortical bone is lost and partly trabecularized at the distal radius. In contrast, no skeletal changes in 1 year occurred at the distal tibia in those women using HRT, which may indicate that HRT can maintain cortical and trabecular bone properties at the weight-

bearing skeleton. This preliminary evidence can assist in designing interventions to address this hypothesis.

The women in our cohort using bisphosphonates had an approximate 3-5% increase in distal radius bone volume fraction and trabecular density, particularly in the inner trabecular region. These increases in the trabecular micro-architecture were consistent with the reported effects of bisphosphonates in postmenopausal women[94]. The lack of observed changes at the distal tibia with our bisphosphonate users may reflect the small sample size and limited power to detect small changes reported with bisphosphonate therapy. Alendronate treatment has shown to decrease trabecular area and increase cortical thickness at the tibia[94].

This study has specific strengths which require consideration. First, our sample of older community-dwelling postmenopausal women represents a clinically relevant population most likely to sustain an osteoporotic related fragility fracture[169,208]. Based on the similar bone health status (proportion of osteopenia and osteoporosis) between our sample and reports from postmenopausal women in North America, Europe, Australia, and Japan[162], we anticipate that the observed bone changes can be generalized to older postmenopausal women in these regions.

Limitations of this study relate to the study duration, possible bias and scanning locations. First, this was a short, one year follow-up study of postmenopausal women. Longer follow-ups are needed to characterize individual changes and identify factors associated with greater bone loss and micro-architectural deterioration. Future research should also define a time interval required to reliably monitor bone changes with HR-pQCT in postmenopausal women. Second, our study was limited to follow-up measures of only 51 of the initial 104 women (49%) and the possibility of attrition bias related to the participants bone health status exists. However, we assume this was not the case because of the similar osteoporosis status at baseline between

the women who returned for the follow-up measures relative to those women who did not return. Third, our results are limited to the distal radius and distal tibia measured with HR-pQCT (XtremeCT) and may not be generalizable to other skeletal sites or measures obtained using other imaging methods.

In summary, this study characterized skeletal changes at the distal radius and tibia using standard HR-pQCT measurements in community-dwelling postmenopausal women over 1 year. The observed loss of trabeculae with concomitant increase in trabecular size at the distal radius and the declined cortical thickness, content, density and area with increase in trabecular area at the distal tibia indicated a site-specific trabecularization of the cortical bone in postmenopausal women.

5: DISCUSSION AND CONCLUSION

5.1 Overview of Findings

The overall goal of this thesis was to provide a careful investigation of precision for all HR-pQCT outcomes, establish the least significant change (LSC) and monitoring time interval (MTI), as well as characterize bone changes in density, geometry, and micro-architecture using HR-pQCT.

5.1.1 Study 1: *HR-pQCT Precision*

The first study of my thesis defined HR-QCT precision errors using: 1) the full array of standard outcomes, 2) two contour methods for the dual-threshold analysis, and 3) 3 different FE models using sufficient degrees of freedom to provide accurate precision errors (with 90% confidence), using unmixed age groups. The primary finding from study 1 was that HR-pQCT precision errors were <10% for bone densitometric, geometric, and mechanical properties; while precision errors were <16% for cortical and trabecular micro-architectural outcomes. These results were comparable to previous studies reporting precision error for standard outcomes[5,13,29,157,195], cortical micro-architecture[5,180], and FE modeling [157,188].

Study 1 also highlighted that postmenopausal women (74±7 years) and young adults (26±8 years) could be measured with comparable precision errors using HR-pQCT. This finding is important because previous research suggested that precision errors derived from young adults would likely underestimate errors in postmenopausal women[149,158]. Further, study 1 demonstrated that manual modification of the endocortical contour did not significantly affect precision error. However, the manual modification of endocortical contours led to generally higher cortical bone properties compared to the automated method—thereby making results more comparable to higher resolution imaging techniques, nevertheless these benefits do not

outweigh the time investment. This is of particular importance as it will lead to time savings and reduced costs for future evaluation of cortical bone micro-architecture.

Interestingly, when comparing the cortical density between the advanced cortical micro-architecture evaluation (AUTO and MOD) to the standard evaluation, the cortical density increased when the cortical thickness increased. Specifically, the average cortical density for the standard evaluation was 773.0 mg HA/cm^3 with an average cortical thickness of 0.523 mm, however, with the AUTO contour the average cortical density was 918.1 mg HA/cm^3 with an average cortical thickness of 1.187 mm (MOD contouring provided the same trends but to a lesser extent). It would be logical to observe a decrease in cortical density with increased cortical thickness because of the inclusion of more cortical pores. However, the increased cortical density observed with the both AUTO and MOD contour methods of the dual-threshold technique was likely the result of using the manufacturer recommended cortical density outcome for which the pores were filled; thereby providing a more comparable outcome to cortical mineralization[180]. This emphasizes the need for careful reporting and comparing of cortical density outcomes between HR-pQCT analysis methods (i.e., standard evaluation and the advanced cortical micro-architecture evaluation).

Regarding FE modeling, the STM and DTM models appeared more precise for modeling the distal radius (STM: 2.8-3.8%; DTM: 3.0-3.8%; E-BMD: 2.6-7.1%) whereas all methods provided comparable precision for modeling the distal tibia (STM: 2.9-4.8%; DTM: 3.0-3.8%; E-BMD: 1.6-2.1%). Results suggested that the E-BMD model could be used when the common region between follow-up scans are high ($\geq$93%), while STM or DTM should be considered when the common region is lower (<93%). These findings provide guidance for future studies investigating bone strength estimates using HR-pQCT-based FE modeling.

All sections of study 1 indicated the importance of acquiring a high percent of image overlap among follow-up scans (i.e., common region) in order to acquire low precision error—especially for subsequent advanced bone analyses (i.e., advanced cortical micro-architecture evaluation and finite element modeling). This highlights the significance of consistent (re)positioning of participants in the cast as well as careful placement of the reference line prior to scanning. These findings are important because they indicate that HR-pQCT can be used to monitor skeletal change, particularly changes in skeletal micro-architecture—which was not possible to quantitatively measure non-invasively, *in vivo* prior to the advent of HR-pQCT.

5.1.2 Study 2: *Monitoring Skeletal Changes*

Study 2 used precision errors outlined in the first study to define the tools needed to assess and monitor skeletal change—specifically the LSC and MTI. The primary findings from study 2 indicated that HR-pQCT follow-up measures in postmenopausal women can be performed every 2 years at the distal radius and every 1 year at the distal tibia to monitor true skeletal changes as indicated by the LSCs. This was the first study to provide MTIs for HR-pQCT and to define the LSC for all standard outcomes using short-term precision—an important attribute because short-term precision is not confounded by skeletal changes. MTI and LSC results are important when designing and interpreting prospective studies (including interventions) in postmenopausal women of similar demographics to that presented in this dissertation.

5.1.3 Study 3: *Characterizing Skeletal Changes*

The primary findings from study 3 characterized natural skeletal changes at the distal radius and tibia over 1 year in postmenopausal women not using bone altering medications (e.g., bisphosphonates or hormone replacement therapy). At the distal radius, annual changes were described primarily as micro-architectural deterioration in the trabeculae. At the distal tibia,

however, annual changes were established in both cortical and trabecular tissues. The observed loss of trabeculae with concomitant increase in trabecular size at the distal radius, as well as the thinned cortex, decreased cortical density and content at the distal tibia indicated a site-specific trabecularization of the cortical bone in postmenopausal women. This is the first study that characterized natural bone changes in postmenopausal women over 1 year using the standard HR-pQCT scanner. Using *in vivo* data, this study confirmed *ex vivo* findings regarding cortical trabecularization at the tibia[180] and added to the literature by reporting a different pattern of cortical trabecularization at the radius in postmenopausal women. The trabecularization of the cortex observed in this study provides evidence regarding the prospective effect of aging at the distal radius and tibia, especially as it pertains to micro-architectural deterioration.

Studies where change is expected (i.e., monitoring or intervention studies) should not only focus on the statistical significance between baseline and follow-up measures or between treatment and control group, but also the effect size of the change or difference between the compared groups[211]. In cases where there is a large effect size, the anticipated MTI may be lower than what is presented in study 2. In contrast, interpreting changes that falls within the precision error of the measurement is challenging and warrants caution when reported.

5.2 Strengths and Limitations

Thesis strengths pertain to participant pool and study design. First, our sample of older community-dwelling postmenopausal women represented a clinically relevant population most likely to sustain an osteoporotic fragility fracture[169,208]. Based on the proportion of DXA-derived femoral neck T-scores, the postmenopausal women involved in these studies had comparable bone health status to the osteoporosis reference standards from North America, Europe, Australia and Japan[161,162], thereby making the data in this thesis generalizable to

postmenopausal women in these regions. Regarding study design, precision errors in postmenopausal women were compared to short-term precision errors observed with a 'best case' sample of young adults, including both females and males. Further, participants were repositioned between measurement times and repeat measures were completed with a minimum of 24 hours between scans. This is important because underestimation of precision error has been reported when precision was calculated using scans repeated on the same day[159]. Also, sufficient number of participants in all precision studies were acquired to attain a minimum of 27 degrees of freedom required to achieve 90% confidence in our precision error estimate[12,149]. Data from all studies was measured from the same operator using the same scanner, thereby minimizing measurement variability and allowing for the most accurate time interval predictions and skeletal change measurements.

Limitations relate to the study duration, small sample size, x-ray tube changes, and lack of independence between follow-up measures. Studies 2 and 3 were based on a short, one year follow-up study of 51 postmenopausal women. Longer follow-ups with multiple measurement years using a larger sample (>51 participants) would more accurately characterize individual changes, identify factors associated with greater bone loss and micro-architectural deterioration, and may provide a more representative estimate of the annual rates of skeletal changes and associated MTIs[9]. A caveat to this research is that skeletal precision, LSC/MTIs, and annual changes may vary according to the cohort's age, ethnicity, disease status, and sex; therefore, monitoring disease progression and skeletal changes associated with intervention will likely require population-specific precision and MTI studies[9]. During the studies in this thesis, the x-ray tube was replaced twice without cross-validation. While this replacement will not affect the precision studies, it may affect the architectural outcomes of studies 4 and 5, which rely on 1

year follow-up data. Because the HR-pQCT evaluation scripts use a common region to translationally match the cross-sectional areas among baseline and follow-up measures (creating a common region), the outcomes are not independent of one another. The use of matched common regions has been shown to reduce precision error by 3-4%[14] and therefore obfuscates the actual precision error estimate of the machine and user. Further, because the precision error and LSC metrics presented in this thesis used a matched common region, applying these metrics to cross-sectional studies may challenge the interpretation of results since matching common regions are not used in cross-sectional comparisons.

5.3 Clinical Significance

Using the standard information provided in all three studies the overarching goal and the clinical significance of this thesis can be summed in one final example. Recall, MTI suggested annual follow-up measures would be sufficient to acquire skeletal changes exceeding the LSC for cortical area, density and thickness, as well as trabecular area at the distal tibia. Therefore, using baseline data from the standard outcomes reported in study 1 (chapter 2), the MTI and LSC information provided in study 2 (chapter 3), and the annual change at the distal tibia provided in study 3 (chapter 4), it can be determined whether true skeletal change occurred at this site beyond the precision error of the HR-pQCT with 95% confidence. In order to be 95% confident that skeletal change over one year at the distal tibia in postmenopausal women was measured there should be a difference between baseline and follow-up of 3.1% (±2.6 mm^2) in cortical area, 0.8% (±6.2 mg HA/cm^3) in cortical density, 3.9% (±31.7 μm) in cortical thickness, and 0.3% (±1.9 mm^2) in trabecular area. The skeletal changes reported in the non-medicated women of study 3 (chapter 4) indicated a difference between baseline and follow-up of -3.1 mm^2 in cortical area, -14.6 mg HA/cm^3 in cortical density, -28.8 μm in cortical thickness, and +2.3 mm^2 in

trabecular area. Measured changes exceed the minimum required difference provided by the LSC for all outcomes except cortical thickness (LSC difference: ±31.7µm; measured difference: -28.8µm). This indicates that we are 95% confident skeletal change was measured for cortical and trabecular areas, and cortical density, but not for cortical thickness; even though the average follow-up measures were statistically different from baseline. This highlights the importance of knowing lab precision for imaging modalities used in investigations anticipating change. Further, this example emphasizes the difference between statistically significant differences between baseline and follow-up measures relative to capturing actual change measured beyond precision error.

5.4 Conclusion

Overall this thesis provides a careful assessment of precision errors using HR-pQCT and is an example for how precision information can be used to plan prospective or longitudinal studies (MTI) as well as for the interpretation of results from investigations anticipating observing skeletal change (LSC).

5.5 Future Directions

Areas of future study include (but are not limited to): population specific studies, cortical porosity accuracy study, finite element model optimization and comparison study, further investigation into the effects of hormone replacement therapy on bone micro-architecture, and a longer term follow-up study to characterize bone changes.

1. As mentioned throughout Study 1, our research is limited by sample size to determine population specific precision beyond ‘postmenopausal women’. While we studied a representative sample of postmenopausal women, skeletal precision may vary according

to time from menopause, disease status (e.g., osteoporosis), and skeletal site assessed; this merits further investigation into population-specific precision studies.

2. As indicated in section 2.2, an objective of study 1 was to investigate the differences between the automatic and modified contour method for the advanced cortical bone micro-architecture evaluation. Future research should determine whether the automatic or manual contouring method more accurately represent cortical bone micro-architecture. Once this information is obtained, it would be prudent to determine how cortical bone micro-architecture changes with age. This is important because bone's mechanical strength is influenced by cortical bone micro-architecture[71,75,173,175,176] and this research will improve our understanding of osteoporosis and factors underpinning bone strength.

3. Another area for further investigation would be to optimize the FE model to more accurately represent falls onto the outstretched hand. Current FE models primarily estimate failure load under axial compressive loading[32,33,44,112,155,188,189,192,212-214]. However, this falling scenario involves a combination of axial compressive loads and "off-axis" dorsal- and lateral-directed loads that result in bending. It would be interesting and important to determine whether the optimized "off-axis" FE model provides better prediction of wrist fractures relative to the currently used compression models.

4. An objective of study 3 was to prospectively characterize skeletal changes in a sub-sample of postmenopausal women using hormone replacement therapy. However, because our sample size was small (i.e. n=8) we were limited to characterize bone micro-architectural changes in this group of women. Future research should go beyond our preliminary evidence to fully discover the effects of hormone replacement therapy on

bone micro-architecture and how bone micro-architecture changes using this pharmaceutical agent. It would also be interesting to apply FE modeling and determine whether bone strength also changes using this medication.

5. Study 3 focused on characterizing the change of bone outcomes from the standard HR-pQCT evaluation over 1 year. Future research should also characterize how bone strength estimates (from finite element modeling) change over at least one year or preferably longer.

6. As indicated in the Study 3 and further demonstrated in the '*Clinical Relevance*' section of this discussion, Study 3 was limited by the sample size and the follow-up time. It would be prudent for future research to follow a larger sample of postmenopausal women for a longer period of time (at least 3 years as defined by our MTIs) in order to fully characterize how bone density, geometry, micro-architecture and strength change in postmenopausal women. This research will improve our understanding of osteoporosis and help to develop new fracture prevention interventions.

7. It would be prudent to consider analysis techniques beyond those provided by the manufacturer—especially for more advanced bone analyses such as cortical and trabecular segmentation (e.g., circumferential rings or texture profiles to separate the cortical and trabecular tissues and identify the endocortex).

REFERENCES

1. Kawalilak CE, Johnston JD, Olszynski WP, Leswick D, Kontulainen SA. Comparison of short term in vivo precision of bone density and micro-architecture at the distal radius and tibia between postmenopausal women and young adults. *Journal of Clinical Densitometry* 2014;17(4):510-517.

2. Kawalilak CE, Johnston JD, Cooper DML, Olszynski WP, Kontulainen SA. Role of endocortical contouring methods on precision of HR-pQCT-derived cortical micro-architecture in postmenopausal women and young adults. *Osteoporosis International.* 2015;Accepted Manuscript.

3. Kawalilak CE, Johnston JD, Olszynski WP, Kontulainen SA. Least significant changes and monitoring time intervals for high-resoltuion pQCT-derived bone outcomes in postmenopausal women. *Journal of Musculoskeletal Neuronal Interactions.* 2015;15(2):190-196.

4. Kawalilak CE, Johnston JD, Olszynski WP, Kontulainen SA. Characterizing micro-architectural changes at the distal radius and tibia in postmenopausal women using HR-pQCT. *Osteoporosis International.* 2014;25(8):2057-2066.

5. Burghardt AJ, Buie HR, Laib A, Majumdar S, Boyd SK. Reproducibility of direct quantitative measures of cortical bone microarchitecture of the distal radius and tibia by HR-pQCT. *Bone.* Sep 2010;47(3):519-528.

6. Medical S. *Scanco Medical Finite Element Software.* Version 1.13 ed. Bruetisellen, Switzerland: SCANCO Medical Ag Fabrikweg 2 CH-8306; 2009.

7. MacNeil JA, Boyd SK. Bone strength at the distal radius can be estimated from high-resolution peripheral quantitative computed tomography and the finite element method. *Bone.* Jun 2008;42(6):1203-1213.

8. Bland JM, Altman DG. Statistical methods for assessing agreement between two methods of clinical measurement. *The Lancet.* 1986;327(8476):307-310.

9. Glüer CC. Monitoring skeletal changes by radiological techniques. *Journal of Bone and Mineral Research.* 1999;14(11):1952-1962.

10. Bonnick SL, Johnston CC, Kleerekoper M, et al. Importance of Precision in Bone Density Measurements. *Journal of Clinical Densitometry.* 2001;4(2):105-110.

11. Panjabi MM, White AA. *Biomechanics in the Musculoskeletal System.* Philadelphia, PA: Churchill Livingstone; 2001.

12. Glüer CC, Blake G, Lu Y, Blunt BA, Jergas M, Genant HK. Accurate assessment of precision errors: how to measure the reproducibility of bone densitometry techniques. *Osteoporosis International.* 1995;5:262-270.

13. Kazakia GJ, Hyun B, Burghardt AJ, et al. In vivo determination of bone structure in postmenopausal women: a comparison of HR-pQCT and high-field MR imaging. *Journal of Bone and Mineral Research.* Apr 2008;23(4):463-474.

14. Laib A, Hauselmann HJ, Ruegsegger P. In vivo high resolution 3D-QCT of the human forearm. *Technology and Health Care.* 1998;6:329-337.-

15. Bouillon R, Burckhardt P, Christiansen C, et al. Consensus development conference: prophylaxis and treatment of osteoporosis. *Osteoporosis International.* 1991;1:114-117.

16. Kamienski M, Tate D, Vega M. The silent thief: diagnosis and management of osteoporosis. *Orthopedic nursing.* May-Jun 2011;30(3):162-171.

17. Caliri A, de Fillipis L, Bagnato GL, Bagnato GF. Osteoporotic fractures: mortality and quality of life. *Panminerva Med.* 2007;49.

18. Cummings SR, Melton LJ, 3rd. Epidemiology and outcomes of osteoporotic fractures. *The Lancet.* 2002;359(9319):1761-1767.

19. Ammann P, Rizzoli R. Bone strength and its determinants. *Osteoporosis International.* 2003;14 Suppl 3:S13-18.

20. Bouxsein ML, Seeman E. Quantifying the material and structural determinants of bone strength. *Best Practice and Research Clinical Rheumatology.* Dec 2009;23(6):741-753.

21. WHO scientific group on the assessment of osteoporosis at primary health care level. WHO Scientific Group on the Assessment of Osteoporosis at the Primary Health Care Level; 7-MAY-2004, 2004; Brussels, Belgium.

22. Cummings SR, Black D, Nevitt MC, et al. Bone density at various sites for prediction of hip fracture. *The Lancet.* 1993;341:72-75.

23. Pasco JA, Seeman E, Henry MJ, Merriman EN, Nicholson GC, Kotowicz MA. The population burden of fractures originates in women with osteopenia, not osteoporosis. *Osteoporosis International.* 2006;17(9):1404-1409.

24. Sornay-Rendu E, Munoz F, Garnero P, Duboeuf F, Delmas PD. Identification of osteopenic women at high risk of fracture: the OFELY study. *Journal of Bone and Mineral Research.* Oct 2005;20(10):1813-1819.

25. Kazakia GJ, Burghardt AJ, Link TM, Majumdar S. Variations in morphological and biomechanical indices at the distal radius in subjects with identical BMD. *Journal of biomechanics.* Jan 11 2011;44(2):257-266.

26. Burr DB. The contribution of the organic matrix to bone's material properties. *Bone.* 2002;31(1):8-11.

27. Kontulainen SA, Kawalilak CE, Johnston JD, Bailey DA. Prevention of Osteoporosis and Bone Fragility: A Pediatric Concern. *American Journal of Lifestyle Medicine.* 2013;7(6):405-417.

28. Hourigan SR, Nitz JC, Brauer SG, O'Neill S, Wong J, Richardson CA. Positive effects of exercise on falls and fracture risk in osteopenic women. *Osteoporosis International.* Jul 2008;19(7):1077-1086.

29. Boutroy S, Bouxsein ML, Munoz F, Delmas PD. In vivo assessment of trabecular bone microarchitecture by high-resolution peripheral quantitative computed tomography. *The Journal of clinical endocrinology and metabolism.* Dec 2005;90(12):6508-6515.

30. Dalzell N, Kaptoge S, Morris N, et al. Bone micro-architecture and determinants of strength in the radius and tibia: age-related changes in a population-based study of normal adults measured with high-resolution pQCT. *Osteoporosis International.* Oct 2009;20(10):1683-1694.

31. Burghardt AJ, Kazakia GJ, Ramachandran S, Link TM, Majumdar S. Age- and gender-related differences in the geometric properties and biomechanical significance of intracortical porosity in the distal radius and tibia. *Journal of Bone and Mineral Research.* May 2010;25(5):983-993.

32. Macdonald HM, Nishiyama KK, Kang J, Hanley DA, Boyd SK. Age-related patterns of trabecular and cortical bone loss differ between sexes and skeletal sites: a population-based HR-pQCT study. *Journal of Bone and Mineral Research.* Jan 2011;26(1):50-62.

33. Mueller TL, van Lenthe GH, Stauber M, Gratzke C, Eckstein F, Muller R. Regional, age and gender differences in architectural measures of bone quality and their correlation to bone mechanical competence in the human radius of an elderly population. *Bone.* Nov 2009;45(5):882-891.

34. Parfitt AM. Age-related structural changes in trabecular and cortical bone: cellular mechanisms and biomechanical consequences. *Calcified tissue international.* 1984;36:S123-S128.

35. Parfitt AM, Mathews CH, Villanueva AR, Kleerekoper M, Frame B, Rao DS. Relationships between surface, volume, and thickness of iliac trabecular bone in aging and in osteoporosis. Implications for the microanatomic and cellular mechanisms of bone loss. *The Journal of clinical investigation.* Oct 1983;72(4):1396-1409.

36. Bousson V, Bergot C, Sutter B, Levitz P, Cortet B, Scientific Committee of the Groupe de Recherche et d'Information sur les O. Trabecular bone score (TBS): available knowledge, clinical relevance, and future prospects. *Osteoporosis International.* May 2012;23(5):1489-1501.

37. Bolotin HH. DXA in vivo BMD methodology: an erroneous and misleading research and clinical gauge of bone mineral status, bone fragility, and bone remodelling. *Bone.* Jul 2007;41(1):138-154.

38. Melton LJ, 3rd, Riggs BL, van Lenthe GH, et al. Contribution of in vivo structural measurements and load/strength ratios to the determination of forearm fracture risk in postmenopausal women. *Journal of Bone and Mineral Research.* Sep 2007;22(9):1442-1448.

39. Stein EM, Liu XS, Nickolas TL, et al. Abnormal microarchitecture and reduced stiffness at the radius and tibia in postmenopausal women with fractures. *Journal of Bone and Mineral Research.* Dec 2010;25(12):2572-2581.

40. Nishiyama KK, Macdonald HM, Hanley DA, Boyd SK. Women with previous fragility fractures can be classified based on bone microarchitecture and finite element analysis measured with HR-pQCT. *Osteoporosis International.* Nov 20 2012;24(5):1733-1740.

41. Sornay-Rendu E, Boutroy S, Munoz F, Delmas PD. Alterations of cortical and trabecular architecture are associated with fractures in postmenopausal women, partially independent of decreased BMD measured by DXA: the OFELY study. *Journal of Bone and Mineral Research.* Mar 2007;22(3):425-433.

42. Melton LJ, 3rd, Christen D, Riggs BL, et al. Assessing forearm fracture risk in postmenopausal women. *Osteoporosis International.* Jul 2010;21(7):1161-1169.

43. Bala Y, Zebaze R, Ghasem-Zadeh A, et al. Cortical Porosity Identifies Women with Osteopenia at Increased Risk for Forearm Fractures. *Journal of Bone and Mineral Research.* Jan 14 2014;29(6):1356-1362.

44. Vilayphiou N, Boutroy S, Sornay-Rendu E, et al. Finite element analysis performed on radius and tibia HR-pQCT images and fragility fractures at all sites in postmenopausal women. *Bone.* Apr 2010;46(4):1030-1037.

45. Krug R, Burghardt AJ, Majumdar S, Link TM. High-Resolution Imaging Techniques for the Assessment of Osteoporosis. *Radiologic Clinics of North America.* 2010;48(3):601-621.

46. Wong AK, Beattie KA, Min KK, et al. A Trimodality Comparison of Volumetric Bone Imaging Technologies. Part II: 1-Yr Change, Long-Term Precision, and Least Significant Change. *Journal of Clinical Densitometry.* 2014.

47. Martini FH, Timmins MJ, Tallitsch RB. *Human Anatomy.* 7th Edition ed. Boston: Pearson Benjamin Cummings; 2012.

48. Larson S. Treatment of osteoporotic fracture. *Scandinavian Journal of Surgery.* 2002;91:140-146.

49. Brandi ML. Microarchitecture, the key to bone quality. *Rheumatology.* Oct 2009;48(Suppl 4):iv3-8.

50. Clarke B. Normal bone anatomy and physiology. *Clinical journal of the American Society of Nephrology : CJASN.* Nov 2008;3 Suppl 3:S131-139.

51. Zebaze RMD, Ghasem-Zadeh A, Bohte A, et al. Intracortical remodelling and porosity in the distal radius and post-mortem femurs of women: a cross-sectional study. *The Lancet.* 2010;375:1729-1736.

52. Atkinson PJ. Quantitative analysis of osteoporosis in cortical bone. *Nature.* 1964;201(4917):373-375.

53. Erlandson MC, Kontulainen SA, Chilibeck PD, Arnold CM, Faulkner RA, Baxter-Jones AD. Former premenarcheal gymnasts exhibit site-specific skeletal benefits in adulthood after long-term retirement. *Journal of Bone and Mineral Research.* Nov 2012;27(11):2298-2305.

54. Ashe MC, Khan KM, Kontulainen SA, et al. Accuracy of pQCT for evaluating the aged human radius: an ashing, histomorphometry and failure load investigation. *Osteoporosis International.* 2006;17(8):1241-1251.

55. Kazakia GJ, Nirody JA, Bernstein G, Sode M, Burghardt AJ, Majumdar S. Age- and gender-related differences in cortical geometry and microstructure: Improved sensitivity by regional analysis. *Bone.* Feb 2013;52(2):623-631.

56. Currey JD. *Bones: Structure and Mechanics.* Princeton, New Jersey: Princeton University Press; 2002.

57. Khosla S, Riggs BL, Atkinson EJ, et al. Effects of sex and age on bone microstructure at the ultradistal radius: a population-based noninvasive in vivo assessment. *Journal of Bone and Mineral Research.* Jan 2006;21(1):124-131.

58. Hansen S, Shanbhogue V, Folkestad L, Nielsen MM, Brixen K. Bone Microarchitecture and Estimated Strength in 499 Adult Danish Women and Men: A Cross-Sectional, Population-Based High-Resolution Peripheral Quantitative Computed Tomographic Study on Peak Bone Structure. *Calcified tissue international.* Oct 22 2014;94:269-281.

59. Seeman E. Age- and menopause-related bone loss compromise cortical and trabecular microstructure. *The Journals of Gerontology. Series A: Biological Sciences and Medical Sciences.* Oct 2013;68(10):1218-1225.

60. Geusens P, Chapurlat R, Schett G, et al. High-resolution in vivo imaging of bone and joints: a window to microarchitecture. *Nature reviews. Rheumatology.* May 2014;10(5):304-313.

61. Aspenberg P, Sandberg O. Distal radial fractures heal by direct woven bone formation. *Acta Orthopaedica Scandinavica.* Jun 2013;84(3):297-300.

62. Martin RB, Burr DB, Sharkey NA. *Skeletal Tissue Mechanics.* New York, NY: Springer; 1998.

63. Martin RB, Ishida J. The relative effects of collagen fiber orientation, porosity, density, and mineralization on bone strength. *Journal of biomechanics.* 1989;22(5):419-426.

64. van Oers RF, Ruimerman R, Tanck E, Hilbers PA, Huiskes R. A unified theory for osteonal and hemi-osteonal remodeling. *Bone.* Feb 2008;42(2):250-259.

65. Cooper DM, Turinsky AL, Sensen CW, Hallgrimsson B. Quantitative 3D analysis of the canal network in cortical bone by micro-computed tomography. *Anatomical record. Part B, New anatomist.* Sep 2003;274(1):169-179.

66. Dempster DW, Compston JE, Drezner MK, et al. Standardized nomenclature, symbols, and units for bone histomorphometry: a 2012 update of the report of the ASBMR Histomorphometry Nomenclature Committee. *Journal of Bone and Mineral Research.* Jan 2013;28(1):2-17.

67. Seeman E. Bone quality: the material and structural basis of bone strength. *Journal of bone and mineral metabolism.* 2008;26(1):1-8.

68. Felsenberg D, Boonen S. The bone quality framework: determinants of bone strength and their interrelationships, and implications for osteoporosis management. *Clinical therapeutics.* Jan 2005;27(1):1-11.

69. Zioupos P, Hansen U, Currey JD. Microcracking damage and the fracture process in relation to strain rate in human cortical bone tensile failure. *Journal of biomechanics.* Oct 20 2008;41(14):2932-2939.

70. Burr DB. Bone material properties and mineral matrix contributions to fracture risk or age in women and men. *Journal of Musculoskeletal Neuronal Interactions.* 2002;2(3):201-204.

71. Currey JD. Changes in the impact energy absorption of bone with age. *Journal of biomechanics.* 1979;12:459-469.

72. Currey JD, Brear K, Zioupos P. The effects of ageing and changes in mineral content in degrading the toughness of human femora. *Journal of biomechanics.* 1996;29(2):257-260.

73. Wang X, Shen X, Li X, Mauli Agrawal C. Age-related changes in collagen network and toughness of bone. *Bone.* 2002;31(1):1-7.

74. Frost HM. Bone's mechanostat: a 2003 update. *The Anatomical Record.* Dec 2003;275(2):1081-1101.

75. McCalden RW, McGeough JA, Barker MB, Court-Brown CM. Age related changes in the tensile properties of cortical bone. *Journal of Bone and Joint Surgery.* 1993;75A(8):1193-1205.

76. Bailey AJ, Sims TJ, Ebbesen EN, Mansell JP, Thomsen JS, Mosekilde L. Age-related changes in the biochemical properties of human cancellous bone collagen: relationship to bone strength. *Calcified tissue international.* 1999;65:203-210.

77. Frost HM. From Wolff's Law to the Utah paradigm: insights about bone physiology and its clinical application. *The Anatomical Record.* 2001;262(4):398-419.

78. Liu R, Schindeler A, Little DG. The potential role of muscle in bone repair. *Journal of Musculoskeletal Neuronal Interactions.* 2010;10(1):71-76.

79. Frost HM. A 2003 update of bone physiology and Wolff's law for clinicians. *Angle Orthodontist.* 2004;74(1):3-15.

80. Frost HM. Wolff's Law and bone's structural adaptation to mechanical use: an overview for clinicians. *Angle Orthodontist.* 1994;64(3):175-188.

81. Chen JH, Liu C, You L, Simmons CA. Boning up on Wolff's Law: mechanical regulation of the cells that make and maintain bone. *Journal of biomechanics.* Jan 5 2010;43(1):108-118.

82. Martin TJ, Seeman E. Bone remodelling: its local regulation and the emergence of bone fragility. *Best Practice & Research: Clinical Endocrinology & Metabolism.* Oct 2008;22(5):701-722.

83. Mackie EJ, Ahmed YA, Tatarczuch L, Chen KS, Mirams M. Endochondral ossification: how cartilage is converted into bone in the developing skeleton. *The international journal of biochemistry & cell biology.* 2008;40(1):46-62.

84. Seeman E, Delmas PD. Bone quality - the material and structural basis of bone strength and fragility. *The New England Journal of Medicine.* 2006;354:2250-2261.

85. Seeman E. Structural basis of growth-related gain and age-related loss of bone strength. *Rheumatology.* Jul 2008;47 Suppl 4:iv2-8.

86. Sommerfeldt DW, Rubin CT. Biology of bone and how it orchestrates the form and function of the skeleton. *European Spine Journal.* Oct 2001;10 Suppl 2:S86-95.

87. Rauch F. The dynamics of bone structure development during pubertal growth. *Journal of Musculoskeletal Neuronal Interactions.* 2012;12(1):1-6.

88. Cauley JA. Estrogen and bone health in men and women. *Steroids.* Jul 2015;99(Pt A):11-15.

89. Vedi S, Croucher PI, Garrahan NJ, Compston JE. Effects of hormone replacement therapy on cancellous bone microstructure in postmenopausal women. *Bone.* 1996;19(1):69-72.

90. Weinstein RS, Hutson MS. Decreased trabecular width and increased trabecular spacing contribute to bone loss with aging. *Bone.* 1987;8(3):137-142.

91. Burr DB. Cortial bone: a target for fracture prevention? *The Lancet.* 2010;375:1672-1673.

92. Reid IR. Short-term and long-term effects of osteoporosis therapies. *Nature reviews. Endocrinology.* Jul 2015;11(7):418-428.

93. Zanchetta MB, Diehl M, Buttazzoni M, et al. Assessment of bone microarchitecture in postmenopausal women on long-term bisphosphonate therapy with atypical fractures of the femur. *Journal of Bone and Mineral Research.* Apr 2014;29(4):999-1004.

94. Burghardt AJ, Kazakia GJ, Sode M, de Papp AE, Link TM, Majumdar S. A longitudinal HR-pQCT study of alendronate treatment in postmenopausal women with low bone density: Relations among density, cortical and trabecular microarchitecture, biomechanics, and bone turnover. *Journal of Bone and Mineral Research.* Dec 2010;25(12):2558-2571.

95. Leslie WD, Morin SN. Osteoporosis epidemiology 2013: implications for diagnosis, risk assessment, and treatment. *Current opinion in rheumatology.* Jul 2014;26(4):440-446.

96. Papaioannou A, Morin S, Cheung AM, et al. 2010 clinical practice guidelines for the diagnosis and management of osteoporosis in Canada: summary. *Canadian Medical Association Journal.* Nov 23 2010;182(17):1864-1873.

97. Burge R, Dawson-Hughes B, Solomon DH, Wong JB, King A, Tosteson A. Incidence and economic burden of osteoporosis-related fractures in the United States, 2005-2025. *Journal of Bone and Mineral Research.* Mar 2007;22(3):465-475.

98. Budhia S, Mikyas Y, Tang M, Badamgarav E. Osteoporotic fractures: a systematic review of US healthcare costs and resource utilization. *Pharmacoeconomics.* 2012;30(2):147-170.

99. Dickenson RP, Hutton WC, Stott JRR. The mechanical properties of bone in osteoporosis. *The Journal of Bone and Joint Sugery.* 1981;63B(2):233-238.

100. Turner CH. Biomechanics of bone - determinants of skeletal fragility and bone quality. *Osteoporosis International.* 2002;13:97-104.

101. Beck T. Measuring the structural strength of bones with dual-energy X-ray absorptiometry: principles, technical limitations, and future possibilities. *Osteoporosis International.* Sep 2003;14 Suppl 5:S81-88.

102. Sanders KM, Nicholson GC, Watts JJ, et al. Half the burden of fragility fractures in the community occur in women without osteoporosis. When is fracture prevention cost-effective? *Bone.* May 2006;38(5):694-700.

103. Stone KL, Seeley DG, Lui L-Y, et al. BMD at multiple sites and risk of fracture of multiple types: long-term results from the study of osteoporotic fractures. *Journal of Bone and Mineral Research.* 2003;18(11):1947-1954.

104. Augat P, Schorlemmer S. The role of cortical bone and its microstructure in bone strength. *Age and ageing.* Sep 2006;35 Suppl 2:ii27-ii31.

105. Nishiyama KK, Macdonald HM, Buie HR, Hanley DA, Boyd SK. Postmenopausal women with osteopenia have higher cortical porosity and thinner cortices at the distal radius and tibia than women with normal aBMD: an in vivo HR-pQCT study. *Journal of Bone and Mineral Research.* Apr 2010;25(4):882-890.

106. Vico L, Zouch M, Amirouche A, et al. High-resolution pQCT analysis at the distal radius and tibia discriminates patients with recent wrist and femoral neck fractures. *Journal of Bone and Mineral Research.* Nov 2008;23(11):1741-1750.

107. Kontulainen S, Hughes JM, Macdonald HM, Johnston JD. The biomechanical basis of bone strength development during growth. *Med Sport Sci.* 2007;51:13-32.

108. Nielson SP. The fallacy of BMD: a critical review of the diagnostic use of dual x-ray absorptiometry. *Clinical Rheumatology.* 2000;19(174-183):174.

109. Genant HK, Engelke K, Prevrhal S. Advanced CT bone imaging in osteoporosis. *Rheumatology.* Jul 2008;47 Suppl 4:iv9-16.

110. Hansen S, Beck Jensen JE, Rasmussen L, Hauge EM, Brixen K. Effects on bone geometry, density, and microarchitecture in the distal radius but not the tibia in women with primary hyperparathyroidism: A case-control study using HR-pQCT. *Journal of Bone and Mineral Research.* Sep 2010;25(9):1941-1947.

111. Varga P, Dall'Ara E, Pahr DH, Pretterklieber M, Zysset PK. Validation of an HR-pQCT-based homogenized finite element approach using mechanical testing of ultra-distal radius sections. *Biomechanics and modeling in mechanobiology.* Jul 2011;10(4):431-444.

112. Pistoia W, van Rietbergen B, Lochmuller EM, Lill CA, Eckstein F, Ruegsegger P. Estimation of distal radius failure load with micro-finite element analysis models based on three-dimensional peripheral quantitative computed tomography images. *Bone.* 2002;30(6):842-848.

113. van Rietbergen B, Pistoia W, Ulrich D, Huiskes R, Ruegsegger P. Prediction of trabecular bone failure parameters using a tissue failure criterion and uFE analysis. *Computer Simulations and Modelling in Medicine.* 2000;1:98-101.

114. Liu XS, Zhang XH, Sekhon KK, et al. High-resolution peripheral quantitative computed tomography can assess microstructural and mechanical properties of human distal tibial bone. *Journal of Bone and Mineral Research.* Apr 2010;25(4):746-756.

115. MacNeil JA, Boyd SK. Accuracy of high-resolution peripheral quantitative computed tomography for measurement of bone quality. *Medical engineering & physics.* Dec 2007;29(10):1096-1105.

116. Pistoia W, van Rietbergen B, Lochmüller EM, Lill CA, Eckstein F, Rüegsegger P. Image-Based Micro-Finite-Element Modeling for Improved Distal Radius Strength Diagnosis. *Journal of Clinical Densitometry.* 2004;7(2):153-160.

117. Cuddihy MT, Gabriel SE, Crowson CS, O'Fallon WM, Melton LJ, 3rd. Forearm fractures as predictors of subsequent osteoporotic fractures. *Osteoporosis International.* 1999;9:469-475.

118. Warriner AH, Patkar NM, Yun H, Delzell E. Minor, major, low-trauma, and high-trauma fractures: what are the subsequent fracture risks and how do they vary? *Current osteoporosis reports.* Sep 2011;9(3):122-128.

119. Compston JE. Osteoporosis. *Clinical Endocrinology.* 1990;33:653-682.

120. *National Osteoporosis Foundation: Clinician's guide to prevention and treatment of osteoporosis.* Washinton, DC: National Osteoporosis Foundation;2010.

121. Lane JM, Serota AC, Raphael B. Osteoporosis: differences and similarities in male and female patients. *The Orthopedic clinics of North America.* Oct 2006;37(4):601-609.

122. Ferrari S. Human genetics of osteoporosis. *Best Practice & Research: Clinical Endocrinology & Metabolism.* Oct 2008;22(5):723-735.

123. Buehring B, Viswanathan R, Binkley N, Busse W. Glucocorticoid-induced osteoporosis: an update on effects and management. *The Journal of allergy and clinical immunology.* Nov 2013;132(5):1019-1030.

124. Morrison A, Fan T, Sen SS, Weisenfluh L. Epidemiology of falls and osteoporotic fractures: a systematic review. *ClinicoEconomics and Outcomes Research: CEOR.* 2013;5:9-18.

125. Deandrea S, Lucenteforte E, Bravi F, Foschi R, La Vecchia C, Negri E. Risk factors for falls in community-dwelling older people: a systematic review and meta-analysis. *Epidemiology.* Sep 2010;21(5):658-668.

126. Blake AJ, Morgan K, Bendall MJ, et al. Falls by elderly people at home: prevalence and associated factors. *Age and ageing.* 1988;17:365-372.

127. O'Loughlin JL, Robitaille Y, Boivin JF, Sulssa S. Incidence of and risk factors for falls and injurious falls among the community-dwelling elderly. *American Journal of Epidemiology.* 1993;137(3):342-354.

128. Campbell AJ, Borrie MJ, Spears GF, Jackson SL, Brown JS, Fitzgerlas JL. Circumstances and consequences of falls experienced by a community population 70 years and over during a prospective study. *Age and ageing.* 1990;19:136-141.

129. Tinetti ME, Baker DI, McAvay G, et al. A multifactorial intervention to reduce the risk of falling among elderly people living in the community. *N Engl J Med.* 1994;331:872-873.

130. Berg WP, Alessio HM, Mills EM, Tong C. Circumstances and consequences of falls in independent community-dwelling older adults. *Age and ageing.* 1997;26:261-268.

131. Crockett K, Arnold CM, Farthing JP, et al. Bone strength and muscle properties in postmenopausal women with and without a recent distal radius fracture. *Osteoporosis International.* May 23 2015.

132. Chiu J, Robinovitch SN. Prediction of upper extremity impact forces during falls on the outstretched hand. *Journal of biomechanics.* 1998;31:1169-1176.

133. DeGoede KM, Ashton-Miller JA. Fall arrest strategy affects peak hand impact force in a forward fall. *Journal of biomechanics.* 2002;35(843-848):843.

134. Gehlbach S, Saag KG, Adachi JD, et al. Previous fractures at multiple sites increase the risk for subsequent fractures: the Global Longitudinal Study of Osteoporosis in Women. *Journal of Bone and Mineral Research.* Mar 2012;27(3):645-653.

135. Barrett-Connor E, Sajjan SG, Siris ES, Miller PD, Chen YT, Markson LE. Wrist fracture as a predictor of future fractures in younger versus older postmenopausal women: results from the National Osteoporosis Risk Assessment (NORA). *Osteoporosis International.* May 2008;19(5):607-613.

136. Mallmin H, Ljunghall S, Persson I, Naessen T, Krusemo U-B, Bergstrom R. Fracture of the distal forearm as a forecaster of subsequent hip fracture: a population-based cohort study with 24 years follow-up. *Calcified tissue international.* 1993;52:269-272.

137. Chan K, Qin L, Lau M, et al. A randomized, prospective study of the effects of Tai Chi Chun exercise on bone mineral density in postmenopausal women. *Archives of Physical Medicine and Rehabilitation.* 2004;85(5):717-722.

138. Tolomio S, Ermolao A, Travain G, Zaccaria M. Short-term adapted physical activity program improves bone quality in osteopenic/osteoporotic postmenopausal women. *Journal of Physical Activity and Health.* 2008;5:844-853.

139. Karinkanta S, Heinonen A, Sievanen H, Uusi-Rasi K, Fogelholm M, Kannus P. Maintenance of exercise-induced benefits in physical functioning and bone among elderly women. *Osteoporosis International.* Apr 2009;20(4):665-674.

140. Karinkanta S, Heinonen A, Sievanen H, et al. A multi-component exercise regimen to prevent functional decline and bone fragility in home-dwelling elderly women: randomized, controlled trial. *Osteoporosis International.* Apr 2007;18(4):453-462.

141. American College of Sports M, Chodzko-Zajko WJ, Proctor DN, et al. American College of Sports Medicine position stand. Exercise and physical activity for older adults. *Medicine and science in sports and exercise.* Jul 2009;41(7):1510-1530.

142. Bainbridge KE, Sowers MF, Crutchfield M, Lin X, Jannausch M, Harlow SD. Natural history of bone loss over 6 years among premenopausal and early postmenopausal women. *American Journal of Epidemiology.* 2002;156(5):410-417.

143. Riggs BL, Wahner HW, Melton LJ, Richelson LS, Judd HL, Offord KP. Rates of bone loss in the appendicular and axial skeletons of women: evidence of substantial vertebral bone loss before menopause. *Journal of Clinical Investigation.* 1986;77:1487-1491.

144. Riggs BL, Melton LJr. Involutional osteoporosis. *N Engl J Med.* 1986;314(26):1676-1686.

145. Uusi-Rasi K, Sievanen H, Pasanen M, Kannus P. Age-related decline in trabecular and cortical density: a 5-year peripheral quantitative computed tomography follow-up study of pre- and postmenopausal women. *Calcified tissue international.* Oct 2007;81(4):249-253.

146. Riggs BL, Melton LJ, Robb RA, et al. A population-based assessment of rates of bone loss at multiple skeletal sites: evidence for substantial trabecular bone loss in young adult women and men. *Journal of Bone and Mineral Research.* Feb 2008;23(2):205-214.

147. Hernandez ER, Revilla M, Seco-Durban C, Villa LF, Cortes J, Rico H. Heterogeneity of trabecular and cortical postmenopausal bone loss: a longitudinal study with pQCT. *Bone.* 1997;20(3):283-287.

148. Kristman VL, Manno M, Cote P. Methods to account for attrition in longitudinal data: do they work? A simulation study. *European journal of epidemiology.* 2005;20(8):657-662.

149. Engelke K, Adams JE, Armbrecht G, et al. Clinical use of quantitative computed tomography and peripheral quantitative computed tomography in the management of osteoporosis in adults: the 2007 ISCD Official Positions. *Journal of Clinical Densitometry.* Jan-Mar 2008;11(1):123-162.

150. Langton CM, Njeh CF. *The Physical Measurement of Bone.* Philadelphia, PA: Institute of Physics; 2004.

151. Shepherd JA, Wang L, Fan B, et al. Optimal monitoring time interval between DXA measures in children. *Journal of Bone and Mineral Research.* Nov 2011;26(11):2745-2752.

152. Kanis JA, Melton LJ, 3rd, Christiansen C, Johnston CC, Khaltaev N. The diagnosis of osteoporosis. *Journal of Bone and Mineral Research.* 1994;9(8):1137-1141.

153. Cranney A, Jamal SA, Tsang JF, Josse RG, Leslie WD. Low bone mineral density and fracture burden in postmenopausal women. *Canadian Medical Association Journal (CMAJ).* Sep 11 2007;177(6):575-580.

154. Langsetmo L, Goltzman D, Kovacs CS, et al. Repeat low-trauma fractures occur frequently among men and women who have osteopenic BMD. *Journal of Bone and Mineral Research.* Sep 2009;24(9):1515-1522.

155. Boutroy S, Van Rietbergen B, Sornay-Rendu E, Munoz F, Bouxsein ML, Delmas PD. Finite element analysis based on in vivo HR-pQCT images of the distal radius is associated with wrist fracture in postmenopausal women. *Journal of Bone and Mineral Research.* Mar 2008;23(3):392-399.

156. Sornay-Rendu E, Boutroy S, Munoz F, Bouxsein ML. Cortical and trabecular architecture are altered in postmenopausal women with fractures. *Osteoporosis International.* Aug 2009;20(8):1291-1297.

157. MacNeil JA, Boyd SK. Improved reproducibility of high-resolution peripheral quantitative computed tomography for measurement of bone quality. *Medical engineering & physics.* Jul 2008;30(6):792-799.

158. Prevrhal S, Engelke K, Genant HK. pQCT: Peripheral Quantitative Computed Tomography. In: Grampp S, ed. *Radiology of Osteoporosis*. 2nd Revised Edition ed. Berlin, Germany: Springer-Verlag Berlin Heidelberg; 2008:143-162.

159. Swinford RR, Warden SJ. Factors affecting short-term precision of musculoskeletal measures using peripheral quantitative computed tomography (pQCT). *Osteoporosis International.* Nov 2010;21(11):1863-1870.

160. Kreiger N, Tenehouse A, Joseph L, et al. The Canadian multicentre osteoporosis study (CaMos): background, rationale, methods. *Canadian Journal of Aging.* 1999;18(3):376-387.

161. Kanis JA. Diagnosis of osteoporosis and assessment of fracture risk. *The Lancet.* 2002;359:1929-1936.

162. Kanis JA, McCloskey EV, Johansson H, Oden A, Melton LJ, 3rd, Khaltaev N. A reference standard for the description of osteoporosis. *Bone.* Mar 2008;42(3):467-475.

163. Medical S. *Xtreme CT Operations Manual.* Version 6.1 ed. Bruettisellen, Switzerland: SCANCO Medical Ag Fabrikweg 2 CH-8306; 2011.

164. Pialat JB, Burghardt AJ, Sode M, Link TM, Majumdar S. Visual grading of motion induced image degradation in high resolution peripheral computed tomography: impact of image quality on measures of bone density and micro-architecture. *Bone.* Jan 2012;50(1):111-118.

165. Laib A, Ruegsegger P. Comparison of structure extraction methods for in vivo trabecular bone measurements. *Computerized Medical Imaging and Graphics.* 1999;23:69-74.

166. Ellouz R, Chapurlat R, van Rietbergen B, Christen P, Pialat JB, Boutroy S. Challenges in longitudinal measurements with HR-pQCT: evaluation of a 3D registration method to improve bone microarchitecture and strength measurement reproducibility. *Bone.* Jun 2014;63:147-157.

167. Hildebrand T, Ruegsegger P. A new method for the model-independent assessment of thickness in 3D images. *Journal of Microscopy.* 1997;185(1):67-75.

168. Laib A, Hildebrand T, Hauselmann HJ, Ruegsegger P. Ridge number density: a new parameter for in vivo bone structure analysis. *Bone.* 1997;21(6):541-546.

169. Riggs BL, Melton LJ, 3rd. The worldwide problem of osteoporosis: insights afforded by epidemiology. *Bone.* 1995;17(5):505S-511S.

170. Spadaro JA, Werner FW, Brenner RA, Fortino MD, Fay LA, Edwards WT. Cortical and trabecular bone contribute strength to the osteopenic distal radius. *Journal of Orthopaedic Research.* 1994;12(2):211-218.

171. Alffram P-A, Bauer GCH. Epidemiology of fractures of the forearm: a biomechanical investigation of bone strength. *The Journal of Bone and Joint Sugery.* 1962;44A(1):105-114.

172. Owen RA, Melton LJr, Johnson KA, Ilstrup DM, Riggs BL. Incidence of Colles' fracture in a North American community. *Am J Public Health.* 1982;72(6):605-607.

173. Augat P, Claes LE. Prediction of fracture load at differenet skeletal sites by geometric properties of the cortical shell. *Journal of Bone and Mineral Research.* 1996;11(9):1356-1363.

174. MacNeil JA, Boyd SK. Load distribution and the predictive power of morphological indices in the distal radius and tibia by high resolution peripheral quantitative computed tomography. *Bone.* Jul 2007;41(1):129-137.

175. Currey JD. The effect of porosity and mineral content on the Young's modulus of elasticity of compact bone. *Journal of biomechanics.* 1988;21(2):131-139.

176. Currey J. Incompatible mechanical properties in compact bone. *Journal of theoretical biology.* Dec 21 2004;231(4):569-580.

177. Patsch JM, Burghardt AJ, Yap SP, et al. Increased cortical porosity in type 2 diabetic postmenopausal women with fragility fractures. *Journal of Bone and Mineral Research.* Feb 2013;28(2):313-324.

178. Bell KL, Loveridge N, Jordan GR, Power CR. A novel mechanism for induction of increased cortical porosity in cases of intracapsular hip fracture. *Bone.* 2000;26:305-313.

179. Bell KL, Loveridge N, Power J, Garrahan N, Meggitt BF, Reeve J. Regional differences in cortical porosity in the fractured femoral neck. *Bone.* 1999;24(1):57-64.

180. Ostertag A, Peyrin F, Fernandez S, Laredo JD, de Vernejoul MC, Chappard C. Cortical measurements of the tibia from high resolution peripheral quantitative computed tomography images: A comparison with synchrotron radiation micro-computed tomography. *Bone.* Feb 26 2014;63C:7-14.

181. Buie HR, Campbell GM, Klinck RJ, MacNeil JA, Boyd SK. Automatic segmentation of cortical and trabecular compartments based on a dual threshold technique for in vivo micro-CT bone analysis. *Bone.* Oct 2007;41(4):505-515.

182. Parfitt AM, Drezner MK, Glorieux FH, et al. Bone histomorphometry: standardization of nomenclature, symbols, and units. *Journal of Bone and Mineral Research.* 1987;2(3):595-610.

183. Jorgenson BL, Buie HR, McErlain DD, Sandino C, Boyd SK. A comparison of methods for in vivo assessment of cortical porosity in the human appendicular skeleton. *Bone.* Apr 2015;73:167-175.

184. Gaerdsell P, Johnell O, Nilsson BE, Gullberg B. Predicting various fragility fractures in women by forearm bone densitometry: a follow-up study. *Calcified tissue international.* 1993;52:348-353.

185. Silva MJ. Biomechanics of osteoporotic fractures. *Injury.* Sep 2007;38(Suppl 3):S69-76.

186. Niebur GL, Feldstein MJ, Yuen JC, Chen TJ, Keaveny TM. High-resolution finite element models with tissue strength asymmetry accurately predict failure of trabecular bone. *Journal of biomechanics.* 2000;33:1575-1583.

187. Pauchard Y, Liphardt AM, Macdonald HM, Hanley DA, Boyd SK. Quality control for bone quality parameters affected by subject motion in high-resolution peripheral quantitative computed tomography. *Bone.* Jun 2012;50(6):1304-1310.

188. Mueller TL, Stauber M, Kohler T, Eckstein F, Muller R, van Lenthe GH. Non-invasive bone competence analysis by high-resolution pQCT: an in vitro reproducibility study on structural and mechanical properties at the human radius. *Bone.* Feb 2009;44(2):364-371.

189. Vilayphiou N, Boutroy S, Szulc P, et al. Finite element analysis performed on radius and tibia HR-pQCT images and fragility fractures at all sites in men. *Journal of Bone and Mineral Research.* May 2011;26(5):965-973.

190. Rizzoli R, Chapurlat RD, Laroche JM, et al. Effects of strontium ranelate and alendronate on bone microstructure in women with osteoporosis. Results of a 2-year study. *Osteoporosis International.* Jan 2012;23(1):305-315.

191. Varga P, Baumbach S, Pahr D, Zysset PK. Validation of an anatomy specific finite element model of Colles' fracture. *Journal of biomechanics.* Aug 7 2009;42(11):1726-1731.

192. Varga P, Pahr DH, Baumbach S, Zysset PK. HR-pQCT based FE analysis of the most distal radius section provides an improved prediction of Colles' fracture load in vitro. *Bone.* Nov 2010;47(5):982-988.

193. van Rietbergen B, Weinans H, Huiskes R, Odgaard A. A new method to determine trabecular bone elastic properties and loading using micromechanical finite-element models. *Journal of biomechanics.* 1995;28(1):69-81.

194. Homminga J, Huiskes R, van Rietbergen B, Ruegsegger P, Weinans H. Introduction and evaluation of a gray-value voxel conversion technique. *Journal of biomechanics.* 2001;34:513-517.

195. Wong AK, Beattie KA, Min KK, et al. A Trimodality Comparison of Volumetric Bone Imaging Technologies. Part I: Short-term Precision and Validity. *Journal of Clinical Densitometry.* Aug 13 2015;18(1):124-135.

196. Genant HK, Engelke K, Hanley DA, et al. Denosumab improves density and strength parameters as measured by QCT of the radius in postmenopausal women with low bone mineral density. *Bone.* Jul 2010;47(1):131-139.

197. Seeman E, Delmas PD, Hanley DA, et al. Microarchitectural deterioration of cortical and trabecular bone: differing effects of denosumab and alendronate. *Journal of Bone and Mineral Research.* Aug 2010;25(8):1886-1894.

198. Laib A, Ruegsegger P. Calibration of trabecular bone structure measurements of in vivo three-dimensional peripheral quantitative computed tomography with 28 um resolution microcomputed tomography. *Bone.* 1999;24(1):35-39.

199. Siris ES, Miller PD, Barrett-Connor E, et al. Identificantion and fracture outcomes of undiagnosed low bone mineral density in postmenopausal women: results from the national osteoporosis risk assessment. *The Journal of the American Medical Association.* 2001;286(22):2815-2822.

200. Liu XS, Cohen A, Shane E, et al. Bone density, geometry, microstructure, and stiffness: Relationships between peripheral and central skeletal sites assessed by DXA, HR-pQCT, and cQCT in premenopausal women. *Journal of Bone and Mineral Research.* Oct 2010;25(10):2229-2238.

201. Leib ES, Lewiecki EM, Binkley N, Hamdy RC. Official position of the international society for clinical densitometry. *Journal of Clinical Densitometry.* 2004;7(1):1-5.

202. Johnell O, Kanis JA. An estimate of the worldwide prevalence and disability associated with osteoporotic fractures. *Osteoporosis International.* Dec 2006;17(12):1726-1733.

203. Sode M, Burghardt AJ, Kazakia GJ, Link TM, Majumdar S. Regional variations of gender-specific and age-related differences in trabecular bone structure of the distal radius and tibia. *Bone.* Jun 2010;46(6):1652-1660.

204. Duckham RL, Frank AW, Johnston JD, Olszynski WP, Kontulainen SA. Monitoring time interval for pQCT-derived bone outcomes in postmenopausal women. *Osteoporosis International.* Jan 24 2013;24(6):1917-1922.

205. Vincent WJ. *Statistics in Kinesiology.* 3rd ed. Champaign, IL: Human Kinetics; 2005.

206. Holzer G, von Skrbensky G, Holzer LA, Pichl W. Hip fractures and the contribution of cortical versus trabecular bone to femoral neck strength. *Journal of Bone and Mineral Research.* Mar 2009;24(3):468-474.

207. Schaffler MB, Burr DB. Stiffness of compact bone: effects of porosity and density. *Journal of biomechanics.* 1988;21(1):13-16.

208. Lauretani F, Bandinelli S, Griswold ME, et al. Longitudinal changes in BMD and bone geometry in a population-based study. *Journal of Bone and Mineral Research.* Mar 2008;23(3):400-408.

209. Mayhew PM, Thomas CD, Clement JG, et al. Relation between age, femoral neck cortical stability, and hip fracture risk. *The Lancet.* 2005;366(9480):129-135.

210. Melton LJ, 3rd, Riggs BL, Keaveny TM, et al. Relation of vertebral deformities to bone density, structure, and strength. *Journal of Bone and Mineral Research.* Sep 2010;25(9):1922-1930.

211. Middel B, van Sonderen E. Statistical significant change versus relevant or important change in (quasi) experimental design: some conceptual and metholodogical problems in estimating magnitude of intervention-related change in health service research. *International jJournal of Integrated Care.* 2002;2(17):1-18.

212. Wong C, Milkkelsen P, Hansen LB, Darvann T, Gebuhr P. Finite element analysis of tibial fractures. *Dan Med Bull.* 2010;57(5):A4148-A4151.

213. Hansen S, Brixen K, Gravholt CH. Compromised trabecular microarchitecture and lower finite element estimates of radius and tibia bone strength in adults with turner syndrome: a cross-sectional study using high-resolution-pQCT. *Journal of Bone and Mineral Research.* Aug 2012;27(8):1794-1803.

214. Chevalley T, Bonjour JP, van Rietbergen B, Ferrari S, Rizzoli R. Fracture history of healthy premenopausal women is associated with a reduction of cortical microstructural components at the distal radius. *Bone.* Aug 2013;55(2):377-383.

APPENDIX A. RETURN BIAS POSSIBILITY

Of the 104 baseline postmenopausal women recruited into the Saskatoon cohort of CaM*os*, 51 women returned for follow-up measurement. Therefore, 51% of the original Saskatoon cohort did not return for follow-up measurements. However, this participant attrition has not biased our follow-up findings because when comparing the osteoporosis status between those that returned (n=33 included study 2; n=18 removed from study 2 because of medication use; total of n=51 included in study 3) relative to those that did not return (n=53) and the total participants of 2011 (n=104), the ratios among normal status, osteopenic, and osteoporotic were similar (Table A1). Further, when comparing the standard HR-pQCT outcomes between those non-medicated postmenopausal women that returned (n=33) and those that did not return (n=53) there were no statistically significant differences (Table A2).

Table A1. Osteoporosis status ratios among those participants that returned for follow-up testing (n=51; n=33 not using bisphosphonates or hormone replacement therapy, n=18 using BIS or HRT) to those participants that did not return for follow-up testing (n=53). These ratios are also combined for the total participants in the baseline testing (n=104).

Included in the study (n=33)			Removed from study based on medication use (n=18)			Did not return for follow-up measures (n=53)		
Normal n (%)	*Osteopenic* n (%)	*Osteoporotic* n (%)	*Normal* n (%)	*Osteopenic* n (%)	*Osteoporotic* n (%)	*Normal* n (%)	*Osteopenic* n (%)	*Osteoporotic* n (%)
11 (33%)	17 (52%)	5 (15%)	4 (22%)	12 (67%)	2 (11%)	17 (32%)	30 (57%)	6 (11%)

Combined (n=51)		
Normal n (%)	*Osteopenic* n (%)	*Osteoporotic* n (%)
15 (29%)	29 (57%)	7 (14%)

Total (n=104)		
Normal n (%)	*Osteopenic* n (%)	*Osteoporotic* n (%)
32 (31%)	61 (59%)	11 (10%)

Table A2. Comparison of standard HR-pQCT outcomes between those participants that returned for follow-up testing (n=33 not using bisphosphonates or hormone replacement therapy) to those participants that did not return for follow-up testing (n=53) for a) radius and b) tibia.

a) Radius		**Returning (n=31)**		**Not Returning (n=49)**			**95% CI**	
		Mean	± SD	Mean	± SD	*P*-value	Lower	Upper
Age	*(years)*	76.6	± 6.5	75.2	± 8.7	0.432	-5.0351	2.1734
Height	*(cm)*	159.8	± 6.2	158.3	± 6.2	0.325	-4.2618	1.4314
Weight	*(kg)*	73.5	± 13.0	68.2	± 13.1	0.082	-11.2817	0.6846
Area								
Total	*(cm^2)*	285.0	± 39.6	274.9	± 37.4	0.253	-27.6147	7.3812
Cortical	*(cm^2)*	38.9	± 13.3	37.9	± 11.9	0.522	-7.7508	3.9666
Trabecular	*(cm^2)*	238.9	± 46.2	226.5	± 38.8	0.219	-31.0262	7.2352
Density								
Total	*(mg HA/cm^3)*	250.8	± 55.2	253.3	± 58.1	0.991	-26.6141	26.3176
Cortical	*(mg HA/cm^3)*	773.1	± 83.6	785.8	± 81.2	0.687	-30.4741	46.0333
Trabecular	*(mg HA/cm^3)*	135.5	± 44.2	133.9	± 37.9	0.874	-19.9552	17.0039
Meta	*(mg HA/cm^3)*	190.1	± 39.8	190.3	± 36.9	0.988	-17.2625	17.5187
Inn	*(mg HA/cm^3)*	97.7	± 49.0	95.0	± 42.0	0.801	-23.0911	17.8908
Micro-architecture								
CtTh	*(μm)*	535.8	± 189.5	532.4	± 174.3	0.703	-0.1009	0.0684
BV/TV	*(%)*	11.3	± 3.7	11.2	± 3.2	0.867	-0.0167	0.0141
TbN	*(1/mm)*	1.8	± 0.5	1.8	± 0.4	0.825	-0.1846	0.2308
TbTh	*(μm)*	61.9	± 10.0	61.0	± 11.5	0.603	-0.0064	0.0037
TbSp	*(μm)*	584.2	± 422.2	526.8	± 230.2	0.411	-0.2054	0.0850
TbSpSD	*(μm)*	352.3	± 368.1	285.0	± 261.4	0.333	-0.2087	0.0715

b) Tibia		**Returning (n=32)**		**Not Returning (n=53)**			**95% CI**	
		Mean	± SD	Mean	± SD	*P*-value	Lower	Upper
Age	*(years)*	76.9	± 6.5	75.1	± 8.3	0.279	-5.3075	1.5495
Height	*(cm)*	159.8	± 6.1	158.3	± 6.1	0.280	-4.2055	1.2310
Weight	*(kg)*	73.5	± 12.8	68.3	± 13.8	0.089	-11.1637	0.8052
Area								
Total	*(cm^2)*	733.5	± 93.8	698.8	± 96.6	0.109	-77.2734	7.8466
Cortical	*(cm^2)*	79.9	± 27.3	82.0	± 25.9	0.867	-10.8936	12.8954
Trabecular	*(cm^2)*	643.5	± 100.9	604.6	± 104.5	0.121	-80.8704	9.5712
Density								
Total	*(mg HA/cm^3)*	239	± 52.4	245.1	± 55.1	0.679	-19.1201	29.1957

Cortical	*(mg HA/cm^3)*	758	± 71.9	768.5	± 79.3	0.730	-28.3638	40.3494
Trabecular	*(mg HA/cm^3)*	159.1	± 38.7	155.7	± 38.9	0.567	-0.0861	0.1561
Meta	*(mg HA/cm^3)*	230.3	± 32.1	227.9	± 36.2	0.769	-19.8154	14.6950
Inn	*(mg HA/cm^3)*	110.7	± 44.7	106.7	± 43.3	0.808	-17.3548	13.5692
Micro-architecture								
CtTh	*(μm)*	748.1	± 262.6	796.2	± 274.4	0.567	-0.0861	0.1561
BV/TV	*(%)*	13.3	± 3.2	13.0	± 3.2	0.773	-0.0165	0.0123
TbN	*(1/mm)*	1.7	± 0.4	1.7	± 0.4	0.394	-0.2481	0.0988
TbTh	*(μm)*	77.8	± 15.4	78.5	± 14.9	0.714	-0.0055	0.0080
TbSp	*(μm)*	550.1	± 252.2	553.6	± 169.2	0.922	-0.0866	0.0955
TbSpSD	*(μm)*	342.7	± 424.6	300.8	± 219.3	0.533	-0.1807	0.0974

** All comparison completed using independent samples t-test using Bonferroni correction for multiple comparisons. Significance accepted at P<0.004.*

APPENDIX B. COPYRIGHT AGREEMENTS

Publication 1:

Kawalilak CE, Johnston JD, Olszynski WP, Leswick D, Kontulainen SA (2014). Comparison of short term in vivo precision of bone density and micro-architecture at the distal radius and tibia between postmenopausal women and young adults. *Journal of Clinical Densitometry*, *17*(4): 541-517.[1]

Dear Chantal,

According to the author agreement you completed, you have the right to reproduce part or all of your research in a thesis or dissertation. Please see this link for further information:http://www.elsevier.com/journal-authors/author-agreement

Let me know if you have any additional questions. Thanks!

Kind regards,
Jessica

::

JESSICA CLEGG
Journal Manager
Journals Production| ELSEVIER
1600 John F Kennedy Blvd, Ste 1800
Philadelphia, PA 19103-2899 USA
Tel +1 (215) 239-3694 | Fax +1 (215) 239-3388
j.clegg@elsevier.com

Journal publishing

Elsevier supports the need for authors to share, disseminate and maximize the impact of their research and these rights, in Elsevier proprietary journals* are defined below:

For subscription articles	**For open access articles**
Authors transfer copyright to the publisher as part of a journal publishing agreement, but have the right to: • Share their article forpersonal (scholarly) purposes(including scholarly rights to create certain derivative works), so long as they give proper attribution and credit to the published work. • Retain patent, trademark and other intellectual property rights (including raw research data). • Proper attribution and credit for the published work.	Authors sign an exclusive license agreement, where authors have copyright but license exclusive rights in their article to the publisher. In this case authors have the right to: • Share their article in the same ways permitted to third parties under the relevant user license (together with personal (scholarly) purposes to create certain derivative works), so long as they give proper attribution and credit to the published work. • Retain patent, trademark and other intellectual property rights (including raw research data). • Proper attribution and credit for the published work.

*Please note that society or third party owned journals may have different publishing agreements. Please see the journal's guide for authors for journal specific copyright information.

Publication 2:

Kawalilak CE, Johnston JD, Cooper DML, Olszynski WP, Kontulainen SA (2015). Role of endocortical contouring methods on precision of HR-pQCT-derived cortical micro-architecture in postmenopausal women and young adults. *Osteoporosis International. E-pub ahead of print.*

Confirmation Number: 11432394

Order Date: 08/26/2015

Order Details Osteoporosis international
Order Detail ID: 68130939
Order License Id: 3696670370537
ISSN: 1433-2965
Publication Type: e-Journal
Publisher: SPRINGER-VERLAG LONDON
Author/Editor: European Foundation for Osteoporosis; National Osteoporosis Foundation; International Osteoporosis Foundation
Permission Status: **Granted**
Permission type: Republish or display content
Type of use: Thesis/Dissertation

Requestor type	Academic institution
Format	Print, Electronic
Portion	chapter/article
Number of pages in chapter/article	10
Title or numeric reference of the portion(s)	Role of endocortical contouring methods on precision of HR-pQCT-derived cortical micro-architecture in postmenopausal women and young adults (DOI 10.1007/s00198-015-3262-3)
Title of the article or chapter the portion is from	N/A
Editor of portion(s)	N/A
Author of portion(s)	Chantal Kawalilak
Volume of serial or monograph	Electronic Publication Ahead of Print
Page range of portion	1-10
Publication date of portion	July 2015
Rights for	Main product
Duration of use	Life of current edition
Creation of copies for the disabled	no
With minor editing privileges	yes

For distribution to	Canada
In the following language(s)	Original language of publication
With incidental promotional use	yes
Lifetime unit quantity of new product	Up to 499
Made available in the following markets	Thesis Dissertation
The requesting person/organization	Chantal Kawalilak/University of Saskatchewan
Order reference number	
Author/Editor	Chantal Kawalilak
The standard identifier	Thesis Dissertation
Title	Monitoring Bone Micro-architecture with a Special Focus on Bone Strength
Publisher	University of Saskatchewan
Expected publication date	Oct 2015
Estimated size (pages)	200

Publication 4:

Kawalilak CE, Johnston JD, Olszynski WP, Kontulainen SA (2015). Least significant changes and monitoring time intervals for high-resolution pQCT-derived bone outcomes in postmenopausal women. *Journal of Musculoskeletal and Neuronal Interactions. 15*(2):190-196.[3]

From the Journal of Musculoskeletal and Neuronal Interactions *Instructions for Authors*:

"Copyright: Authors submitting manuscripts to JMNI retain the copyright of the article if it is published."

Publication 5:

Kawalilak CE, Johnston JD, Olszynski WP, Kontulainen SA (2014). Characterizing micro-architectural changes at the distal radius and tibia in postmenopausal women using HR-pQCT. *Osteoporosis International, 25*(8):2057-2066.[4]

Confirmation Number: 11432375

Order Date: 08/26/2015

Order Details: Osteoporosis international
Order Detail ID: 68130878
Order License ID: 3696660676349
ISSN: 1433-2965
Publication Type: e-Journal
Publisher: SPRINGER-VERLAG LONDON
Author/Editor: European Foundation for Osteoporosis; National Osteoporosis Foundation; International Osteoporosis Foundation
Permission Status: **Granted**
Permission type: Republish or display content
Type of use: Thesis/Dissertation

Requestor type	Academic institution
Format	Print, Electronic
Portion	chapter/article
Number of pages in chapter/article	10
Title or numeric reference of the portion(s)	Characterizing micro-architectural changes at the distal radius and tibia in postmenopausal women using HR-pQCT (DOI 10.1007/s00198-014-2719-0)
Title of the article or chapter the portion is from	N/A
Editor of portion(s)	N/A
Author of portion(s)	Chantal Kawalilak
Volume of serial or monograph	25
Issue, if republishing an article from a serial	8
Page range of portion	2057-2066
Publication date of portion	April 2014
Rights for	Main product
Duration of use	Life of current edition
Creation of copies for the disabled	no
With minor editing privileges	yes
For distribution to	Canada

In the following language(s)	Original language of publication
With incidental promotional use	yes
Lifetime unit quantity of new product	Up to 499
Made available in the following markets	Thesis Dissertation
The requesting person/organization	Chantal Kawalilak/University of Saskatchewan
Order reference number	
Author/Editor	Chantal Kawalilak
The standard identifier	Thesis Dissertation
Title	Monitoring Bone Micro-architecture with a Special Focus on Bone Strength
Publisher	University of Saskatchewan
Expected publication date	Oct 2015
Estimated size (pages)	200